E.O. Paton Electric Welding Institute of the National Academy of Sciences of Ukraine

International Scientific-Technical and Production Journal

The Paton WELDING JOURNAL

November 2015
No.11

Published since 2000

English translation of the monthly «Avtomaticheskaya Svarka» (Automatic Welding) journal published in Russian since 1948

Founders
E.O. Paton Electric Welding Institute, NASU
International Association «Welding»

Publisher
International Association «Welding»

Translators
A.A. Fomin, O.S. Kurochko, I.N. Kutianova
Editor
N.A. Dmitrieva
Electron galley
D.I. Sereda, T.Yu. Snegiryova

Address
E.O. Paton Electric Welding Institute,
International Association «Welding»
11, Bozhenko Str., 03680, Kiev, Ukraine
Tel.: (38044) 200 60 16, 200 82 77
Fax: (38044) 200 82 77, 200 81 45
E-mail: journal@paton.kiev.ua
www.patonpublishinghouse.com

State Registration Certificate
KV 4790 of 09.01.2001
ISSN 0957-798X

Subscriptions
$348, 12 issues per year,
air postage and packaging included.
Back issues available.

CONTENTS

THE 80th ANNIVERSARY OF THE CHAIR OF WELDING PRODUCTION OF NTUU «KIEV POLYTECHNIC INSTITUTE»

Evgy O. Paton, the founder of the Chair, and his sons Vladimir (*left*) and Boris (*right*) near new universal automatic welding machine TS-17 (1949)

In 1935, on the initiative of Evgeny O. Paton, the outstanding scientist and engineer, the academician of the UkrSSR, the Chair of Welding Production was founded at Mechanical Faculty of Kiev Polytechnic Institute, and preparation of mechanical engineers on specialty «Equipment and Technology of Welding Production» was organized. The need in education of the specialists of such a profile was caused by the requirements of intensive development of the domestic industry, transport, construction and many other branches of the national economy. By transferring the students from other specialties the first groups of students were formed for educating the welding engineers at the second and third years of study. The first graduation of engineers of welding specialty (17 persons) took place in 1938, and within 3 years 104 welding specialists were educated and trained.

Many research workers of the Electric Welding Institute of the Academy of Sciences of the UkrSSR, organized in 1934, took an active part in the educational process at the Chair in those years, in particular, V.I. Dyatlov, V.V. Severnitsky, A.M. Sidorenko, F.E. Sorokovsky. For teaching the profile disciplines the staff members from other chairs of the Institute were also invited. Among them the Ass. Profs I.P. Trochun and N.V. Pines, the Assistant G.K. Blavdzevich, and M.M. Bort, the Chief metallurgist of the aircraft plant. The required number of rooms for educational process and research works was allocated for the Chair. At that stage the formation of new engineering specialty «Equipment and Technology of Welding Production» took place. For the first time the methodological grounds for education and training of welding engineers were developed, including an integrated system of education based on close relation between the educational institution and production.

From the beginning of its foundation the Chair was headed by the Academician E.O. Paton. However, his high duties as the Director of Electric Welding Institute impeded his work in KPI, and in 1938 he was forced to leave the institution, further he still continued to render a comprehensive assistance to the Chair, permanently embodying the originally laid idea of affinity and cooperation of both organizations.

Evgeny Paton was an outstanding scientist and teacher, and that fact had a rather beneficial effect on the quality of preparation of the welding specialists. In those years as the basis of educating the welding engineers E.O. Paton laid the important methodological principles consisting in need of combining the theoretical and practical training of students, subordinating the content of the training specialists to the practical problems of welding production, high requirements to the work of students over the educational material, in extensive use of modern achievements of science and technology of welding for education. The scientific and pedagogical staff of the Chair carefully preserves these principles even at the present time.

In 1938, the Ass. Prof. V.L. Ulasik became the head of the Chair. The outbreak of the war in 1941 interrupted education of welding specialists. KPI was evacuated to Tashkent. Many teachers, staff, postgraduate and undergraduate students were mobilized, some of them moved to the plants producing defensive products. Due to

Unveiling of monument Evgeny Paton at NTUU «KPI»

the absence of teaching personnel the education of welding production engineers in Tashkent was not carried out.

In 1944, after return of KPI from evacuation to Kiev, the Chair of Welding Production immediately resumed its activity. From July to November 1944 the Cair was headed by Prof. G.I. Pogodin-Alekseev, and then from the end of 1944 to 1947 by the Ass. Prof. I.P. Trochun, and for a short period in 1947, by the Ass. Prof. M.N. Gapchenko and the Assistant M.M. Bort. There was a strong lack of qualified scientific and pedagogical staff. Nevertheless in short terms the staff members and the students of the Chair managed to restore the classrooms and laboratories destroyed during the war. The Chair was equipped with the necessary welding equipment. As a result, in fact, the new educational and laboratory facilities were created with total area of about 700 m^2. The first post-war graduation of mechanical engineers on specialty «Equipment and Technology of Welding Production» was held in 1947. It became possible due to the great contribution of Prof. K.K. Khrenov, who headed the Chair from 1947 to 1957. After K.K. Khrenov the Chair was headed by Prof. I.P. Trochun (1957–1967) and Prof. V.I. Dyatlov (1967–1969). Since 1965, at the Chair the education and training of electromechanical engineers on specialty «Electrothermal Equipment» with the specialization in electric welding installations was opened.

In 1969, to the position of the Head of the Chair (as a combining job) Prof. B.S. Kasatkin, the Head of Department of the Electric Welding Institute, was invited, who headed the Chair until June 1972. This event contributed to the significant widening and strengthening of comprehensive and creative cooperation between the Chair and the E.O. Paton Electric Welding Institute, especially in the field of scientific research. The contractual research works and training of scientific personnel were essentially boosted through postgraduate courses and competition. At the same time, the difficulties associated with the limited educational, laboratory and scientific base of the Chair were noticeable more significantly.

In the early 1970s, the Government of Ukraine took the decision to found the Educational Center for the joint training and improving the qualification of welding engineers on the facilities of KPI and PWI. The new educational and laboratory building (now the 23rd building of the National Technical University of Ukraine «KPI») of 6000 m^2 area was built. In September, 1977 the Chair moved to the new educational and laboratory facilities, equipped with the modern equipment and devices. For educational work the PWI leading scientists G.I. Leskov, A.I.

Chvertko, A.G. Potapievsky, V.R. Ryabov, V.N. Zamkov, V.E. Moravsky, V.I. Makhnenko, B.A. Movchan, A.A. Rossoshinsky et al. were invited to the Chair on the terms of a combining job.

Since 1972 to 1974, the Chair was headed by Prof. M.N. Gapchenko, and since 1974 it was headed by Prof. I.R. Patskevitch.

From 1962 to 1978, under the supervision of V.P. Chernysh the works on creation of methods of magnetic control of solidification of weld pool metal (V.P. Chernysh, V.V. Syrovatka, I.V. Malinkin, V.D. Kuznetsov et al.) were carried out at the Chair. The obtained results confirmed the possibility of active influence on the process of primary solidification by electromagnetic stirring of weld pool and showed that stirring leads to refinement of weld metal structure, and change in depth and shape of penetration.

In 1978, from the Chair of Welding Production the Chair of Welding Equipment was detached under the directorship of Prof. V.P. Chernysh, where the works on the control of solidification of weld pool metal by the magnetic influence were continued, further developed in the works of Prof. R.N. Ryzhov, Dr. V.A. Pakharenko et al.

From May, 1989 to April 27, 2015, the Chair of Welding Production was headed by Prof. V.M. Prokhorenko (the graduate from the Chair in 1962).

In 1991, from the Chair of Welding Production the Chair of Restoration of Machine Parts was detached, which by that time was headed by the Ass. Prof. V.M. Dukhno, and from October, 1993 it was headed by Prof. V.N. Korzh. It was charged with preparation of specialists on specialty «Equipment and Technology for Improving Wear Resistance of Machine Parts». At present time the Chair is called the Chair of Surface Engineering and is headed by Prof. V.D. Kuznetsov.

On the basis of the Chair of Welding Production in 1975 the Welding Faculty resumed its work, whose dean until 2002 was Prof. A.M. Slivinsky, the graduate of the Chair of Welding Production in 1960. Since 2002 until now the Welding Faculty is headed by Prof. S.K. Fomichev, who headed the Chair of Electric Welding Equipment since 2001.

Today the Faculty consists of three special chairs: Welding Production, Electric Welding Equipment and Surface Engineering. The Faculty prepares bachelors in the direction «Welding», as well as specialists on «Equipment and Technology of Welding Production», «Welding Machines», «Equipment and Technology of Increasing Wear Resistance and Restoration of Machine Parts», and masters in the field of welding science and technology on the basis of bachelor preparation. Currently, about 400 students are studying at the Faculty. Besides the education of students of the Faculty the scientists carry out a wide range of scientific research on the most relevant and advanced directions.

On the territorial facility of building of the Welding Faculty, the Welding Training Center was founded in 1977, where the UNIDO workshop and courses for improving the qualification of domestic specialists in the field of welding and nondestructive testing of welded joints and training courses for welders-workers were opened. The Chair of Welding Production takes also an active part in the work of the Educational Center. At the moment this direction is actively realized in the program of double diploma — International Welding Engineer (IWE), International Welding Technologist (IWT) and International Welding Inspector (IWI) (according to standard DSTU ISO 14731:2008). This diploma is realized on the basis of the Welding Faculty and the teachers of the chairs of the Welding Faculty form the working group on training specialists on the basis of laboratories of the Chair.

At the end of 1994, on the initiative of A.M. Slivinsky, the Dean of the Welding Faculty, and the Ukrainian Welding Society according to the general resolution of the National Academy of Sciences of Ukraine and the Ministry of Education of Ukraine, the Ukrainian Committee for Welder Certification (UCWC) was founded. Its technical director was V.T. Kotik, the Ass. Prof. of the Chair of Welding Production. During the period of the UCWC activity, more than 700 experts were trained and certified, and more than 230 commissions on certification of welders were opened in Ukraine. The database on certifying commission and certified welders (annually certified about 10,000 persons), created by the UCWC, provide a rapid control of the certification processes as well as obtaining the information on the status and dynamics of development of welding production in Ukraine. Thus, the system of welders certification in Ukraine demonstrated its necessity, relevance and effectiveness, providing the high quality of welding works.

Since the moment of its foundation the research work gained the extensive development at the Chair. The postgraduate courses were organized and successfully operate. The postgraduate students and many staff members of the Chair defended their theses for candidate of technical sciences degree. The teachers of the Chair published a number of books, which received a wide recognition. At the Chair the steadily developing research directions were formed. In particular, the staff members of the Chair under the general supervision of Prof. K.K. Khrenov carried out a number of works related to the investigation of welding arc (V.E. Moravsky, G.B. Serdyuk,

Staff members of the Chair of Welding Production (September, 2015)

G.V. Vasiliev, L.A. Byalotsky). In 1949, K.K. Khrenov published fundamental monograph «Electric welding arc», which became the first summarized work on the subject. These works on study of arc discharge were continued on a new qualitative level with the use of electronic oscillography of arc in order to study the transient processes (L.A. Zhdanov, V.L. Kovalenko). The results of these investigations are reflected in the thesis for Cand. of Tech. Sci. Degree of V.L. Kovalenko (2013). As a result, a new complex criterion for evaluation of stability of existence of arc discharge was proposed, which includes power and technological characteristics of the arc, the features of existence of alternating current arc were explained.

The other demanded direction of research activity of the Chair was the creation of new original slag systems for ceramic fluxes and development of their compositions intended for welding and surfacing, as well as the technology of manufacture of ceramic fluxes (D.M. Kushnerev, I.M. Zhdanov, M.P. Grebelnik et al.). The results of investigations on the development and application of ceramic fluxes are described in monograph of K.K. Khrenov and D.M. Kushnerev «Ceramic fluxes» published in 1954. The works were continued in 1970–2015 by A.M. Slivinsky, V.N. Kopersak, V.I. Prokhorov, V.T. Kotik, O.A. Gaevsky, L.A. Zhdanov and N.M. Strelenko. During that time the unique ceramic flux for welding the metal after oxy-fuel cutting (A.M. Slivinsky, V.T. Kotik), fused flux AN-44 for welding of low-carbon steels of increased strength (A.M. Slivinsky, V.M. Prokhorov, B.N. Kopersak), fused flux AN-69 for surfacing (A.M. Slivinsky, L.A. Zhdanov), agglomerated flux ANK-45 (jointly with the PWI Department) and flux ANK-73 for surfacing (L.A. Zhdanov, N.M. Strelenko) were developed. The results of the work are reflected in numerous publications and protected by the copyright certificates and patents of Ukraine.

The development of original technologies for surfacing of cutting tool, worn-out parts of machines and mechanisms are also an important direction of work of the Chair of Welding Production. The works of V.D. Kuznetsov, N.A. Gorpenyuk, Yu.A. Yuzvenko, M.S. Samotryasov and B.N. Gorpenyuk should be noted.

The important works on theoretical problems of welding were performed under the supervision of V.I. Dyatlov, who defended the thesis for Dr. of Tech. Sci. Degree on these directions in 1963. They include original developments in the field of theory of freely expanding and contracted welding arc, calculations of conditions of automatic submerged arc welding, electrode metal transfer and a number of other investigations. The theoretical models of V.I. Dyatlov on arc processes, electrode metal transfer, metallurgical interaction in submerged arc welding did not loose their relevance even today. Prof. V.I. Dyatlov dealt not only with fusion welding, but also with solid-state welding. At the Chair under his supervision the thesis for Cand. of Tech. Sci.

Degree on diffusion welding in the glow discharge of magnetic and nonmagnetic steels was made by D.I. Kotelnikov, who later defended the thesis for Dr. of Tech. Sci. Degree on the same subject.

Under the supervision of M.N. Gapchenko at the Chair a number of works was carried out aimed at the study of weldability, brittle fracture of metals and modernization of technology of welding steels and alloys. The results of investigations are summarized in monograph of M.N. Gapchenko «Brittle fractures of welded joints and structures», as well as in his thesis for Dr. of Tech. Sci. Degree defended in 1969. Later the investigations of technological strength and weldability for nickel alloys, stainless and high-strength steels were continued by A.A. Slivinsky. The results of these investigations in 1998–2015 were published in numerous articles, including foreign ones, and they were also included into educational book «Weldability of structural materials».

The works in the field of gas-flame treatment of metals, carried out under the supervision of M.M. Bort and A.D. Kotvitsky, gained a great development in 1950–1960. Especially the oxygen cutting of metal of large thicknesses at low pressure, pack cutting of metal, development of the whole series of installations for cutting the round profile, hot crops of steel casting, hot rolling, etc. should be noted. The fundamentally new types of cutters were created, which found a wide application in industry. The development of plasma welding, surfacing and cutting of materials was headed by M.N. Gapchenko. The significant results were obtained under the supervision of V.N. Korzh in the field of creation of equipment and technologies for welding using hydrogen-oxygen flame. The results of these investigations formed the basis of the thesis for Dr. of Tech. Sci. Degree of V.N. Korzh defended in 1991.

The works in the field of welding stresses and deformations were developed under the supervision of I.M. Zhdanov and I.P. Trochun, who developed the simple and descriptive methods for engineering calculations of welding stresses and deformations in metal structures. The main results of these investigations are presented in monograph of I.P. Trochun «Inner forces and deformations in welding». The investigations of thermal deformation processes in welding (the works of I.M. Zhdanov, I.M. Chertov, E.A. Korshenko, V.M. Prokhorenko, A.S. Karpenko, V.N. Korzh, B.V. Medko, A.K. Gonchar et al.) were intensively developed in the 1960s, carried out under the supervision of I.M. Zhdanov. The main directions of research are the study of regularities of formation of deformations and stresses in welding process, regularities of brittle fracture, creation of new experimental methods of investigations and devices, development of methods for reducing residual stresses and deformations.

The results of investigations of influence of stress-strain state of welded structures on brittle fracture of welded joints are reflected in the thesis for Dr. of Tech. Sci. Degree of V.M. Prokhorenko «Methods for calculating stress intensity factors and crack opening in welded joints with account for residual stresses», the defence of which was held in 1989. The further investigations of stressed state of welded structures were carried out in the direction of development of new engineering methods of calculation based on the modern conceptions about the kinetics of deformations in welding. The result of these studies was the thesis for Cand. of Tech. Sci. Degree of D.V. Prokhorenko. The research results described above were partially included into educational books «Stresses and deformations in welding» by B.S. Kasatkin, V.M. Prokhorenko, I.M. Chertov, as well as «Stresses and deformations in welded joints and structures» by V.M. Prokhorenko, D.V. Prokhorenko, published, respectively, in 1987 and 2009. In the recent years the study of stress-strain state in welding is successfully continued by the young generation of researchers D.V. Prokhorenko and A.A. Perepichaj using numerical methods of mathematical modeling based on finite element method. In particular, they carried out modeling of stress-strain state of the main pipeline at the site of repair of crack-like defect, study of thermomechanical processes in surfacing the weld on the surface of a semi-infinite body, calculation of stresses and deformations for different technological schemes of welding of butt joints of thin metal. One of the results of these studies was the thesis for Cand. of Tech. Sci. Degree of A.A. Perepichaj.

In the 1980s, at the Chair the new scientific directions appeared. Under the supervision of I.R. Patskevitch the development of matters of the technology of welding cast iron and investigations of surface phenomena in welding was started. The wettability and leaking of different pairs of liquid metals in isothermal and non-isothermal conditions were studied. The effect of external influences on the mentioned phenomena was determined. The results of these works are described in monograph of I.R. Patskevich, V.R. Ryabov and G.F. Deev «Surface phenomena in metals during welding» (1991). Their works were continued by V.P. Bojko, who created a unique experimental installation for investiga-

tion of high-temperature processes of wetting and interphase interactions at the gas–slag–metal boundary. According to the results of research works the numerous papers were published. The methods of increasing the accuracy of producing welded structures were intensively developed under the supervision of I.M. Zhdanov. The works were continued by V.V. Lysak. According to the results of the work the thesis for Cand. of Tech. Sci. Degree was defended and an original method for welding of thin sheet material was developed.

Many interesting results were obtained by V.V. Batyuk with the staff members of the Chair (B.A. Bobin, S.N. Minakov, I.N. Grisha et al.) in the direction of development of devices and technology of non-destructive testing of residual welding stresses in different welded structures.

The investigations in the field of temperature conditions of weld pool and electrode metal drops were carried out by V.M. Dykhno and S.M. Getmanets, and later they formed the basis of thesis for Cand. Tech. Sci. Degree and made a significant contribution to the study of heat content of electrode metal drops and pool in argon arc welding.

Since the late 1980s, at the Chair under the supervision of S.K. Fomichev a large complex of works was carried out to improve the corrosion resistance of welded structures, the materials of these investigations formed the basis for the thesis for Dr. of Tech. Sci. Degree defended by him in 1994. Since 1987, at the Chair under the supervision of I.P. Belokur the matters of flaw detection and quality control of welded joints are intensively developed. The results of research works in this direction are reflected in his thesis for Dr. of Tech. Sci. Degree, defended in 1991, and in his numerous publications.

Since the 1990s, at the Chair the direction is actively developed associated with the development of CAD systems of technological processes of fusion welding using the computer technology. Under the supervision of I.F. Korinets and with the participation of V.P. Bojko and Yu.I. Okhaj the mathematical models for melting of steel and titanium base metals, solid and flux-cored wires and heating of covered electrode were developed. As a result, the original methods of calculation of conditions of mechanized and automatic arc welding in shielding gases and under flux were developed.

Modern scientific and technical directions of the Chair of Welding Production. The research directions of the Chair were formed in the close creative relationships with the PWI, with the participation of not only the leading scientists of the Institute, but also Boris E. Paton himself. Prof. B.E. Paton, the Director of the PWI and the President of the NAS of Ukraine, personally assisted in solving the problems of material and technical base, training of scientific personnel of the Chair and solving the strategic tasks of development of welding production. Below the basic problematic directions of work of the Chair are considered.

Technologies and metallurgical processes in electric arc welding:

- creation of theoretical models for calculation of gas phase composition, effect of welding consumables on composition of weld metal, content of gases and nonmetallic inclusions in it during arc welding on the basis of physical thermodynamic modeling;
- investigation of metallurgical processes in welding and development of new fused agglomerated fluxes and flux-cored wires for welding and surfacing;
- study of weld metal tendency to crack formation on the basis of technological samples;
- investigation of arc discharge in welding and its technical characteristics on the basis of complex factors of stability and transient processes using synergic power sources;
- investigation and modeling of features of pore formation in welding;
- modeling of thermal processes of electric arc welding;
- investigation of influence of thermal deformational cycles of welding on phase composition and structure of welded joint metal;
- technological features of welding using modulated current with synergic regulation of arc;
- creation of mathematical models of base and electrode metal melting in arc fusion welding and optimization of welding processes in shielding gases on their basis.

Stresses and deformations in welding:

- modeling and calculation of welding stresses, deformations and displacements of elements of welded structures using finite element method basing on the modern computer technologies;
- study of influence of technological schemes of welding on residual displacements of longitudinal axis of welded structures and development of optimal technological sequence of their welding;
- modeling of stress-strain state of welded structures for beam and arc welding methods;
- determination of energy input of thermal straightening of welded one-dimensional structures using engineering calculation methods.

Diffusion welding and brazing of metals, alloys and composite materials:

- mathematical modeling of thermal deformation processes during diffusion welding and brazing;
- development of technologies of diffusion welding and brazing with the controlled stress-strain state;
- investigation of influence of surface modification by highly-concentrated energy flows on properties of diffusion-welded and brazed joints;
- creation of new materials for producing diffusion-welded and brazed joints.

The active development of the direction is provided owing to the support of the PWI management and staff members, in particular, K.A. Yushchenko and I.V. Krivtsun, the Academicians of the NASU, V.F. Khorunov, the Corr.-Member of the NASU, and the staff members of the National Shipbuilding University (Nikolaev). The great contribution to the performance of works on control of stress-strain state in the process of producing joints in the solid state was made by V.I. Makhnenko, the Academician of the NASU, and to producing of metal-ceramic joints by O.K. Nazarenko, the Corr.-Member of the NASU.

Many of the graduates of the Chair became prominent workers of science and welding production. Among the graduates from the Chair there are many candidates and doctors of technical sciences. In this article it is difficult to mention the names of all the prominent graduates of the Chair. We only note that many of them became the academicians of the NASU and managers of large enterprises and organizations.

In the period of 2005–2015, a significant breakthrough in raising the scientific potential of the Chair and Welding Faculty in general was done. This became possible due to the implementation of a target program of preparation of Candidates and Doctors of sciences, signed by Prof. B.E. Paton and M.Z. Zgurovsky, the Academician of the NASU, the Rector of NTUU «KPI», and is realized at their active support. In the frames of this program at the Welding Faculty 5 Doctors and 10 Candidates of Technical Sciences were prepared.

Recently, the Chair has a fruitful cooperation with well-known companies Fronius Ukraine and Binzel Ukraine GmbH, as well as the PWI Pilot Plant of Welding Equipment and Pilot Plant of Welding Materials, where our graduates are working. These companies are equipping the laboratories of the Chair with innovative equipment, provide information stands and welding consumables, carry out lectures-presentations on the latest achievements in the field of welding production. The students visit these enterprises with a great interest.

The staff members of the Chair take an active part in the development of international cooperation. In particular, Prof. V.V. Kvasnitsky, Ass. Profs L.A. Zhdanov and A.A. Slivinsky, and the Head of the laboratory A.A. Grinyuk take an active part in the international projects of the Chinese-Ukrainian E.O. Paton Welding Institute. The joint research and educational programs with the Belarusian State University, Otto-von-Guericke University Magdeburg (Germany), Federal University of Uberlandia (Brazil) and organizations of other countries, are actively carried out.

During 80 years the Chair of Welding Production prepared thousands of highly-skilled specialists, who played an important role in development of welding science and production. Our graduates successfully work not only in Ukraine but also in many other countries like Germany, USA, Canada, Russia, Australia, New Zealand and Israel.

Students of the Chair in its history. Many glorious pages to the history of the Chair were written down by its students. They worked actively in the student construction brigades in Tyumen, Sakhalin and other regions of the former Soviet Union and also in Czech Republic.

In 1985–1987, the specialized student brigades of the Chair participated in the large-scale scientific and technical experiment on the construction of pipelines of polyethylene pipes for gasification and water supply of towns of Novoodessa district of Nikolaev (Ukraine) region. This was a good example of fruitful cooperation of the Chair with the PWI, when the students under the supervision of teachers participated in the implementation of developments of the scientists.

The students of the Chair participate constantly in the Ukrainian student competitions on welding and occupy the first and prize places in the individual and team standings. The master and postgraduate students deliver papers at the annual scientific conferences. In 2010, our team occupied a prize place at the All-Ukrainian engineering competitions and represented Ukraine at the European competitions. The Chair was always famous by its activists, who participated in organization of the Faculty Days — edition of the multi-issue student newspaper, organization of broadcasting in our building, creation of the student library of several thousand books on welding. The students of the Chair contribute to the victories of sport teams of the Faculty in football, basketball, shaping and achieve high results in individual sports like track-and-field

athletics, wrestling, boxing, gymnastics, weightlifting, sport archery. The best students of the Chair as to the results of study, research and social works receive scholarships of Evgeny O. Paton and Boris E. Paton, as well as scholarships of the Rector of NTUU «KPI» and the mayor of Kiev.

At different times many foreign students from China, Iran, Vietnam, Cuba, Poland, Hungary, Bulgaria and other countries studied at the Chair. Our Ukrainian students in their turn have an opportunity to study abroad. We have a double diploma programs with Otto-von-Guericke University Magdeburg and the Federal University of Uberlandia. More than a dozen of our students have already received the master diplomas of Ukrainian and German sample, as well as Ukrainian and Brazilian sample. In the recent years the staff members of the Chair were essentially renewed. It was joined by young and perspective personnel. Over the last 10 years the staff members of the Chair defended 6 theses for Cand. of Tech. Sci. Degree, and at the present time most of the teachers are the associate professors of the Chair. The Chair is headed by Prof. V.V. Kvasnitsky.

Participation of the Chair in development of defense industry of Ukraine. From the moment of foundation of the Chair its staff members under the supervision of Evgeny O. Paton took an active part in the work on defense subjects. The graduates of the Chair worked in the defense industry and contribution of welders to creation of tank and other machinery in 1941–1945 is well-known. Such assistance has become urgent as well in our days.

Since September, 2014, the initiative group of the staff members and students of the Welding Faculty under the supervision of Dr. A.A. Slivinsky (students A. Suprun, E. Bilytsky, post-graduate student A. Bogach, staff member S. Nestulya, Ass. Prof. L. Zhdanov et al.) is carrying out works on manufacture and assembly of protective anti-cumulative screens for armored vehicles of the ATO forces.

Due to cooperation with the Central Research Institute of Armament and Military Equipment of the Armed Forces of Ukraine into the design of screens and technology of their manufacture a number of improvements was introduced. The screens successfully passed ballistic tests at the site of the Ministry of Defence of Ukraine. The application for a patent was drawn up and the works on adoption of the screens of the given type for the armament are carried out. Today by the efforts of students a single production in the mechanical workshop of the Welding Faculty was developed into a serial production of screens at one of the enterprises of Kiev. At the moment, the Faculty carries out a complete design and technological support of the screens manufacture, a set of technical documentation on the screens for the main models of light-armoured vehicles of the AFU — BTR-80 and BMP-2 was developed.

Assembly of anti-cumulative screens on armored personnel carrier BTR-80 of the Armed Forces of Ukraine in the ATO zone by the Chair staff members

During combat missions of the AFU, under the enemy fire, due to anti-cumulative screens mounted on armoured vehicles the lives of many military men were saved. The staff members of the Chair received official thanks from the AFU command.

By the specialists of the Welding Faculty the protective screens were manufactured and installed on armored vehicles of the mobile units of special operation forces of Ukraine. The cooperation with the Ukrainian defense enterprises on working out the technological recommendations on welding of armor steels of foreign production and vibration processing of welded armor structures was arranged.

At the present time the further investigations on the processing of working elements of the screens are carried out to improve the effectiveness of protection and guarantee the destruction of the warhead of anti-tank ammunition.

The staff members of the Chair of Welding Production of the National Technical University of Ukraine «Kiev Polytechnic Institute» celebrate the 80th anniversary, being fully resolved to conduct a high-level preparation of welding specialists for the independent state of Ukraine.

S.K. Fomichev, V.P. Bojko,
V.V. Kvasnitsky, L.A. Zhdanov,
A.A. Slivinsky,
V.L. Kovalenko, NTTU «KPI»

STRUCTURE AND PROPERTIES OF WELD METAL MODIFIED BY NANOOXIDES

V.D. KUZNETSOV and **D.V. STEPANOV**
NTTU «Kiev Polytechnic Institute»
37 Pobeda Ave., 03056, Kiev, Ukraine. E-mail: v.kuznetsov@kpi.ua

Given are the results of investigation of structure and properties of weld metals at introduction of nanooxide powders into weld pool. It is shown that portion of nanooxides, being introduced in the weld pool, should not exceed 0.5 % in a range of recommended modes of welding of low-alloy steels. It is determined that nanooxides introduction results in formation of mainly non-metallic inclusions in nanosize range of 0.07–0.13 μm as well as in 0.3–0.8 μm range. At that increased content of carbon, titanium, oxygen, aluminum and manganese are observed in them in comparison to reference welds. It is shown that introduction of 0.5 % titanium nanooxide reduces content of brittle constituents of the structure and content of acicular ferrite rises to 40 %, that results in 2 times increase of impact toughness together with simultaneous increase of yield strength. It is shown that modifying of weld metal by titanium and aluminum nanooxides reduces solidification interval, that can indicate their effect as 2nd type inoculants. 15 Ref., 3 Tables, 6 Figures.

Keywords: *weld, low-alloy steel, nanopowder, nanooxides, structure, non-metallic inclusions, mechanical properties, solidification interval*

Analysis of investigations and publications of recent years indicates a role of non-metallic inclusions (NMI) as factor for regulation of structure and properties of cast metal. It is shown [1, 2] that inclusions engineering can be used for steel microstructure optimizing. Inclusions (oxides, sulfides, carbides) of <1 μm size, promoting nucleation of acicular ferrite (AF), are referred to a separate group due to their small size, and they are called dispersoids having no negative effect on reduction of mechanical properties, but determining the conditions of metal microstructure formation.

Works [3–6] studied effect of NMI size on heterogeneous nucleation of AF structure as well as content and peculiarities of distribution of NMI in presence of aluminum oxides, titanium oxides and nitrides.

Systematic researches in this direction were made by staff members of the E.O. Paton Electric Welding Institute. Works [7–13] experimentally studied and theoretically grounded effect of carbides, nitrides and oxides on level of AF formation and increase of mechanical properties of weld metal of low-alloy steels.

Peculiarity of works indicated above is study of role of NMI, including of nanosize range, being formed in weld metal at corresponding changes of concentration of introduced elements and their reactions with oxides, nitrides, carbides formation, as well as when not more than 1 μm size elements are introduced via charge of flux-cored wire and in form of nanosize powder inoculants.

Development of works in this direction requires accumulation and analysis of experimental data applicable to range of low-alloy steels as well as schemes of introduction of nanosize particles in the weld pool.

Aim of this work is investigation of effect of NMI on structure and properties of weld metals at direct introduction of nanooxide powders in the weld pool.

Investigations for detection of general dependencies were carried out in welding of low-alloy steels 09G2S and 10G2FB with Sv-10KhGN2SMFTYu wire as well as steel A-514 (18GSKhNF) with Sv-09G2S wire. In all the cases welding was performed in Ar + 28 % CO_2 gas mixture at 12.3 kJ/cm heat input.

Nanocomponents were introduced in the weld pool in form of addition alloy after pressing and baking of homogeneous mixture of iron powder of 40 μm fraction and nanosize powders of aluminum or titanium oxides (27–41 nm) with set volume relationship.

Prepared addition alloy was used as consumable electrode of set length and diameter, embeded in a groove along the butt length before welding [14]. In this case effect of processes, related with passing of nanopowders via arc, was eliminated.

Examination of structure and NMI were carried out by methods of optical and electron microscopy using Neophot-30 microscope, electron scanning microscope JSM 35CF with attachment for local X-ray analysis INCA Energy 350 as well

as computer programs developed at the E.O. Paton Electric Welding Institute for analysis of microstructure constituents and distribution of NMI by size and composition. Thermal-physical characteristics of cast metal were investigated using NETZSCH thermal analyzers DSK 404F1.

Investigations showed that amount of nanopowder introduced in the weld pool results in change of amount of NMI in the weld metal.

Dependence of general volume fraction of NMI on content of aluminum nanooxides in the weld are given in Figure 1.

If NMI fraction in the reference weld makes 0.45 % then introduction in the weld pool of nanopowder of aluminum oxide in 0.5 % amount promotes for rapid increase of fraction of NMI to 0.65 %. Introduction of aluminum oxide nanopowder in 0.5–2.5 vol.% range does not have significant effect on volume fraction of NMI. Further growth to more than 2.5 % of nanopowder results in rise of NMI volume fraction from 0.70 to 0.86 %.

However, results of evaluation of structural changes for indicated range of introduced nanopowders showed that exceed of volume fraction above 0.5 % is not accompanied by significant structural changes.

Figure 2 for example shows structure of weld metal in welding of 09G2S steel for indicated range of changes of volume fraction of aluminum oxide nanopowder.

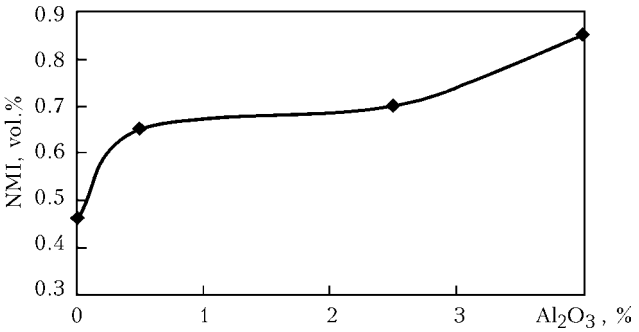

Figure 1. Dependence of NMI volume fraction on content of aluminum nanooxides in weld metal in welding of steel 09G2S using Sv-0KhGN2SMFTYu wire

Formation of structure, the main constituents of which are precipitation of polygonal ferrite, acicular and lamellar ones with ordered and disordered secondary phases, takes place in the weld metal under initial conditions. The peculiarity of this structure is presence of coarse constituents of indicated morphological forms of ferrite (Figure 2, *a*). Microhardness of constituents changes from *HV* 145 to *HV* 187.

Microstructure of weld metal with addition of Al_2O_3 nanopowder in 0.5 % amount has refined dispersed structure mainly consisting of upper bainite, partially lower and acicular ferrite (Figure 2, *b*). Microhardness of constituents changes from *HV* 264 to *HV* 304.

Weld metal with addition of Al_2O_3 nanopowder in amount of 2.5 % volume fraction has microstructure of intra-granular ferrite and ferrite with ordered and disordered secondary phases

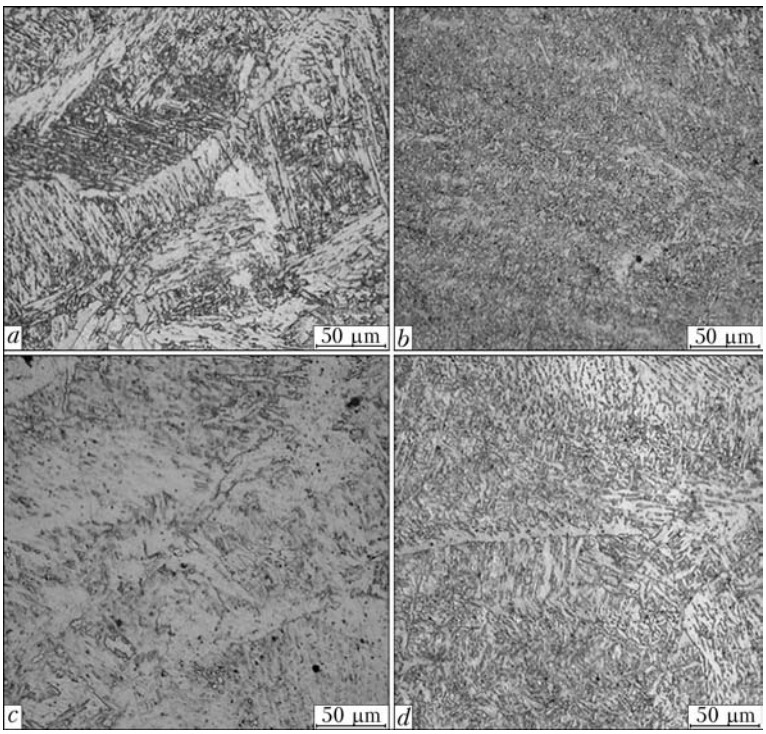

Figure 2. Microstructure of reference weld (*a*) and weld with addition of nanopowder Al_2O_3 in amount of 0.5 (*b*), 2.5 (*c*) and 4.5 (*d*) %

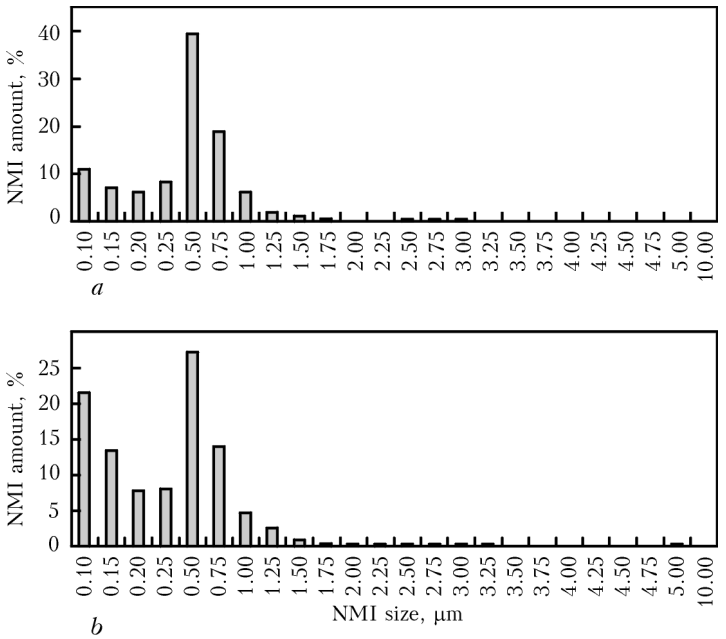

Figure 3. Histogram of NMI distribution by size: *a* — in reference weld; *b* — in weld with addition of aluminum oxide in 0.5 % amount

(Figure 2, *c*). Microhardness of constituents virtually does not change and stays in *HV* 180–189 limits.

Addition of Al_2O_3 nanopowder in amount of 4.5 % results in formation in the structure of intra-granular ferrite with precipitates of AF and ferrite with ordered secondary phases (Figure 2, *d*). Microhardness of constituents changes from *HV* 188 to *HV* 236.

It can be concluded that the main role in formation of structure with increased strength and toughness properties plays nanooxides being introduced only in small amount (0.5 %), and increase of their concentration, apparently, promotes for coagulation and coalescence with NMI of material during solidification of the weld pool and has no significant effect on structure formation.

In fact, computer processing of results of distribution of NMI by size allowed selecting three size ranges from total data array, i.e. inclusions of to 0.3 μm, from 0.3 to 0.8 μm and more than 0.8 μm.

The peculiarity of NMI in the weld metal is their smaller size range at nanooxides introduction into the weld pool (Figure 3).

Thus, if from 5 to 10 inclusions of the reference weld fall for 0.10–0.25 μm and from 5 to 40 inclusions for 0.5–1 μm size range, then in the case of nanooxide introduction the first range covers from 8 to 22 inclusions and the second from 5 to 27 inclusions.

Found dependencies are also verified by the results of processing of size of only spherical inclusions by index of diameter of equivalent circumference. For example, Figure 4 gives the hystograms on volume content and distribution of such inclusions in the weld metal for initial state and with inclusion of nanooxides.

The main part of spherical inclusions from 4 to 6 % falls for the range of up to 0.3 μm size as well as for the ranges of 0.3–0.8 μm and more in the initial state without addition of nanopowder oxide. At that, up to 9 % precipitation of particles of 0.31–0.37 μm size are observed (Figure 4, *a*).

Addition of TiO_2 nanopowder in 0.5 vol.% amount promotes for rise from 6 to 14 % of part of spherical inclusions of 0.3 μm as well as 0.30–0.55 μm size. At that, no inclusion of more than 0.8 μm size can be virtually observed (Figure 4, *b*).

Results of local spectral analysis of chemical composition of the inclusions showed that significant increase of carbon, oxygen, aluminum, sulfur, titanium, manganese concentration is observed in each of them independent on size. This is particularly obvious for carbon, oxygen and sulfur (several orders).

Introduction of nanooxides, in keeping the general pattern on content of indicated elements, somewhat changes it to the side of larger content of oxygen, aluminum and titanium, that indicates presence of oxides of these elements in the inclusions.

Analysis of triple diagrams of oxides of SiO_2–Al_2O_3–MnO and TiO_2–Al_2O_3–MnO systems for the most typical range of inclusion size 0.3–0.8 μm also verifies increased content of Al_2O_3 and TiO_2 oxides (Figure 5).

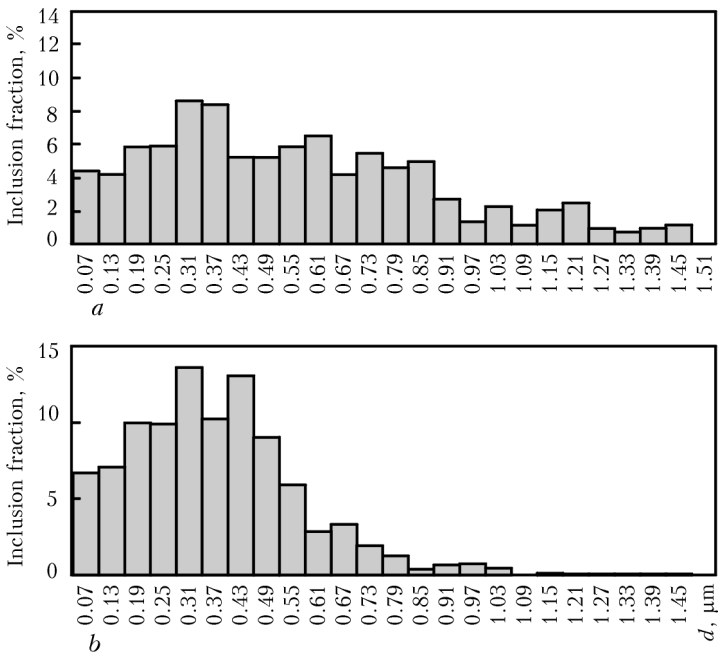

Figure 4. Histogram of distribution of inclusions in weld metal by diameter of equivalent circumference d: a — in initial condition; b — weld with 0.5 vol.% TiO_2 nanooxide in welding of 10G2FB steel

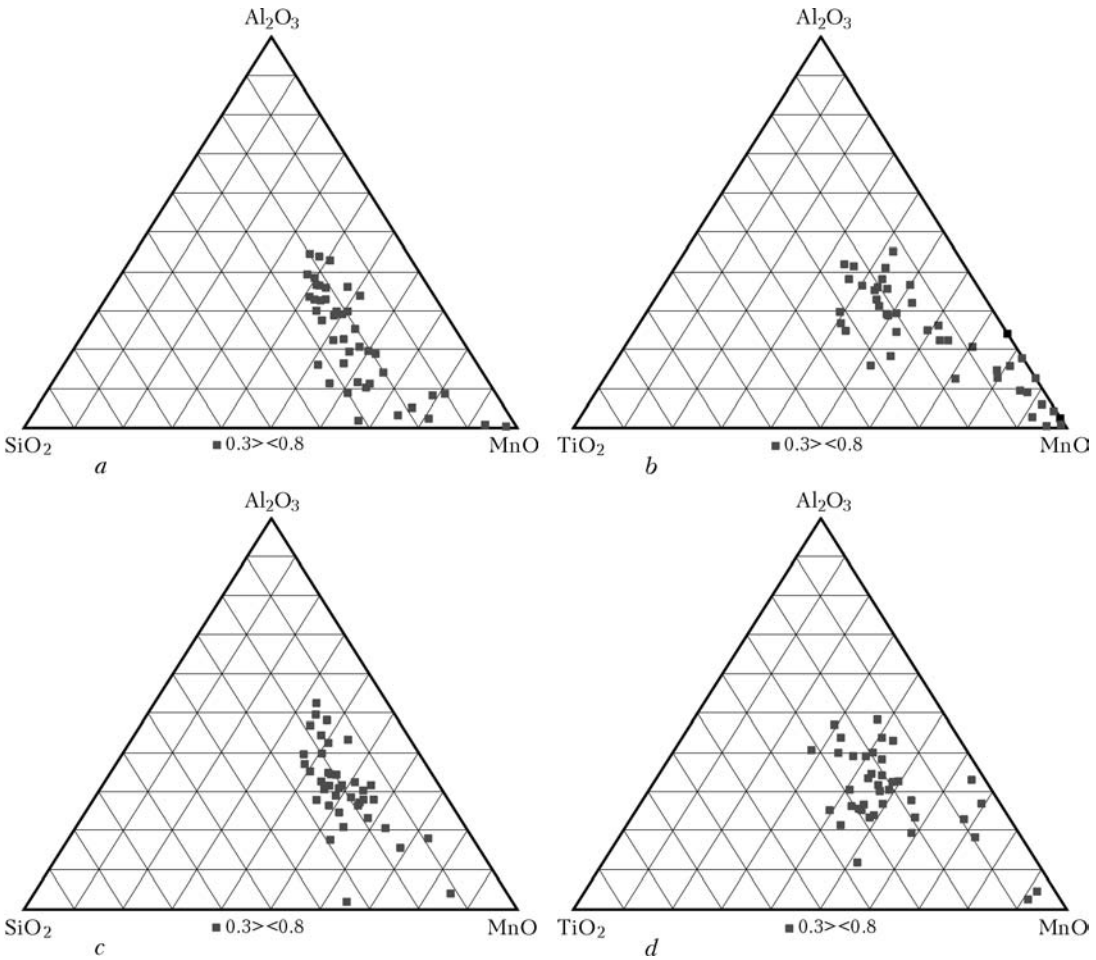

Figure 5. Triple diagrams of oxides of SiO_2–Al_2O_3–MnO and TiO_2–Al_2O_3–MnO system: a, b — reference weld; c, d — weld with 0.5 % TiO_2

Table 1. Typical morphological forms of ferrite in weld metal structures

Studied weld	Constituents of microstructure of weld metal, %					
	BF	LF	AF	UB	LB	WF
Reference weld without nanooxides	Up to 10	10–20	Up to 10	20–40	20–40	Up to 35
Weld with 0.5 % TiO_2 nanooxide	Up to 10	Up to 10	20–40	10–20	10–15	Up to 15

Thus, if significant part of inclusions of one as well as another systems in the reference weld contains from 50 to 90 % MnO, up to 40 % of Al_2O_3 and to 20 % TiO_2 (Figure 5, *a*, *b*), then introduction in the weld pool of 0.5 % TiO_2 provides for high MnO concentration only in separate inclusions, and presence of Al_2O_3 as well as TiO_2 in the inclusions exceeds to 55 and 40 %, respectively (Figure 5, *c*, *d*).

Thus, complex analysis of inclusions indicates significant difference in their sizes, distribution density and content in metallic matrix at nanooxide introduction, which has effect on weld metal structure.

In fact, results of metallographic analysis determined that the most wide-spread morphological forms of ferrite in the weld metal structure are block ferrite (BF), lamellar ferrite (LF), intra-granular AF, Widmanstatten ferrite (WF), upper (UB) and lower bainite (LB). Percent content of each of forms in the investigated welds in welding of 10G2FB steel is given in Table 1.

Initial structure of welds is characterized by increased content of brittle constituents (BF, WF, UB) and formation of AF to 10% with high coefficient of shape (L/B of 4–7) and aciculars of up to 20 μm length.

Microstructure of weld metal has sufficiently high content of intra-granular polygonal ferrite with precipitation along the boundaries of grains of xenomorphic ferrite (Figure 6, *a–c*). Welds with such structure are characterized by low level of toughness and ductility of metal. Values of microhardness of structural constituents vary from *HV* 231 to *HV* 253.

Weld metal structure with TiO_2 in 0.5 % amount is characterized by reduced content of brittle constituents (BF, WF, UB) and increased AF content to 40 % with more favorable coefficient of shape (L/B of 3–5) and aciculars' length to 5 μm in comparison with reference structure (Figure 6, *d–f*).

Welds with such structure are characterized by combination of sufficiently high level of indices of toughness, ductility and strength. The

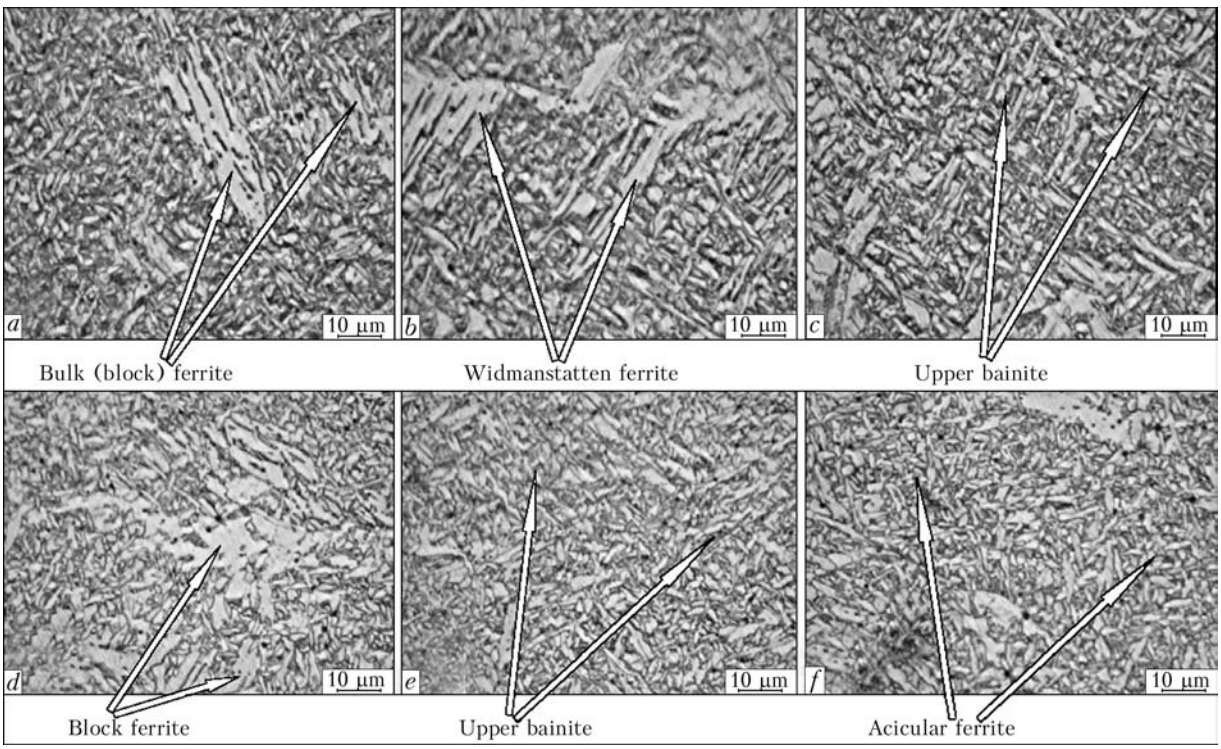

Figure 6. Typical structure of weld metal without nanooxides (*a–c*) and with 0.5 vol.% TiO_2 (*d–f*)

Table 2. Results of mechanical tests of weld metal in welding of A-514 (18GSKhNF) steel using 09G2S wire

Studied metal	Yield strength σ_y, MPa	Tensile strength σ_t, MPa	Relative elongation, %	Reduction in area, %	Impact toughness KVC, kJ/m^2
Without nanopowders	357	542	21	61	4.6
With TiO_2 nanooxide in 0.5 % amount	514	647	18	54	9.3

measurements show that microhardness of structural constituents varied from HV 230 to HV 250.

Thus, introduction of nanooxides, in particular titanium, in the weld pool results in positive structural changes from the point of view of formation of tough morphological forms of ferrite, that promotes for increase of weld metal mechanical properties (Table 2).

As follows from data of Table 2, increase of yield strength for 157 MPa and strength for 105 MPa is observed at introduction of titanium nanooxides in the weld pool. At that, impact toughness also increases 2 times. Thus, the common point, independent on grade of investigated low-alloy steel and type of introduced nanooxides, is change of size, distribution density, composition of the inclusions as well as their positive effect on structure and mechanical properties of weld metal.

Role of introduced nanooxides in structure-forming is also shown by data of thermograms of differential scanning calorimetry. The investigations found the differences in melting temperatures as well as in solidification of metal modified by nanooxides (Table 3).

The general dependence is some reduction of weld metal melting temperature at nanooxides introduction. It is the well-known fact that nanostructural materials differ by significantly lower melting temperature [15], therefore, some reduction of liquidus temperature can be related with presence of nanooxides in the weld metal. Reduction of melting temperature is developed in different ways for titanium and aluminum oxides. Thus, if melting temperature of the reference metal is 1543.4 °C, then its reduction to 1535.8 °C is observed at introduction of 0.5 % TiO_2 and to a greater extent, i.e. 1522.5 °C, at 1 % Al_2O_3.

At the same time, increase of solidification temperature of weld metal, modified by nanooxides, except for 1 % Al_2O_3, is observed. At that, the general dependence is in reduction of interval of solidification of modified metal, independent on investigated range of changes of volume fraction of introduced nanooxides.

Thus, it makes 43.9 °C for the reference metal, then observed reduction for the investigated range of changes of each of nanooxides is virtually

Table 3. Thermal-physical characteristics of weld metal

Metal content	T_L, °C	T_S, °C	ΔT, °C
Reference	1543.4	1499.5	43.9
0.5 % TiO_2	1535.8	1524	11.8
1 % TiO_2	1540.6	1527.7	12.9
0.5 % Al_2O_3	1541.9	1518.6	23.3
1 % Al_2O_3	1522.5	1499	23.5

Note. T_S — solidus temperature; T_L — liquidus temperature; ΔT — solidification interval.

the same and it is ΔT = 23.3 °C for aluminum oxide and ΔT = 11.8 °C for titanium oxide.

It can be concluded based on this that effect of nanooxides can be observed already in solidification stage, that changes its conditions to the side of quicker propagation, may be as a consequence of appearance of additional centers of nucleus formation on the inclusions, i.e. their effect as 2nd type inoculants.

This stage of investigations does not allow determining one-valued role of nanooxides in mechanism of regulation of weld metal structure formation. They also can play a role of 3rd type inoculants. In the melt they can draw heat for own heating and reduce melt temperature under certain conditions of melting, that results in growth of solidification rate. Besides, as it was determined in works of the E.O. Paton Electric Welding Institute, their effect can also be observed at the second stage of the secondary solidification effecting austenite transformation resistance.

Accumulation and analysis of experimental data in this direction allows outlining the most significant sides of NMI effect, including for nanosize range, on weld structure formation.

Conclusion

It is shown that increase from 0.5 to 4.5 % of volume fraction of nanooxides introduced in the weld pool results in increase from 0.46 to 0.87 of general NMI portion in the weld metal, at that significant structural changes take place at introduction of nanooxide, volume fraction of which does not exceede 0.5 %. Typical in this case is increase of fraction of inclusions of small

size range 0.07–0.50 μm. Inclusions in the weld metal modified by nanooxides have increased content of oxygen, aluminum and titanium, that indicates their prime composition from oxides of these elements.

Introduction of titanium nanooxide promotes for reduction of brittle constituents of ferrite and increase of content of acicular ferrite. This results in increase of mechanical properties of the weld metal, in particular impact toughness. Introduction of nanooxides reduces weld metal solidification range, that can indicate their effect as 2nd type inoculants.

1. Takamura, J., Mizoguchi, S. (1990) Roles of oxides in steels performance — Metallurgy of oxides in steels. In: *Proc. of 6th Int. Iron and Steel Conf.* (Tokyo, Japan, 1990), Vol. 1, 591–597.
2. Grong, O., Kolbeinsen, L., van der Eijk, C. et al. (2006) Microstructure control of steels through dispersoid metallurgy using novel grain refining alloys. *ISIJ Int.*, **46**, 824–831.
3. Lee, T.K., Kim, H.J., Kang, B.Y. et al. (2000) Effect of inclusion size on the nucleation of acicular ferrite in welds. *Ibid.*, **40**, 1260–1268.
4. Yamamoto, K., Hasegawa, T., Takamura, J. (1996) Effect of boron on intra-granular ferrite formation in Ti-oxide bearing steel. *Ibid.*, **36**, 80–86.
5. Vanovsek, W., Bernhard, C., Fiedler, M. et al. (2013) Influence of aluminium content on the characterization of microstructure and inclusions in high-strength steel welds. *Welding in the World*, Issue 1, **57**, 73–83.
6. Seo, J.S., Kim, H.L., Lee, C. (2013) Effect of Ti addition on weld microstructure and inclusion characteristics of bainitic GMA welds. *ISIJ Int.*, 53**(5)**, 880–886.
7. Golovko, V.V., Grigorenko, G.M., Kostin, V.A. (2011) Influence of nanoinclusions on formation of weld metal structure of ferritic-bainitic steels (Review). *Zbirnyk Nauk. Prats NUK*, **4**, 42–49.
8. Pokhodnya, I.K., Golovko, V.V., Stepanyuk, S.M. et al. (2012) Study of effect of titanium nanocarbides on formation of microstructure and properties of weld. *FKhMM*, **6**, 68–75.
9. Golovko, V.V., Stepanyuk, S.M., Ermolenko, D.Yu. (2012) Study of influence of nanoformation in metal on microstructure formation of weld and its mechanical properties. In: *Transact. on Building, materials science, machine-building*, Issue 64, 155–159.
10. Golovko, V.V., Pokhodnya, I.K. (2013) Effect of non-metallic inclusions on formation of structure of the weld metal in high-strength low-alloy steels. *The Paton Welding J.*, **6**, 2–10.
11. Golovko, V.V., Stepanyuk, S.N., Ermolenko, D.Yu. (2014) Technology of welding of high-strength low-alloy steels with introduction of titanium-containing inoculants. In: *Nanosized systems and materials in Ukraine*, 395–399. Kiev: Akademperiodika.
12. Golovko, V.V., Stepanyuk, S.M., Ermolenko, D.Yu. (2015) Effect of titanium-containing inoculants on structure and properties of weld metal of high-strength low-alloy steels. *The Paton Welding J.*, **2**, 14–18.
13. Grigorenko, G.M., Kostin, V.A., Golovko, V.V. et al. (2015) Effect of nanopowder inoculants on structure and properties of cast metal of high-strength low-alloy steels. *Sovr. Elektrometallurgiya*, **2**, 32–41.
14. Kuznetsov, V.D., Loboda, P.I., Fomichov, S.K. et al. *Method of electric arc welding with introduction of nanocomponents into weld pool*. Pat. 98985 UA. Int. Cl. B 23K 9/16. Fill. 15.12.14. Publ. 12.05.15.
15. Ragulya, A.V., Skorokhod, V.V. (2007) *Consolidated nanostructural materials*. Kyiv: Naukova Dumka.

Received 21.10.2015

EFFECT OF COOLING MODE AFTER DIFFUSION WELDING AND BRAZING ON RESIDUAL STRESSES IN GRAPHITE–COPPER EDGE JOINTS

V.V. KVASNITSKY[1], **G.V. ERMOLAEV**[2] and **M.V. MATVIENKO**[3]
[1]NTUU «Kiev Polytechnic Institute»
37 Pobeda Ave., 03056, Kiev, Ukraine. E-mail: kvas69@ukr.net
[2]National Shipbuilding University
9 Geroiv Staliningrada Ave., 54025, Nikolaev, Ukraine. E-mail: welding@nuos.edu.ua
[3]Kherson Branch of National Shipbuilding University
44 Ushakov Ave., 73022, Kherson, Ukraine. E-mail: matvienkomv@i.ua

Studied is stress-strain state at different modes of cooling of cylindrical assemblies from graphite and copper in plastic and elastic stages considering short-term plastic deformations as well as creep. Effect of cooling mode on plastic deformations in butt zone and axial stresses on assemblies' surface, determining possibility of fracture of brittle graphite was jound. 7 Ref., 3 Tables, 12 Figures.

Keywords: *diffusion welding, brazing, graphite–copper joint, stress-strain state, cooling modes, residual stresses, mathematical modeling*

Graphite products are used in combination with many metals in current equipment. Graphite having high electric and heat conduction is widely used in development of current-carrying or current-collecting devices of different assemblies and machines, graphitized electrodes, sealing arrangements etc., where joining with metals is necessary. Brazing and diffusion welding [1, 2] are used for that. The general problem for both methods of joining are residual stresses caused by different thermal coefficients of linear expansion (TCLE) of materials to be joined. Residual stresses in ductile materials being joined usually result in degradation of shape and size, and can promote crack formation and fracture in graphite, which is a brittle material.

Metals with close to graphite TCLE are selected for reduction of stresses in metal-graphite assemblies. Many assemblies use titanium, which is not equal to graphite on electric and heat conduction. The best choice for indicated devices is copper, but it has significantly larger TCLE than graphite, that often results in crack formation in graphite after assembly cooling.

Our earlier researches [3, 4] were dedicated to investigation of dependencies of formation of stress and deformation fields in the butt zone in diffusion welding (DW) and brazing of parts from dissimilar materials. This information is necessary for updating assembly structure and production of quality joint. Some general dependencies of formation of residual stresses were received for metal–ceramics joints in bush-to-bush joint assemblies, in which Young's modules of joined materials are equal [5]. But they are an order different in graphite and copper, that can have significant effect on stress-strain state (SSS) of the assembly in their joining. Therefore, investigation of SSS formation in copper-non-metallic assemblies is a relevant task.

Researches of graphite (ceramics)-to-metals joints showed that fracture is initiated by cracks appearing in the butt in non-metallic part [1]. Metal surface after complete fracture includes thin graphite layer as shown in Figure 1.

Aim of the investigation is study of peculiarities of SSS formation in cooling after DW and brazing of metal-graphite assemblies and effect of graphite and copper joining technology on it by computer modeling.

Investigations were carried out by computer modeling method using license software complex ANSYS (vers. 10). Axially symmetric problems

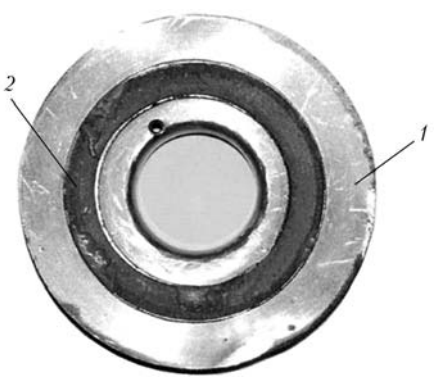

Figure 1. Fracture surface of metal (*1*) to graphite (*2*) joint

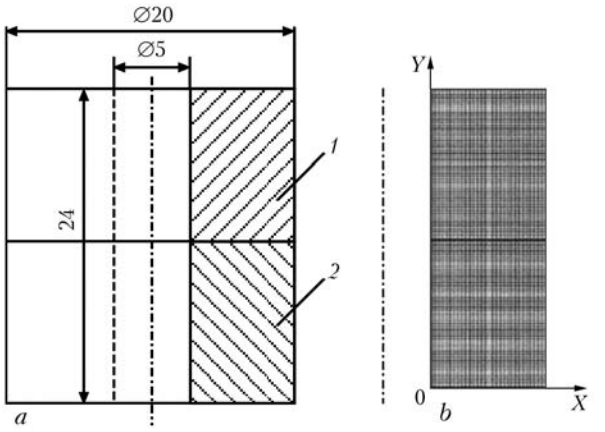

Figure 2. View of B–B assembly (*a*) and its finite element model (*b*): *1* — copper bush; *2* — graphite bush

with finite elements of PLANE 182 type were solved.

Edge joints, which are usually used in current-carrying devices, were taken for investigations. Modeling was carried out for bush-to-bush (B–B) assembly. This model in comparison with bar or cylinder is more informative since has two-side surfaces and being easily transformed in cylinder with inner radius equal zero, and rules of SSS formation in cylinder–cylinder type assemblies are also preserved for bar–bar type assemblies as shown in works [6, 7].

View of B–B assembly and section of its finite element model are shown in Figure 2. This model can be used for joints made by pressure brazing, eliminating brazing metal interlayer due to its small thickness.

Table 1 shows thermal-physical properties of copper and graphite, taken in calculations.

Assembly cooling in 900 to 500 °C range, in which creep resistance has a significant effect on stress relief, was considered for investigation of general dependencies of SSS formation.

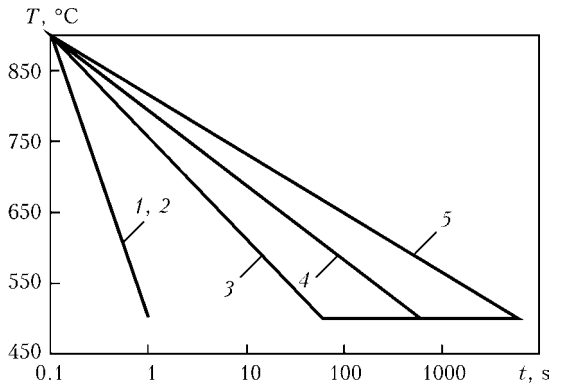

Figure 3. Thermal cycles of cooling for studied five variants (*1–5*)

Modeling was carried out for 5 variants of temperature reduction in indicated interval:

- elastic solution at temperature reduction to 500 °C (variant 1);
- elastic-plastic solution at quick reduction of temperature to 500 °C (variant 2), where creep deformations are negligibly small;
- elastic-plastic solution considering creep at gradual reduction of temperature to 500 °C in course of 60 s and further holding during 6000 s at 500 °C (variant 3);
- elastic-plastic solution considering creep at gradual reduction of temperature to 500 °C during 600 s and further holding at 500 °C up to 6000 s (variant 4);
- elastic-plastic solution considering creep at gradual reduction of temperature to 500 °C during 6000 s (variant 5).

Figure 3 provides for thermal cycles for considered variants.

Copper creep rate in variants 3–5 was determined by equation

$$\dot{\varepsilon} = C_1 \sigma^{C_2} e^{\frac{C_3}{T}},$$

Table 1. Thermal-physical properties of materials joined

Material	Temperature, °C	Young's modulus $E \cdot 10^3$, MPa	Poisson's coefficient	TCLE$\cdot 10^6$, 1/deg	Yield strength, MPA	Strengthening modulus$\cdot 10^3$, MPa
Graphite	20	9.3	0.18	4.8	–	–
	200	9.4		5.0	–	–
	400	9.8		5.1	–	–
	700	10.3		5.5	–	–
	900	10.8		5.7	–	–
Copper	20	125	0.34	16.7	69	1.5
	200	110		17.2	60	1.3
	400	100		17.8	45	0.9
	700	60		19.4	17.3	0.8
	800	40		20.5	11.5	0.7
	900	38		19.8	8.5	0.6

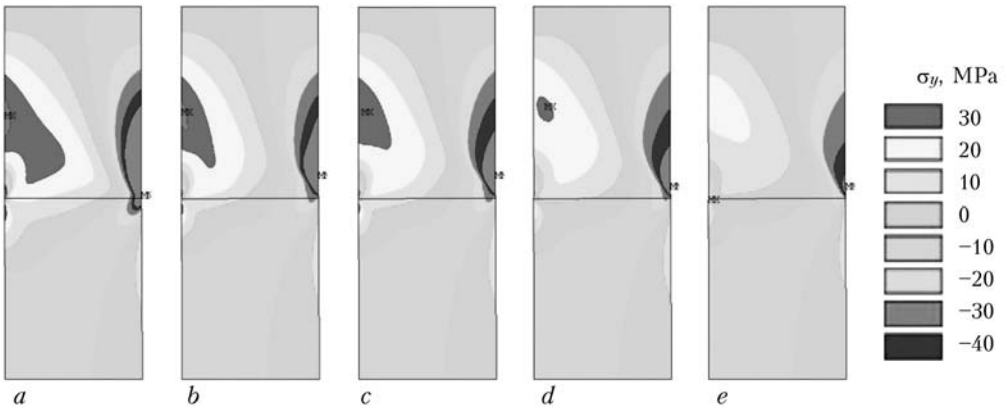

Figure 4. Axial stresses after cooling to 500 °C in variants 1 (*a*), 2 (*b*), 3 (*c*), 4 (*d*) and 5 (*e*)

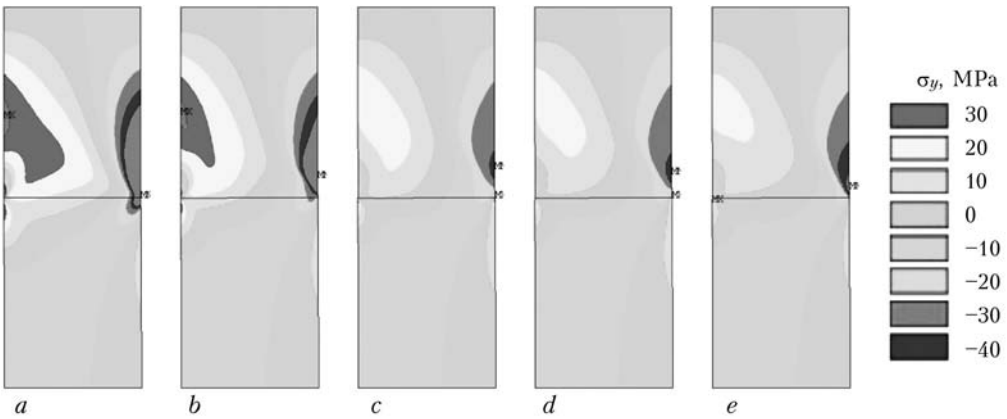

Figure 5. Axial stresses after cooling and holding in variants 1 (*a*), 2 (*b*), 3 (*c*), 4 (*d*) and 5 (*e*)

where $C_1 = 1.67 \cdot 10^{-30}$, $C_2 = 5$, $C_3 = 25872$ are the equation coefficients, received by us experimentally in investigation of copper creep.

Fields and diagrams of distribution of stresses, deformations and movements at different stages of cooling, including the moments of end of temperature reduction (all variants) and end of holding at 500 °C (variants 3 and 4), were analyzed. Further only fields and diagrams of axial stresses are given. They, as shown in work [5], are the main reason of brittle fracture of materials with low TCLE.

Analysis of stress fields for different cooling variants showed that all stress constituents, including equivalent ones, significantly change at cooling rate variation, in particular in copper (Figure 4). Further holding at 500 °C (variants 3 and 4) promotes more changes in them (Figure 5). At that radial, circumferential, tangential and equivalent stresses are concentrated close to the butt, and axial stresses are in internal and external surfaces of the bush.

Plastic deformation are distributed in accordance to stresses, i.e. from copper side in the vicinity to the butt, to the most extent at distance of around 1/4 of bush thickness from its external surface (Figures 6 and 7).

Analysis of fields and values of plastic deformations (Table 2) showed that instantaneous deformations in copper reduce from 1.4 % in variant 1 to zero in variant 5 with increase of cooling time. Creep deformations at temperature reduc-

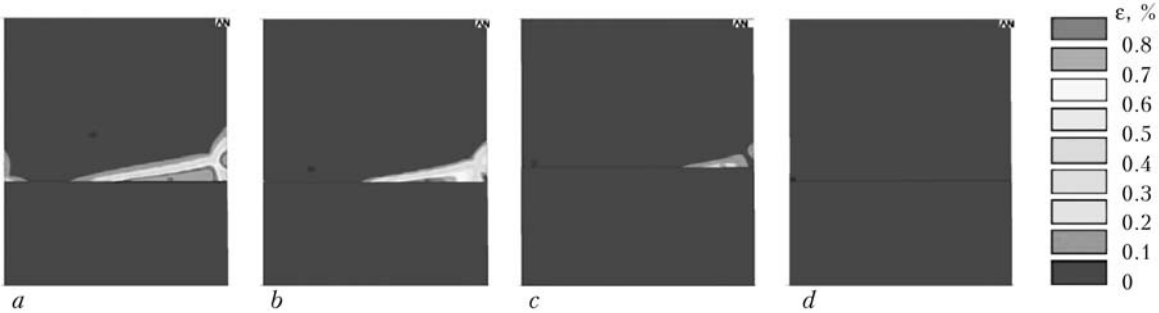

Figure 6. Equivalent deformations of instantaneous plasticity after cooling to 500 °C in variants 2 (*a*), 3 (*b*), 4 (*c*) and 5 (*d*)

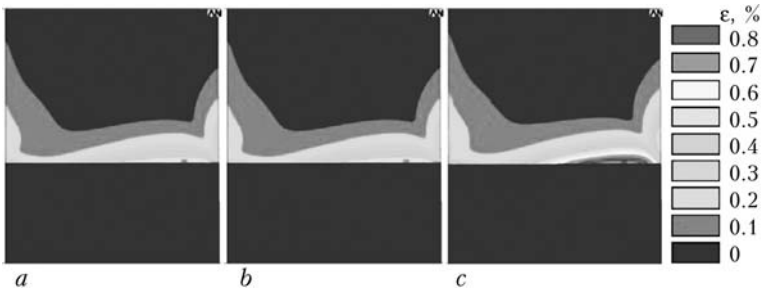

Figure 7. Equivalent creep deformations after cooling and holding in variants 3 (*a*), 4 (*b*) and 5 (*c*)

tion stage, on the contrary, significantly increase with rise of cooling time to 500 °C (from 0.4 % in variant 3 to 1.05 % in variant 5). Total plastic deformations at cooling stage reduce from 1.4 % in variant 2 to 1.05 % in variant 5.

Creep deformations show insignificant rise (0.19 and 0.22 %) in process of holding at constant temperature 500 °C (variants 3 and 4). As a result, total creep deformations for the whole period of cooling and holding at 500 °C increase with rise of cooling time and corresponding decrease of time of holding from 0 (variant 2) to 1.05 % (variant 5), whereas sum ones (instantaneous and plastic) reduce from 1.4 % (variant 2) to 1.05 % (variant 5).

Thus, increase of cooling rate is more efficient than increase of time of holding after temperature decrease from the point of view of development of short-term plastic deformations in copper. And, vice versa, slow cooling is more efficient from the point of creep deformations.

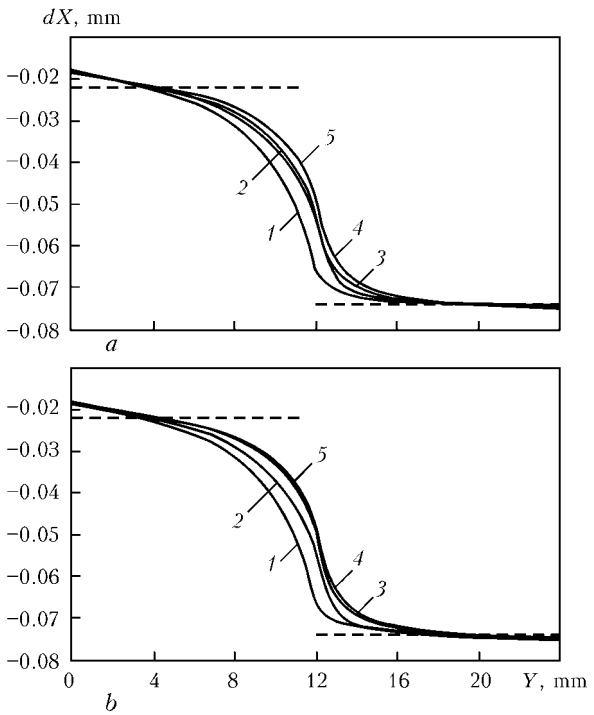

Figure 8. Diagrams of radial movements of points of bush external surface after cooling to 500 °C (*a*) and after cooling and holding (*b*) for variants 1–5 (*1–5*)

Nature of fields of short-term and creep plastic deformations are also distinguished (Figures 6 and 7). The short-term deformations are mostly concentrated close to the butt in its part adjacent to the external surface (Figure 6). The creep deformations cover all butt area at distance comparable with bush thickness (Figure 7). At that, they significantly reduce (Figures 6, *b* and 7, *a*) in process of long-term holding at 500 °C (variant 3).

Effect of plastic deformations in copper on axial stresses appearing on graphite side surface is caused by two mechanisms. On the one hand, in accordance with the general principles of mechanics, plastic deformation of copper provides for reduction of level of stresses in it and, respectively, preserve assembly equilibrium conditions in graphite. On the other hand, they effect bend shape of generatrix, which also influences the level and nature of stress distribution in copper [5]. Nature of this effect is ambiguous. Plastic deformations in copper can increase as well as reduce surface curvature, respectively increasing or reducing stress level.

Elastic and plastic deformation of bush material result in change of its surface shape. Analysis of diagrams of radial movements of points of external surface showed (Figure 8) that the nature of generatrix bending is almost kept the same, as at equal rigidity of materials being joined [5]. However, their skew-symmetries relatively to butt plane at elastic loading (variant 1) are significantly violated. The generatrix from the side

Table 2. Maximum plastic (equivalent) deformations in copper, %

Variant	End of cooling			End of holding	Sum
	Instantaneous deformations	Creep deformations	Sum	Creep deformations	
2	1.40	0	1.40	0	1.40
3	0.90	0.40	1.30	0.59	1.49
4	0.23	0.75	0.98	0.97	1.21
5	0	1.05	1.05	1.05	1.05

of more rigid material (copper) shows less bending, approaching to free contraction state (see dashed line in Figure 8). The situation is opposite and the bend is significantly increased from the side of less rigid material (graphite).

Bend in more rigid, but ductile material (copper) increases and that in less rigid elastic material (graphite) reduces, shape of bend of the generatrix approaches to symmetric one in appearance of plastic instantaneous and creep deformations (variants 2–5). In other words, the short-term plastic deformations, developing at quick cooling, and creep deformations (variants 3–5) compensate higher rigidity of copper in elastic state in comparison with graphite and equalize deformations of external surface in the butt region.

At that, the diagrams of radial movements of points of external surface after cooling and holding are virtually matched in variants 3–5 regardless some differences in value of maximum plastic deformations in copper (see Table 2).

Nature of radial movement of the points of internal side surface is more complex (Figure 9). A convex part of the graphite surface (material with lower TCLE) in immediate proximity to the butt (1–2 mm) gradually passes into a concave one with the removal from it. The situation is different in copper (material with larger TCLE), in which concave surface close to the butt gradually passes into a convex one with the removal from it.

Such a complex bend shape of the generatrix on internal surface of the bush is explained in work [5] by oncoming effect of two factors. On the one hand, this is a difference of mutual shift of upper and lower parts of the bush due to different change of their diameters, and, on the other hand, it is various change of section width at temperature contraction of materials of upper (metal) and lower (graphite) parts of the assembly.

Mutual shift of upper and lower parts of the bushes results in formation of convexity on the external and concavity on the internal surface of material with lower TCLE (graphite). Different change of width results in formation of convexity on the both sides of this material. As a consequence of simultaneous effect of both factors a nature of bend of the external surface, i.e. outside convexity, is preserved and the internal one being significantly changed.

Presence (effect) of two mechanisms of movement is also verified by absence of symmetry of the fields of plastic deformations and diagrams of tangential stresses relatively to middle of the bush thickness. Quantitative characteristic of effect of shift of the bush parts can be a level of

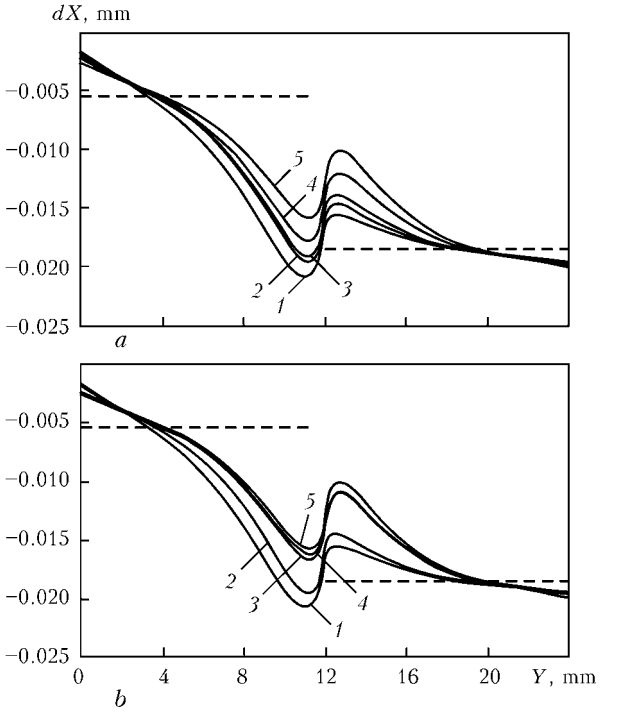

Figure 9. Diagrams of radial movements of points of bush internal surface after cooling to 500 °C (*a*) and after complete cooling and holding (*b*) for variants 1–5 (*1–5*)

tangential stresses in the middle of bush thickness (around 20 MPa).

Nature of bend of the internal surface is preserved at change of cooling rate, but value of movement is reduced at decrease of cooling rate (variants 3–5). Difference in movements is reduced at further holding (see Figure 9).

Axial stresses are distributed in accordance with surface deformation (Figures 10 and 11). They are compressive on the external surface in upper copper bush (with larger TCLE) and tensile ones in graphite lower part (with lower TCLE) (see Figures 4, 5 and 10).

After cooling tensile stresses for all variants reach maximum value (around 14 MPa) close to the butt (at 2–3 mm distance), and show gradual 2 times reduction at approaching to it (Figure 10, *a*). Further holding at 500 °C in variants 3 and 4, when creep deformations are added to short-term deformations, results in the fact that maximum stresses in graphite near the butt, on the contrary, rapidly increase to 30–35 MPa (Figure 10, *b*) and maximum point is right up to the butt.

The distribution is much more complex (see Figure 11) on the internal surface. Axial stresses in the lower graphite bush are of the tensile nature, they reduce to the zero step-by-step (at 2–3 mm distance from the butt) and transform in the compressive ones at removal from the joint, and then they again reduce to the zero at the edge.

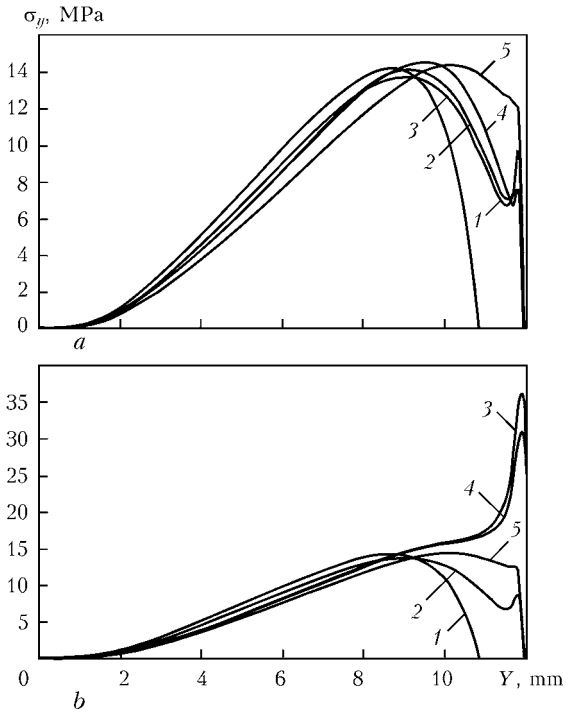

Figure 10. Diagrams of axial stresses on external surface of graphite after cooling (*a*) and after cooling and holding at 500 °C (*b*) for models 1–5 (*1–5*)

Table 3 and Figure 12 for convenience of comparison of the variants provide for the values and diagrams of maximum tensile stresses in graphite after cooling to 500 °C and holding at this temperature during 6000 s.

Analysis of the Table and Figures show that the internal surface is exposed to the most danger

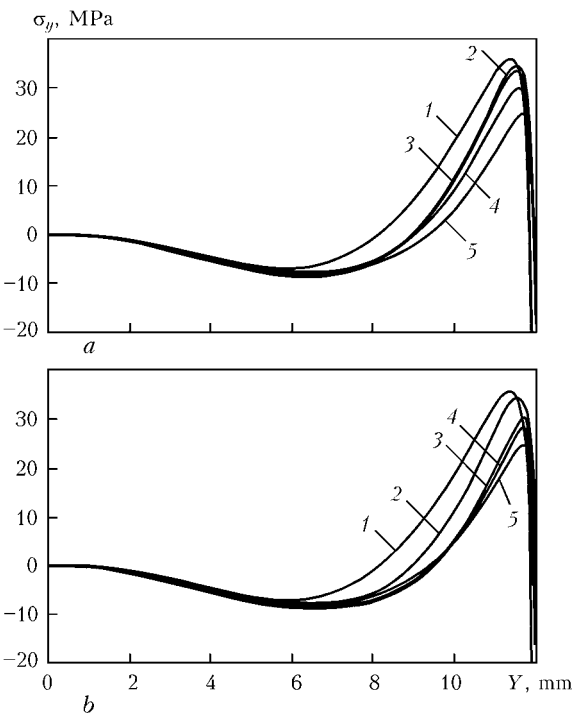

Figure 11. Diagrams of axial stresses on internal surface of graphite after cooling (*a*) and after cooling and holding at 500 °C (*b*) for models 1–5 (*1–5*)

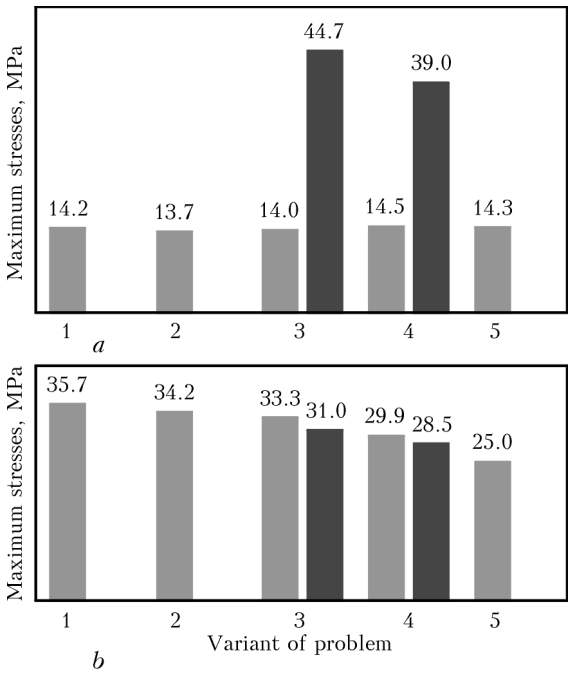

Figure 12. Maximum tensile stresses on external (*a*) and internal (*b*) surfaces of graphite in variants 1–5 after cooling to 500 °C and holding at this temperature (variants 3 and 4)

from the point of view of crack formation in graphite after cooling. At that, for all variants except for variant 5, the maximum tensile stresses reach bending strength of graphite (45 MPa for MPG-8 graphite and 34.3 MPa for MPG-6 and MPG-7 graphite). Variants 3 and 4 are dangerous for the external surface. Using them holding after cooling will result in larger tensile stresses.

Thus, the optimum, from the point of view of reduction of danger of crack formation in graphite after cooling to 500 °C, shall be variant 5 (gradual reduction of temperature from 900 to 500 °C during 6000 s) at which tensile stresses do not exceed 25 MPa.

Variants with quick cooling and further holding are not reasonable, since large stresses are developed on the external surface of graphite at them.

Further cooling of the assembly to 20 °C takes place under conditions of growth of yield point

Table 3. Maximum tensile stresses in graphite, MPa

Variant	On external surface		On internal surface	
	End of cooling	End of holding	End of cooling	End of holding
1	14.2	–	35.7	–
2	13.7	–	34.2	–
3	14.0	44.7	33.3	31.0
4	14.5	39.0	29.9	28.5
5	14.3	14.3	25.0	25.0

and creep resistance. Creep rate reduces and residual stresses exceed graphite strength limit (more than 65 MPa) even in cooling from 500 to 20 °C during 3.8 h.

Thus, regardless the effective influence of deformations of instantaneous plasticity and creep in 900–500 °C temperature interval, application of DW or brazing of copper (silver) braze alloys can result in assembly fracture.

Sufficiently high temperatures of DW are to be noted when considering technological variants of graphite-to-copper joining. Work [2] investigates three variants of graphite-titanium DW, namely with nickel interlayer of 10–30 μm thickness deposited on graphite by galvanic method, with nickel foil of 10 μm thickness, and directly graphite to titanium. Temperature of 850 °C was taken in welding with nickel interlayer, and that without interlayer made 1100 °C. Such high temperatures of DW do not allow using these methods in given assemblies.

Brazing allows regulating a stress level by changing temperature interval of cooling via selection of braze alloys with necessary melting temperature, providing serviceability of the assemblies under specific conditions. The calculations showed that application of low-temperature braze alloys with melting temperature up to 250 °C guarantees production of defect-free joints. For example, POS-50 braze alloy with melting temperature 209 °C provides for tensile strength equal 36 MPa, i.e. at graphite level. Taking into account lead toxicity, it is reasonable to use substitutes of tin-lead braze alloys, for example, low-temperature ones developed at the E.O. Paton Electric Welding Institute, in which lead is replaced by small amounts of silver. If graphite wetting by braze alloy requires higher temperature, than brazing is reasonable to be carried out by two-step technology with pretinning of graphite surface. Thus, graphite-to-copper brazing with further slow cooling is more practical. Time of cooling is to be calculated for specific assembly using copper creep parameters.

Conclusions

1. All constituents of stresses and deformations are significantly changed with cooling rate variation. Further holding at 500 °C changes them more.

2. Reduction of cooling rate from the point of view of development of plastic deformations is more efficient than increase of holding time after temperature reduction to 500 °C. This promotes for reduction of the level of stresses in the assembly at cooling.

3. Internal surface has the highest risk of crack formation after cooling, where in all variants, except for variant 5, the maximum tensile stresses reach graphite bending strength.

4. Variant 5 (gradual reduction of temperature from 900 to 500 °C during 6000 s), at which tensile stresses do not exceed 25 MPa, is considered the most optimum from the point of view of reduction of danger of crack formation in graphite after cooling to 500 °C.

5. Variants with quick cooling and further holding are not reasonable since large stresses on the external surface of graphite are developed at them.

6. Brazing with low-temperature lead-free braze alloys is the most practical for production of copper-graphite assemblies from low-strength graphite.

1. Ermolaev, G.V., Kvasnytsky, V.V., Kvasnytsky, V.F. et al. (2015) *Brazing of materials*: Manual. Ed. by V.F. Khorunov at al. Mykolaiv: NUK.
2. Kazakov, N.F. (1976) *Diffusion welding of materials*. Moscow: Mashinostroenie.
3. Kvasnitsky, V.V., Ermolaev, G.V., Matvienko, M.V. (2008) Influence of plastic deformation on stress-strain state in diffusion welding of dissimilar metals applicable to cylinder–cylinder and bush–bush assemblies. *Zbirnyk Nauk. Prats NUK*, **1**, 100–107.
4. Makhnenko, V.I., Kvasnitsky, V.V., Ermolaev, G.V. (2008) Stress-strain state of diffusion bonds between metals with different physical-mechanical properties. *The Paton Welding J.*, **8**, 2–6.
5. Kvasnitsky, V.V., Ermolaev, G.V., Matvienko, M.V. (2009) Influence of strength and creep resistance on residual stress-strain state of metal-ceramic joints. *Zbirnyk Nauk. Prats NUK*, **3**, 83–92.
6. Kvasnitsky, V.V., Ermolaev, G.V., Matvienko, M.V. (2008) Influence of geometry of dissimilar materials parts on stress-strain state in diffusion welding. *Ibid.*, **5**, 42–46.
7. Kvasnitsky, V.V., Matvienko, M.V., Ermolaev, G.V. (2009) Influence of the ratio of dimensions of cylindrical parts from dissimilar materials on their stress-strain state in diffusion welding. *The Paton Welding J.*, **8**, 17–20.

Received 21.07.2015

THERMAL-PHYSICAL PECULIARITIES OF GAS-SHIELDED PULSE-ARC WELDING USING NON-CONSUMABLE ELECTRODE (Review)

A.A. SLIVINSKY, L.A. ZHDANOV and **V.V. KOROTENKO**
NTUU «Kiev Polytechnic Institute»
37 Pobeda Ave., 03056, Kiev, Ukraine. E-mail: o.slyvinsky@gmail.com

The work studies the main problems of development and possible perspectives for further improvement of inert-gas non-consumable pulse-arc welding. Main technological possibilities and thermal-physical peculiarities of the process are given depending on variation of welding mode parameters. Considered are the directions for development of methods of mathematical modeling of welding process and possible ways of their improvement. Necessity in further investigations of the process for determination of parametric dependencies and development for engineering and scientific purposes of optimum modes of pulse-arc welding using tungsten cathode was grounded. 41 Ref., 7 Figures.

Keywords: *pulse TIG welding, thermal cycles, mode rigidity, gas-dynamic characteristics, transition processes, discretization, precision, thermocouple, finite element method.*

TIG welding starts active development in period of aircraft and space engineering, namely in the 1960s of the last century. Today TIG welding is one of the most wide-spread methods for joining of metals and alloys. It is widely used in industry branches with high requirements to welds and structures, particularly in aircraft and rocket production [1–6].

Equipment for alternating current welding with pile-up of pulses for aluminum joining was developed till the end of 1960s. It was based on mechanical contactors and performed non-consumable pulse-arc welding. At that, low-amperage stationary arc was kept between the pulses, that allowed for significant process stabilization and increase of welded joint quality [7–9].

Development of TIG welding together with application of different consumables and auxiliary materials (fluxes, pastes, filler wires and gas mixtures) is based on methods and means of change of process energy characteristics, that provides for efficient influence on heat input in welding [10]. Thus, in proper time application was found for such methods of welding as step-arc welding [11] and modulated current welding [12].

Further development of element base, power electronics as well as microprocessor and digital equipment resulted in expansion of amount of controlled values and regulated parameters of the mode. It is 7–10 for pulse-arc welding in modern current power sources. At that, pulse current (I_p), break current (I_b), duration of pulse (t_p) and breaks (t_b), time of pulse growth (t_{up}) and time of pulse drop (t_{down}) and shape of pulse have direct effect on peculiarities of existence of arc discharge. Arc voltage is set by length of inter-arc gap, i.e. set by operator.

Obviously that correct selection of welding mode is a complex and long process. Therefore, synergetic power sources, in which a program sets the optimum relationship of parameters of mode in the power source, find more and more application at current time. In order to receive corresponding software program, providing necessary mode of power source, an operator shall set material, its thickness, electrode diameter, welding position and welding current (stationary or pulse mode). At that, application of advanced computer technologies using PC and communication technologies, namely Ethernet and WiFi, are provided for easy selection of welding mode parameters. Development of PC–welding power source systems has already allowed tracing all parameters of welding mode as well as carrying their analysis and adjustment in automatic mode directly via software set on PC (ewm Xnet technology) [13] from EWM and Fronius Digital Revolution [14]).

Number of investigations was carried out and large amount of welding equipment with different capabilities was developed from the appearance of non-consumable pulse welding up to present moment. However, large number of parameters of welding mode regulation complicates its selection and designation for specific task. It is

particularly relevant for sheet metal, where increase of efficiency is important, but formation of burning through and significant deformation of structure shall not be allowed. Modern advanced technologies of regulation of process of pulsed-current argon-gas tungsten-electrode arc welding (PTIGW) do not always allow achieving optimum result, first of all, due to large set of process regulated parameters and their relationships. Therefore, investigation of their effect on geometry of welded joint, which depends on weld pool shape and being determined by physical characteristics of plasma of arc discharge, is still relevant task.

Balance between efficiency and quality of welded joint is to be kept in welding of sheet metal. Heat supply in pulse mode input allows significant expansion of possibilities of regulation of heat input into base metal and its penetration. In general, base metal penetration and weld formation can be represented using the following scheme.

Input of heat Q takes place in course of current pulse of t_p duration. It provokes melting of base metal with formation of weld pool in form of point $Q = q_a t_p$, where q_a is the arc effective power, and t_p is the duration of pulse of principle current. The weld pool is cooled till complete or partial solidification in course of t_b. The next heat pulse will melt the same spot weld pool at $S = v(t_p + t_b)$ distance from previous point, where v is the welding speed.

In such a way, the weld is formed by means of periodical melting of separate points with set step S. Level of points overlapping is determined by their size and step. Amount of heat per unit of weld length makes $Q/S = q_a t_p / v(t_p + t_b)$, where $q_a t_p / t_p + t_b$ is the average power of periodic arc.

Study [15] shows that process of pulse arc welding to a first approximation can be considered as welding process with direct current arc of $q_r / q_a(1 + t_b / t_p)$ power. Calculated current at that makes $I_r = I_p / (1 + t_b / t_p)$. Relationship t_b / t_p characterizes current frequency and stipulates penetration ability of periodic arc. The greater it is at the same calculated current I_r (average power), the more pulse current (pulse power) is. Dimensionless t_b / t_p value is a technological parameter characterizing ability to penetration of periodic (pulse) arc at set pulse energy and cycle duration. It is called rigidity of mode of pulse arc welding (G).

Thus, pulse arc penetration ability can be effected by change of mode rigidity and absence of variation in current value. Comparative investigations on stationary and pulse arc welding of 3 mm thick 12Kh18N9T steel, given in [15], showed that increase of rigidity promotes for rise of value of total heat efficiency (Figure 1) under conditions of equal average rate of heat input and welding speed.

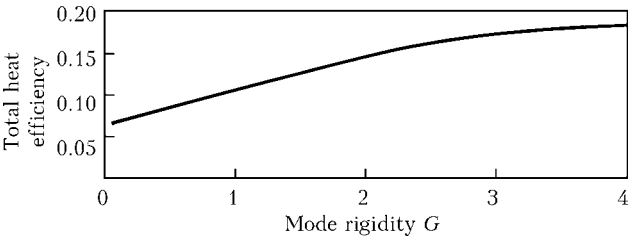

Figure 1. Mode rigidity versus total heat efficiency [15]

The attention is also paid to the fact [15] that increase of G under condition of similar penetration provides for reduction of zones of plastic deformations (heating above 600 °C) (Figure 2).

Work [16] according to the results of measurement of thermal cycles showed that rise of mode rigidity at the same currents significantly reduces HAZ (temperature in test points being at 2 mm distance from welding axis decreased per 200 °C at rise of G from 0.3 to 3). The results published in [17] (Figure 3) verify this. Thus, it can be stated that mode rigidity has decisive effect on form of welding thermal cycles and time of weld pool existence and can serve as general integral parameter of PTIGW process.

Studying PTIGW processes, in addition to time characteristic of pulses, requires outlining such parameters of modes as pulse current (I_p), base current value (I_b) and welding speed (v), which determine a rate of energy input. If I_p is the parameter, first of all, effecting the base metal penetration, then I_b, according to [18], is used for stabilizing arc discharge. Thus, I_b zero value promotes for rise of possibility of so-called erratic arc, that results in undetermined location of areas of arc excitation on electrode and reduces arc process stability.

Another peculiarity of PTIGW is deformation of shape of arc discharge with possible lagging of anode spot. Author of study [19] explains this

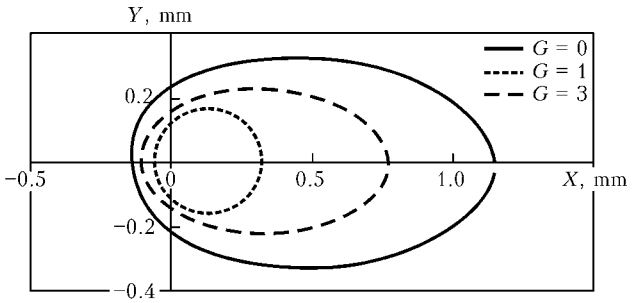

Figure 2. Calculation isotherms T = 600 °C at different modes of welding using pulsed and stationary arc [15]

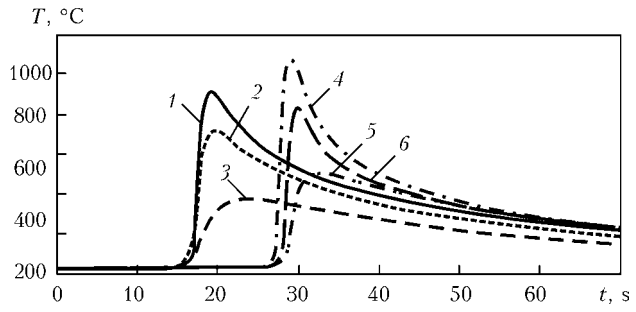

Figure 3. Thermal cycles measured in welding with pulsed (*1–3*) and stationary (*4–6*) arc for points at 4, 6 and 8 mm distance from weld axis [17]

effect by the fact that evaporation of base metal, taking place during current pulse, supplies to arc discharge the atoms of lower ionizing potential than that of shielding gas atoms, but simultaneously promotes for decrease of level of heat contraction of arc column, that, in turn, results in high values of voltage drop during the break. This generates contradiction between available favorable conditions of arc existence on weld metal melted by current pulse and necessity of its movement in less favorable conditions of cold metal.

Based on principle of Steenbeck thermodynamic minimum [20], lags of anode spot shall appear on molten metal from time to time in processes of welding, since the molten metal provides for minimum arc voltage. The anode spot moves synchronously with molten metal pool, lagging from electrode movement before voltage of stretched arc do not become equal to anode process excitation voltage. Due to this arc movement can be of stepwise nature. Such a lag of anode spot results in significant for oscillation of arc voltage per 10–15 V [21], that, in turn, provokes oscillations of heat power and as a consequence unstable base metal penetration.

Thus, it can be noted that spatial instability of moving arc significantly limits area of allowable parameters of welding mode. Therefore, supporting of arc column ionizing requires keeping some arc current before the next pulse within the time gaps between pulses. Thus, stability of PTIGW process can be reached namely with the help correct selection of base current value, keeping arc column ionization, and frequency of pulses.

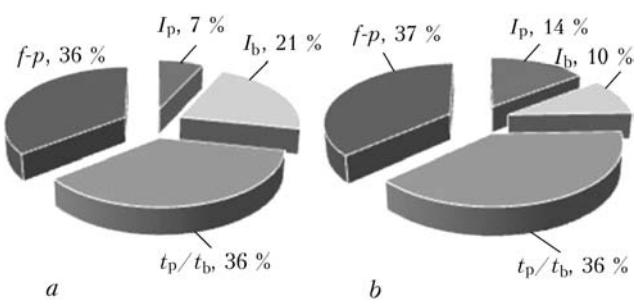

Figure 4. Diagrams of distribution of effect of main parameters of PTIGW (*a*) and HF-PTIGW (*b*) on base metal penetration [26]

A great deal of current investigations [22–25] is dedicated to selection of optimum parameters. Quantitative verification of investigations is represented in overwhelming majority by mathematical dependencies being received using Taguchi method. Effect of parameters of mode of pulse-arc welding on base metal penetration for the range of current pulsing frequency up to 10 (PTIGW) and 100–250 Hz (HF-PTIGW) was evaluated in [26] by given procedure. It can be seen from diagram (Figure 4) that t_p/t_b relationship (value reverse to mode rigidity) and current pulsing frequency *f-p* have the main effect on process of penetration and formation of welded joint in PTIGW as well as HF-PTIGW. At the same time, such parameters of mode as base and pulse currents have the least effect on penetration. However, these are the parameters influencing welding process stability and, respectively, quality of welded joint formation.

There is a great deal of works dedicated to PTIGW process simulation. At that, physical-mathematical modeling of characteristics of arc pulse discharge is usually a basis for experimental data, received with the help of arc sounding method [27, 28].

Results of mathematical modeling of arc discharge between tungsten cathode and copper water-cooled anode, given in [29], showed that existence of arc discharge in welding using pulse-periodic mode is accompanied by significant changes of electromagnetic, thermal and gas dynamic characteristics of arc plasma.

Presented results of simulation show that transition processes play an important role in heat input distribution over the base metal. Their experimental investigation can be carried out based on analysis of electron oscillograms of energy parameters of arc discharge, i.e. current and voltage.

Selection of characteristics of primary probes and registration devices, namely analog-digital transducers (ADT), is very important when performing such oscillographic testing. Procedure on selection of the primary probes for generation of suitable digital signal image is described in details in work [30], and principles of selection of ADT for oscillographic testing are given in [31].

Current approaches to simulation of physical processes, taking place in arc discharge plasma during PTIGW, described in works [32–36], provides for application of finite element method

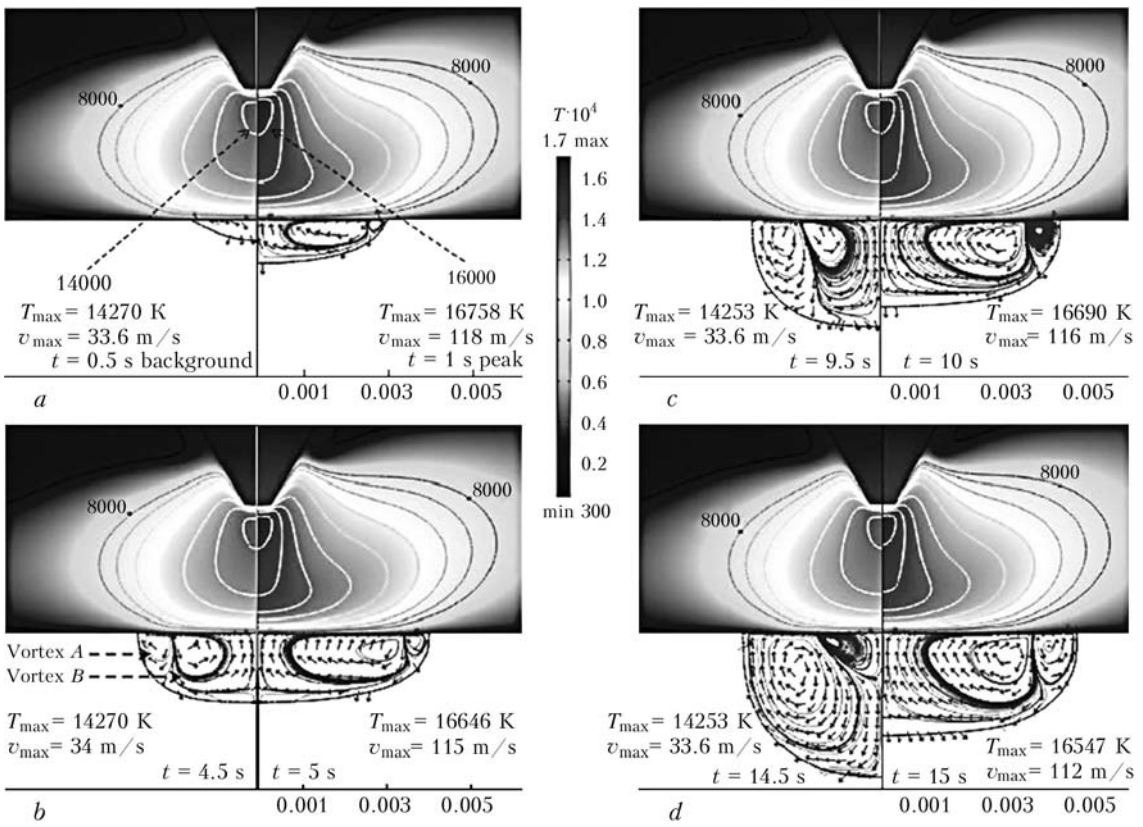

Figure 5. Results of simulation of magnetic-hydro-dynamic processes in weld pool for periods of effect of base current (*left*) and pulse current (*right*) at time moment of 1 (*a*), 5 (*b*), 10 (*c*) and 15 (*d*) s from the PTIGW beginning at I_p = = 160 A, I_b = 80 A and *f-p* = 1 Hz [36]

(FEM). Thus, results, received in [36], are based on application of infra-red chamber and numerical FEM-simulation using ComsolScript complex. At that, calculation of temperature distribution in cathode and anode area and in plasma arc is carried out using a system of main classic Maxwell's equations. Simulation of magnetic-hydro-dynamic processes showed that different various take place in weld pool at different moments of time and they significantly depend on electrodynamic characteristics of plasma column as well as its temperature (Figure 5).

It was determined that the maximum temperature of tungsten cathode made 3500 K in pulse moment and 3200 K at break moment. The maximum temperature of plasma area was 14250 K in break moment and 16540 K at pulse current effect. It is the well-known fact that these values significantly depend on material of anode, value of welding current and distance between the electrodes. Results of calculation also show nature of change of penetration depth and width depending on amount of pulses at the same point of metal. This allows talking about heat saturation depending on amount of pulses (Figure 6).

The main thesis of results presented in [36] is a statement of authors that no change of shape takes place in cross-section of the weld pool in pulse arc welding even at significant difference in base and pulse values of current, that allows for regulating these parameters in a wide range during sheet metal welding. At the same time, this work assumed the following simplifications during simulation, namely thermodynamic equilibrium takes place in arc plasma, and effect of metal vapors is not considered. The latter assumption significantly reduces efficiency of application of this model on practice. In general case, it should be noted that the model is designed for spot welding, i.e. when power source is stationary. This also introduces significant errors in prediction of base metal penetration.

It is the well-known fact that structural transformations in metal and stress-strain state of welded joint and structure in whole have decisive effect on welded joint mechanical properties. These factors are determined by nature of welding heat processes. And if simulation of stationary welding process is sufficiently well described in scientific sources, then of information on calculations of heat processes in non-consumable pulse-arc welding is not enough. It is the well-known fact that thermal-physical situation in pulse-arc welding has significant differences from that in stationary arc welding, i.e. process of heat distribution becomes non-stationary, cyclic

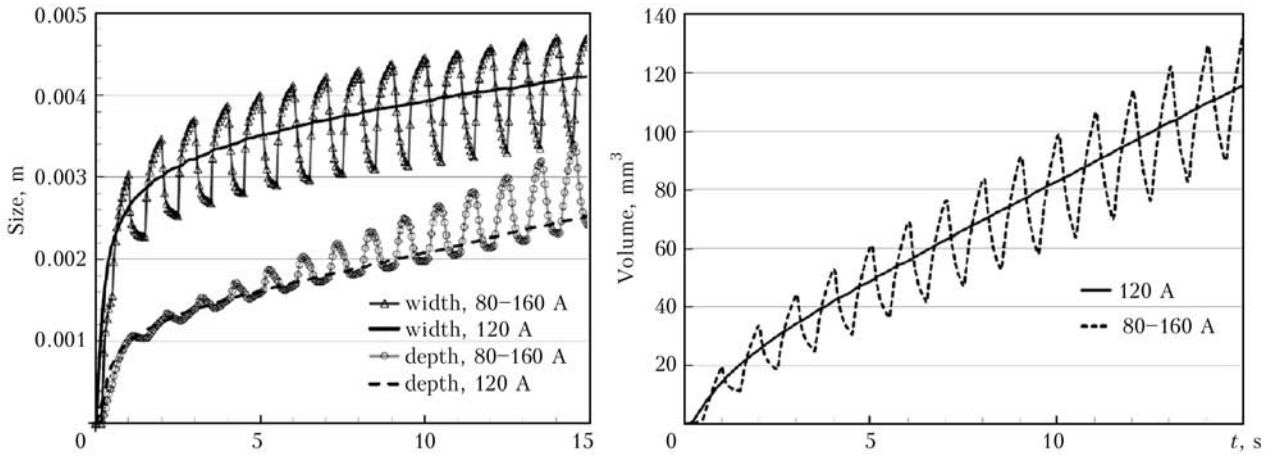

Figure 6. Comparison of geometry characteristics of weld pool for DC welding and PTIGW [36]

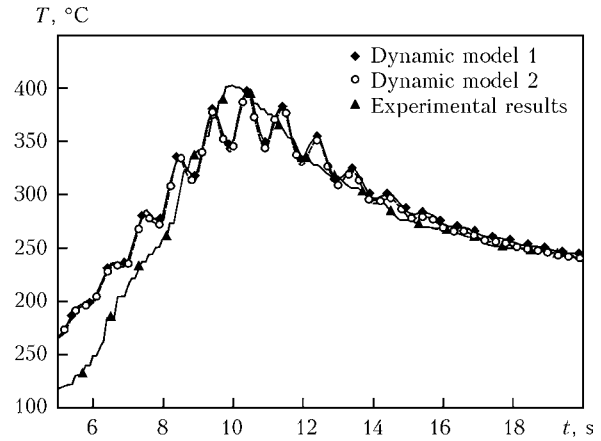

Figure 7. Welding thermal cycles, received experimentally and at FEM-simulation, for points located at 40 mm distance from beginning of welding, 6 mm from weld axis and at 4 mm depth for I_p = 160 A, I_b = 80 A, *f-p* = 1 Hz, t_p = = 0.5 s and t_b = 0.5 s [41]

change of processes of heating and cooling in each point of weld and near-weld zone takes place.

Schemes of spot, linear and volumetric power sources are used for calculation of heat processes in TIG welding. The basics for calculation of heat processes in welding were founded, as everybody knows, by Rozental and Rykalin. Series of simplifications are mainly used in application of Rykalin calculation schemes for non-consumable pulse-arc welding. Works [37, 38] can be an example. Their results are rather qualitative than quantitative, and, besides, such an approach does not allow predicting the weld pool shape and it makes it inconvenient for determination of pulse welding optimum parameters.

Application of volumetric heat sources [39] is necessary for more accurate prediction of penetration depth as well as thermal condition of base metal. Procedure of FEM-simulation of heat processes is the most widely used at current time. It considers volumetric heat sources of ellipsoid form and in first approximation recall a weld pool shape [40]. Work [41] provides for the results of PTIGW simulation for heat source represented in form of parabola of rotation with normal (Gaussian) power distribution. At that, size of the source was experimentally determined, using images received with the help of speed infra-red CCD-camera. The simulation was carried out in two different statements, namely when the heat source is set in form of parabola of rotation at the moment of base current influence, and in form of Gaussian model (Figure 7, dynamic model 1) at the moment of principle current influence, as well as in the case when it is represented in form of Gaussian model for the moment of break and moment of pulse of heat source (Figure 7, dynamic model 2).

It can be seen from given thermal cycles that both dynamic models provide for satisfactory conformity with experimental thermal cycle on maximum temperatures, but that can not be said about nature of oscillation of temperatures received experimentally and mathematically. It is obvious that welding with periodic change of power, typical for PTIGW process, also promotes for periodic change of metal temperature, that can't be observed on experimental curve received by authors of work [41]. Probably, such mismatch is related with peculiarities of measurement equipment. Except for similarity of temperature calculation and experiment, an important factor is a prediction of penetration shape, that is difficult to realize using proposed procedure.

Conclusion

It is determined based on results of reference data on peculiarities of gas-shielded nonconsumable-electrode pulse-arc welding that the main problem with practical application of this method is

absence of possibility for prediction of effect of welding mode parameters on physical and technological properties of arc discharge and, as a result, weld geometry characteristics.

It is shown that the main technological characteristic of this method of welding is mode rigidity.

It is found that such parameters of modes as current and voltage in the pulse as well as base values of current and voltage, particularly, short-term changes of energy parameters of arc discharge, have to be outlined in addition to pulse time characteristics during PTIGW analysis.

Requirements to ADT, which is used for registration of energy parameters of PTIGW process and transition processes, were formulated based on analysis of reference data and Nyquist theorem. Besides, application of synchronized video registration of pulse arc discharge is relevant for further decoding of oscillograms.

Results of simulation of physical processes in plasma and magnetic-hydro-dynamic processes in the weld pool show that various processes take place in the pool at different moments of time and they significantly depend on electrodynamic characteristics of plasma column as well as on its temperature.

Finite-element modeling of heat processes of tungsten-electrode pulse-arc welding requires application of calculation scheme of volumetric heat source of ellipsoid form and presence of calculation-experimental time dependencies of the main macroparameters for specific mathematical description of time variable of arc power.

Thus, available experimental data and results of simulation of PTIGW process reflect existence of arc discharge plasma at moments of current pulse generation and its effect on behavior of weld pool metal. Processes, accompanying appearance of the main arc discharge in pulse and its extinction, i.e. transition short-term processes, are not considered due to absence of accurate experimental data. This verifies relevance of development of optimum procedure for further investigation of these processes under PTIGW conditions, which allows development of more accurate procedure for prediction of effect of welding mode on geometry and technological characteristics of welded joint.

1. Brodsky, A.Ya. (1956) *Tungsten-electrode argon-arc welding*. Moscow: Mashgiz.
2. Petrov, A.V. (1961) *Technology of inert-gas arc welding*: Reference book on welding, Vol. 2, 327–375. Ed. by E.V. Sokolov. Moscow: Mashgiz.
3. (1985) Actual problems of welding of non-ferrous metals. In: *Proc. of 11th All-Union Conf*. Kiev: Naukova Dumka.
4. (1985) *Metals science of aluminium alloys*. Ed. by S.T. Kishkin. Moscow: Nauka.
5. Russo, V.L. (1962) *Inert-gas welding of aluminium alloys*. Leningrad: Sudpromgiz.
6. Shakhanov, S.B. (2007) *Theory and technology of welding production in rocket industry*: Manual. St.-Petersburg: Balt.GTU.
7. Gurevich, S.M., Zamkov, V.N., Kushnirenko, N.A. (1965) Increase of penetration efficiency of titanium alloys in argon-arc welding. *Avtomatich. Svarka*, **9**, 1–7.
8. Alov, A.A., Shmakov, V.M. (1962) Argon-arc welding with auxiliary argon flow. *Svarochn. Proizvodstvo*, **3**, 13–16.
9. Terry, S.A., Tyler, W.T. (1958) Inert-gas tungsten-arc welding. *Welding and Metal Fabr.*, **2**, 58–61.
10. Paton, B.E. (1963) Further development of systems of automatic control and regulation of welding processes. *Avtomatich. Svarka*, **5**, 1–6.
11. Razmyshlyaev, A.D., Patrikeev, A.I., Maevsky, V.R. (1988) Calculated definition of pool contour in step-by-step-arc welding of thick metal. *Svarochn. Proizvodstvo*, **5**, 35–37.
12. Vagner, F.A. (1980) *Equipment and methods of pulsed arc welding*. Moscow: Energiya.
13. Network-based welding processes analyzing, controlling and managing. pdf. *https*//www.ewm-group.com/ru/service/downloads/ brochures-handouts-and-manuals/2698-ewm-xnet-brochure/download.html
14. (2002) Weld+vision FRONIUS MAGAZINE, **11**. pdf. *http*://www.fronius.com/cps/rde/xbcr/SID-76553F1D-04EC16FD/fronius_brasil/4000062136_weld_ vision_Nr 9_en.pdf
15. Petrov, A.V., Slavin, G.A. (1966) Study of technological features of pulsed arc. *Svarochn. Proizvodstvo*, **2**, 1–4.
16. Slyvinsky, O.A., Bojko, V.P., Prepiyalo, A.O. (2013) Mathematical modeling of heat processes in argon-arc welding of thin stainless steel of ferrite class. In: *Proc. of 6th All-Ukr. Interbranch Sci.-Techn. Conf. of Students, Post-Graduate Students and Researches on Welding and Related Processes and Technologies* (Kiev, 29–31 May 2013), 14.
17. Slyvinsky, O.A., Korotenko, V.V. (2014) Mathematical modeling of heat processes of pulsed tungsten argon-arc welding of thin stainless steel. In: *Proc. of 7th All-Ukr. Interbranch Sci.-Techn. Conf. of Students, Post-Graduate Students and Researches on Welding and Related Processes and Technologies* (Kiev, 14–16 May 2014), 19.
18. Kovalev, I.M. (1973) Some methods for stabilizing of unstable arc with non-consumable electrode. *Svarochn. Proizvodstvo*, **6**, 3–5.
19. Kovalev, I.M. (1972) Space stability of moving arc with non-consumable cathode. *Ibid*., **8**, 1–3.
20. Finkelnburg, V., Mekker, G. (1961) *Electric arc and thermal plasma*. Moscow: IL.
21. Kozakov, Yu.M., Stolbov, V.I., Koryagin, K.B. (1986) Lagging of anode spot of moving welding arc. *Svarochn. Proizvodstvo*, **10**, 19–21.
22. Kim, D., Rhee, S. (2001) Optimization of arc welding process parameters using a genetic algorithm. *Welding J*., **July**, 184–189.
23. Giridharan, P.K., Murugan, N. (2009) Optimization of pulsed GTA welding process parameters for welding of AISI 304L stainless steel sheets. *Int. J. Advanced Manufact. Technology*, Issue 5, **40**, 478–489.
24. Babu, S., Senthil Kumar, T. (2008) Optimizing pulsed current gas tungsten arc welding parameters of AA6061 aluminium alloy using Hooke and Jeeves algorithm. *Transact. of Nonferrous Metals Soc. of China*, **18**, 1028–1036.
25. Chakravarthy, M.P., Ramanaiah, N., Sundara Siva Rao, B.S.K. (2013) Process parameters optimization

for pulsed TIG welding of 70/30 Cu–Ni alloy welds using Taguchi technique. *Int. J. Mechanical, Aerospace, Industrial, Mechatronic and Manufact. Eng.*, *7*(**4**), 342–348.
26. Arivarasu, M., Devendranath Ramkumar, K., Arivazhagan, N. (2014) Comparative studies of high and low frequency pulsing on the aspect ratio of weld bead in gas tungsten arc welded AISI 304L plates. *Proc. Eng.*, **97**, 871–880.
27. Dyatlov, V.I. (1961) Volt-ampere characteristic of constricted electric arc. *Avtomatich. Svarka*, **1**, 23–26.
28. Rabkin, D.M., Ivanova, O.N. (1968) Investigation of arc in tungsten arc welding. *Ibid.*, **5**, 16–20.
29. Krivtsun, I.V., Krikent, I.V., Demchenko, V.F. (2013) Modelling of dynamic characteristics of a pulsed arc with refractory cathode. *The Paton Welding J.*, **7**, 13–23.
30. Zhdanov, L.A., Slyvinsky, A.M., Kotyk, V.T. et al. (2003) Possibility of analog-digital converter application for study of alternating current welding arc. *Mashynoznavstvo*, **2**, 38–41.
31. Zhdanov, L.A., Slyvinsky, A.M., Kopersak, V.M. et al. (2004) Study of alternating current welding arc by personal computer. *Nauk. Visti NTUU KPI*, **3**, 49–55.
32. Wu, C.S., Gao, J.Q. (2001) Analysis of the heat flux distribution at the anode of a TIG welding arc. *Comput. Mater. Sci.*, **24**, 323–327.
33. Lu, F., Tang, X., Yao, Yu.S. (2006) Numerical simulation on interaction between TIG welding arc and weld pool. *Ibid.*, **35**, 458–465.
34. Tanaka, M., Lowke, J.J. (2007) Predictions of weld pool profiles using plasma physics. *J. Phys. D: Appl. Phys.*, **40**, 1–23.
35. Traidia, A., Roger, F., Guyot, E. (2010) Optimal parameters for pulsed gas tungsten arc welding in partially and fully penetrated weld pools. *Int. J. Therm. Sci.*, **49**, 1197–1208.
36. Traidia, A., Roger, F. (2011) Numerical and experimental study of arc and weld pool behavior for pulsed current GTA welding. *Int. J. Heat and Mass Transfer*, **54**, 2163–2179.
37. Petrov, A.V. (1967) Application of sources method for calculation of heat processes in pulsed-arc welding. *Fizika i Khimiya Obrab. Materialov*, **5**, 15–25.
38. Vagner, F.A. (1975) Calculation of temperatures in product during pulsed welding with exponential pulse shape. *Avtomatich. Svarka*, **7**, 13–15.
39. Kiselev, S.N., Kiselev, A.S., Kurkin, A.S. et al. (1998) Modern aspects of computer modeling of heat, deformation processes and structure formation in welding and related technologies. *Svarochn. Proizvodstvo*, **10**, 16–24.
40. Goldak, J.A., Chakravarti, A., Bibby, M. (1984) A new finite element model for welding heat sources. *Metallurg. Transact. B*, Vol. 15, 229–305.
41. Zhang Tong, Zheng Zhentai, Zhao Ru (2013) A dynamic welding heat source model in pulsed current gas tungsten arc welding. *J. Materials Proc. Technology*, **213**, 2329–2338.

Received 28.07.2015

MAIN TENDENCIES IN DEVELOPMENT OF PLASMA-ARC WELDING OF ALUMINIUM ALLOYS*

A.A. GRINYUK[2, 3], V.N. KORZHIK[1, 2], V.E. SHEVCHENKO[1, 2], A.A. BABICH[2], S.I. PELESHENKO[4], V.G. CHAJKA[2], A.F. TISHCHENKO[2] and G.V. KOVBASENKO[2]

[1]Chinese-Ukrainian E.O. Paton Welding Institute
(Guangdong General Research Institute of Industrial Technology)
(Guangzhou Research Institute of Non-Ferrous Metals, PRC)
[2]E.O. Paton Electric Welding Institute, NASU
11 Bozhenko Str., 03680, Kiev, Ukraine. E-mail: office@paton.kiev.ua
[3]NTUU «Kiev Polytechnic Institute»
6/2 Dashavskaya Str., 03056, Kiev, Ukraine. E-mail: andrey_grinyuk@ukr.net
[4]South China University of Technology
510641, Guangzhou, PRC. E-mail: sviatoslav@qq.com

Publications, describing the characteristic technologies of aluminium alloy welding by an arc constricted by high-velocity inert gas flow were analyzed. It is shown that plasma-arc welding (PAW) is further development of the process of nonconsumable-electrode inert-gas welding. It is established that during development of PAW of aluminium alloys, there was a transition from alternating sinusoidal current to reverse polarity direct current, and furtheron to variable polarity asymmetrical current with rectangular current waveform. A more promising direction of improvement of PAW equipment is transition from specialized power sources to modular design of PAW system, based on power sources applied for nonconsumable electrode welding and plasma modules. Further path of improvement of the processes of aluminium alloy PAW is combined or hybrid application of several heat sources, including the constricted arc and consumable-electrode arc. In the authors' opinion, hybrid consumable-electrode PAW with hollow anode and axial wire feed in the most promising variant. 41 Ref., 17 Figures.

Keywords: *plasma-arc welding, aluminium alloys, alternating sinusoidal current, variable polarity asymmetrical current, hybrid plasma-arc welding, consumable electrode*

Aluminium and aluminium alloys take up the second place after steel as to production and consumption. Owing to a set of physical and mechanical, corrosion and technological properties, aluminium-based light alloys are successfully applied not only in development of flying vehicles, but also in other sectors of industry and construction. Volumes of aluminium alloy application in military equipment items, in shipbuilding, in fabrication of automotive and railway vehicles, in electrical engineering, in manufacture of cryogenic and chemical apparatuses, in agricultural and food industry are considerable. Alongside a multitude of diverse welding processes, arc welding processes are more widely applied to produce aluminium alloy permanent joints, which can be divided into nonconsumable and consumable electrode welding. Nonconsumable electrode welding is applied in fabrication of structures from semi-finished products of aluminium alloys 2–12 mm thick. In its turn, nonconsumable electrode welding is performed by freely expanding and constricted arc.

The first mention of plasma jet energy application for metal treatment dates back to 1950s [1]. Nowadays the plasma jet is used for welding, cutting, coating deposition, surface hardening, etc. Transferred and non-transferred constricted arc is applied for metal treatment. At transferred arc application the electric discharge runs between the electrode and the item, and in the case of non-transferred arc the discharge runs between the electrode and the plasma nozzle. In this case, the treated item is exposed only to a plasma jet blown out through small diameter nozzle by inert gas flow.

Fusion welding with heating by constricted plasma arc is a further development of inert-gas nonconsumable-electrode welding process [2]. Another inner water-cooled copper nozzle is

*Work was performed with financial support within Program of Foreign Experts in PRC #WQ20124400119, R&D Project of Innovation Group of Guangdong Province #201101C0104901263 and International Project of Ministry of Science and Technology of PRC # 2013DFR70160.

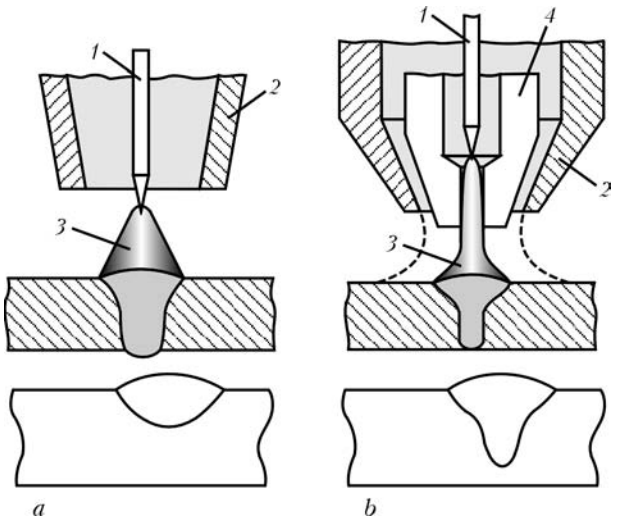

Figure 1. Schematic of the process and shape of weld penetration in nonconsumable electrode arc (*a*) and plasma-arc (*b*) welding: *1* — tungsten electrode, *2* — shielding gas nozzle; *3* — welding arc; *4* — plasma-forming nozzle

added to the torch design. Gas, blown out through inner nozzle hole of small diameter (from 1 to 5 mm) forms a layer of thermal and electric insulation around the arc, preventing its free expansion. Welding zone is protected by inert gas flow from larger diameter outer nozzle (Figure 1), and arc column temperature and its voltage rise [2].

On the whole, analysis of the experience of plasma arc application for welding showed that it is a more versatile source of metal heating in welding, compared with electric arc in nonconsumable and consumable electrode welding. Compared to these methods, plasma provides deeper penetration of metal at simultaneous reduction of its melting volume, and it also has the following advantages:

- higher plasma arc temperature (up to 18,000–25,000 K);
- smaller arc diameter;
- arc cylindrical shape (unlike the regular conical shape);
- plasma arc pressure on the metal 6–10 times higher than that of a regular one;
- ability to maintain the arc at low currents (0.2–30 A).

Plasma arc application in welding also ensures absence of metal spattering, smaller heating of base metal and, consequently, its smaller deformation, no need for edge preparation (grooving) in many cases due to high penetrability of the plasma arc, higher cost effectiveness and efficiency (by 2–3 times and more), reduction of the cost of machining at butt preparation for welding, and of weld treatment after welding by 3–5 times and more, lower consumption of welding consumables by 3 to 5 times or more, weld quality improvement and possibility of 100 % automation of the processes of welding the longitudinal and circumferential welds.

According to GOST 2601–84 «Metal welding. Terms and main definitions», fusion welding with heating by an arc constricted by gas flow, is called plasma welding. In our opinion, such a definition is more suitable to the process of welding by non-transferred constricted arc, which is usually not used for welding. Therefore, it is more correct to apply the term «plasma-arc welding», which specifies participation of both the arc energy, and plasma jet energy, in part heating.

Plasma-arc welding with alternating sinusoidal current. A feature of aluminium alloy arc welding is the need to break up the surface refractory oxide film. For its effective breaking up, plasma-arc welding (PAW) should be performed at reverse polarity direct current or at variable polarity current [3].

Similar to the case of nonconsumable electrode welding with freely expanding arc, the first experiments on PAW of aluminium alloys were conducted with application of alternating sinusoidal current of 50 Hz frequency. At the end of 1960s, PWI performed intensive studies of this process [4, 5]. To ensure constricted arc running, a pilot arc module was added to a standard machine for nonconsumable electrode aluminium welding. The pilot arc ran between the electrode and plasma-forming nozzle, ionizing the gap between the electrode and the item. At application of sinusoidal AC, oxide film breaking up proceeds in reverse polarity half-wave at electrode positive. Up to 70 % of the arc heat evolves in the electrode. In 1970–1971 the method of PAW with sinusoidal AC was applied in ship-building. An advanced automatic machine «Aluminij-1» for nonconsumable electrode welding of aluminium alloys and UDG-701 power source were proposed for its realization [6]. This welding process did not become widely accepted later on. There is no information in publications about batch-produced machines for PAW at sinusoidal AC.

Plasma-arc welding at reverse polarity direct current. PAW at reverse polarity was applied for the first time for joining 6.35 mm aluminium alloy sheets by the staff of Thermal Dynamics Corporation [7]. The first studies in the Soviet Union on application of DCRP date back to the beginning of 1970s [8, 9].

The best cathode breaking up of the film (cathode cleaning) in nonconsumable electrode welding is achieved at reverse polarity. Plasmatron electrode assembly is the anode, and the item proper is the cathode. PAW at DCRP is easier to implement, compared to sinusoidal AC welding. For instance, standard welding rectifiers can

be used as the constricted arc power source. Nonetheless, this PAW process has a significant drawback — a considerable amount of heat evolves in the electrode assembly at reverse polarity welding, leading to electrode premature failure.

In order to extend the service life of electrode assembly, its intensive cooling is performed, tungsten rods of large diameter (8–10 mm) or special copper electrodes with inserts of refractory materials (tungsten, hafnium) are used. To extend plasmatron life, its components are made massive, that increases its overall dimensions.

Stability of running of a constricted direct current arc at reverse polarity depends on the quality of part surface preparation for welding. Presence of unremoved oxide films on the surface of items being welded can cause wandering of the heating spot, because of different emissivity of the oxide film and cleaned base metal [8, 9]. At small currents this wandering will become more pronounced.

The process was widely applied for manufacturing items from aluminium alloys for cryogenic applications [10]. UPS-301 and UPS-503 machines were manufactured in the USSR for PAW at DCRP, and welding could be also performed with surfacing machine UPNS-304.

Studies of this variant of PAW of aluminium are intensively pursued in Russia. Company «Shipbuilding and Ship Repair Center» developed PPN-200 semi-automatic machine for PAW of aluminium at DCRP. Nonconsumable electrode welding machine Master-2500 of Kemppi is used as the power source [11]. Company «Plazmek» Group developed a versatile PAW station, including an inverter power source, module for pilot arc generation and plasma gas feeding, independent water-cooling unit and proprietary plasmatrons. List of companies, manufacturing equipment for direct current PAW is extensive: it can include companies from North and South America, Europe and Asia. The following equipment models can be noted: DigiPLUS A7P and DigiPLUS A7PO of IMC Engenharia de Soldagem (Brazil), Ultima150 of Thermal Arc (USA), PI400 Plasma of Svejsemaskinefabrikken Migatronic A/S (Denmark), Plasmaweld 402 of L-TEC Schweisstechnik (Germany), PSI 350plus of Kjellberg Finsterwalde Schweisstechnik und Verschleissschutzsysteme (Germany), Tetrix 552 RC Plasma CW of EWM Hightec Welding Automation (Germany), PW400 of Arcraft Plasma Equipment PVT. Ltd (India), Plasma 500XP of Powwel Co. Ltd (Korea), and others.

To increase the effectiveness of PAW at DCRP, Russian scientists proposed pulsed feed of plasma gases [12–14].

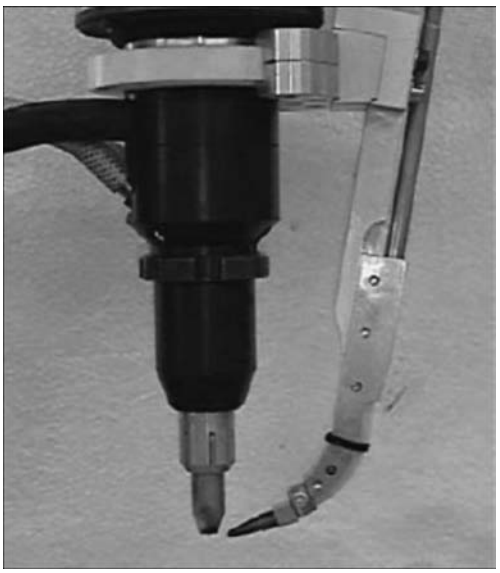

Figure 2. Appearance of Plasmatron welding torch (Inocon Technologie GmbH) [16]

One of the negative points of DCRP application for PAW of aluminium alloys is a strong proneness of this welding process to hydrogen gas porosity in the weld metal [15].

Plasmatron welding process proposed by Inocon Technologie GmbH (Austria) is one of the variants of PAW of aluminium alloys at direct current [16]. An ingenious shape of the welding torch is a feature of the welding process (Figure 2). As reported by Inocon Technologie GmbH staff, such a scheme of the welding process allows temperature in the active heating spot to be increased (Figure 3), and welding to be performed without an additional module of pilot arc generation.

Plasma-arc welding of aluminium alloys with alternation of electrode and plasma-forming nozzle polarities. To reduce the adverse impact of heat evolved in the electrode at current passage during reverse polarity half-wave, and preserve sufficient cathode cleaning of the weld, PWI staff proposed an original method for applying voltage to the plasmatron [17]. During straight polarity half-wave the arc ran between the tungsten electrode and the item, and during the reverse polarity half-wave the arc was excited between the item and copper plasma-forming nozzle. Owing to such a schematic of energy application to the plasmatron, good penetration was achieved, tungsten electrode resistance was improved, and the arc running during reverse polarity half-wave, ensured effective breaking up of the oxide films. However, this equipment for PAW of aluminium alloys was not put into batch production. At present, German scientists revisited the idea of separate feeding of energy to the electrode and the plasma-forming nozzle. Their machine for

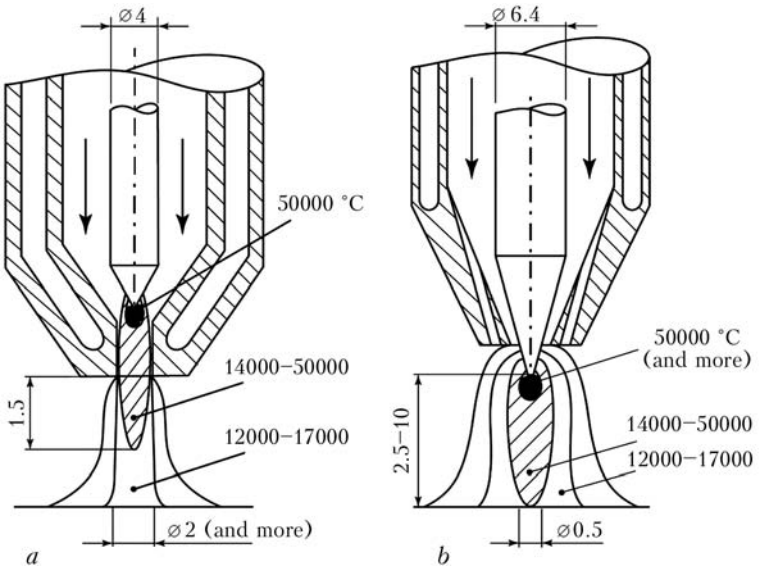

Figure 3. Temperature distribution in traditional torch for PAW (*a*) and Plasmatron welding torch of Inocon Technologie GmbH (*b*) [16]: *a* — heat flow surface density of 10^3–10^5; *b* — 10^6 W/cm^2

PAW with alternation of the electrode and the plasma-forming nozzle polarity also is still at the laboratory stage.

Plasma-arc welding by variable polarity asymmetrical current with rectangular waveform. Process of PAW by variable polarity asymmetrical current with rectangular current waveform, called Variable Polarity Plasma Arc (VPPA) welding, was registered by Hobart Brothers Inc. in 1978 [18]. A special module, forming an additional pulse at transition from straight to reverse polarity, was incorporated into the design of welding machines generating sinusoidal welding current, to ensure continuous arcing. Rectangular waveform of welding current allowed ensuring reliable arc excitation at polarity reversal without application of a special module. To lower the thermal impact on the torch electrode assembly, PAW by variable polarity current with rectangular waveform was performed with prevalent flowing of straight polarity current. Minimum admissible duration of current flowing at reverse polarity is selected to ensure effective cathode breaking up of the oxide films. The ratio of duration of current flowing at straight and reverse polarity was equal to approximately 3:1. Current amplitude at reverse polarity was approximately by 30–40 A higher than at straight polarity (Figure 4) [19]. Reduction of the amount of heat evolving in electrode

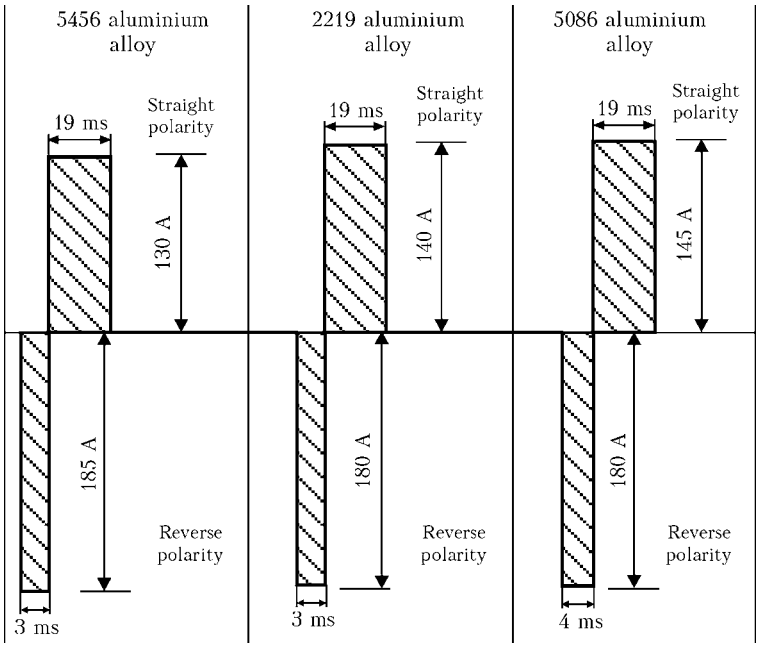

Figure 4. Amplitude and duration of current flowing at straight and reverse polarity for VPPA welding aluminium alloys of different composition [18]

assembly allowed increasing plasmatron performance and reducing its geometrical dimensions.

In 1972, Sciaky proposed to Boeing to use variable polarity asymmetrical current with rectangular waveform for PAW of aluminium alloys [20]. Sciaky power source, however, did not provide arcing stability at variable polarity asymmetrical current. In 1974, Hobard Brothers Inc. started development of a power source and set of equipment for PAW at variable polarity asymmetrical current of rectangular waveform for Boeing. In 1979, the first such set of equipment for PAW was supplied to Marshall Space Flight Center. The set was based on VP-300-S power source, actual values of welding current were monitored with Cyber-Tig 11 Series 800 Programmer. This set of equipment and its subsequent analogs were widely used for fabrication of fuel tanks for liquid hydrogen and oxygen of Space Shuttle system [21–23]. In 1990s, Hobart Brothers Inc. stopped manufacturing equipment for VPPA welding process. At the same time, the demand of US space industry in the field of PAW of aluminium alloys by variable polarity asymmetrical current is satisfied by products of Liburdi, Canada (LTP400-VP power source) (Figure 5) and AMET, USA (VPC450 power source). High cost of equipment and complexity of operation did not promote wide acceptance of this welding process by industry.

VPPA welding at asymmetrical current was the most effectively applied for gravity welding of joints without using backing elements with forming grooves. Such a process was called «keyhole» (Figure 6). In this process the plasma jet penetrates right through the weld pool molten metal, forming a through-thickness channel, which exists during the entire period of welding. Through-thickness penetration of the plasma jet completely eliminates oxide film inclusions in the weld, and also reduces item deformation, due to homogenizing of heating of the parts being welded by height. 100 % argon was used as plasma gas, and 100 % helium was the shielding gas.

More active application of PAW of aluminium alloys by variable polarity asymmetrical current began from 2000s. In Europe, a number of such companies as Merkle (Germany), EWM (Germany), Castolin (Switzerland), SBI (Austria), Migatronic Automation (Denmark) started batch production of equipment for PAW by variable polarity asymmetrical current with rectangular waveform. Some of these systems — Tetrix 350 AC/DC Plasma (EWM) and PMI-380 AC/DC (SBI), can be used both for automatic and for manual PAW of aluminium alloys.

At the start of 1990s, PWI performed investigations of PAW of aluminium alloys by variable polarity asymmetrical current with rectangular

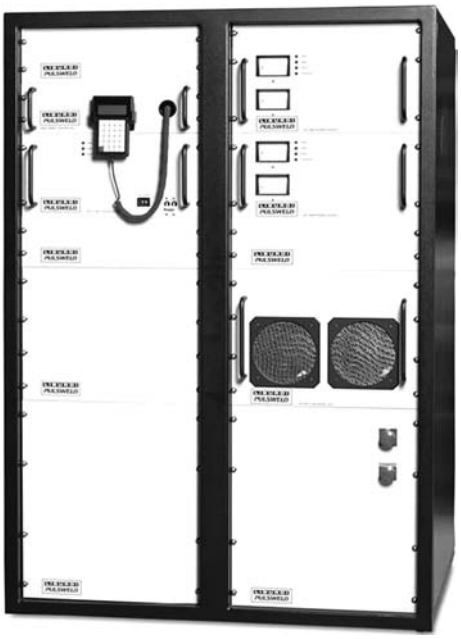

Figure 5. Appearance of LTP400-VP power source (Liburdi) for welding by VPPA process [18]

waveform using thyristor power sources with inductive energy storages. Investigation results showed that just temporary asymmetry is sufficient for sound weld formation, i.e. prevalence of the time of straight polarity current flowing and equality of straight and reverse polarity current amplitudes [24, 25].

In 2001, Fronius (Austria), based on PWI technical assignment developed a set of equipment for PAW of aluminium alloys by variable polarity asymmetrical current with rectangular waverform. The complex includes MW450 power source, FPM plasma module, filler wire feed

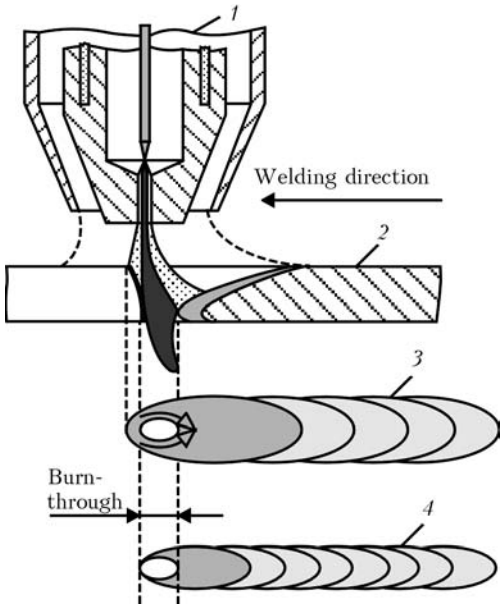

Figure 6. Block diagram of PAW in «keyhole» mode (ISF Aachen scheme) [22]: *1* — plasma torch; *2* — weld; *3* — weld surface; *4* — weld root

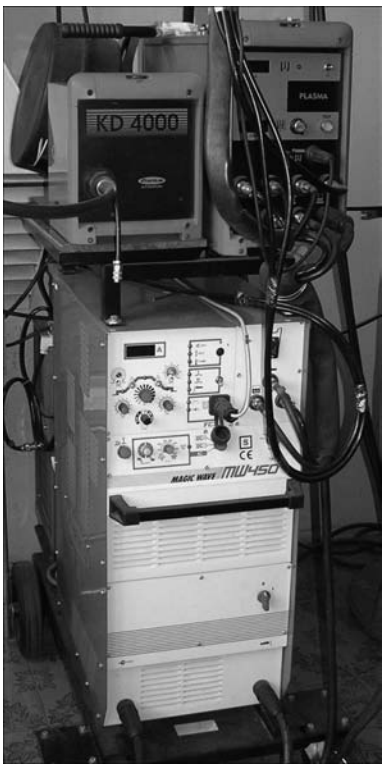

Figure 7. Fronius equipment for PAW of aluminium alloys by variable polarity asymmetrical current

mechanism KD 4000, plasmatron displacement system, welding process control system FPA 2003-Plasma, and independent water cooling unit (Figure 7). This equipment complex was used in PWI to develop a technology of PAW of aluminium–lithium alloys by variable polarity asymmetrical current [26, 27].

Unlike equipment for PAW of aluminium alloys of other companies, PAW system from Fronius is made by power source–plasma module scheme. Such a design allows selection of a power source of required power to solve the defined tasks. If not more than 150 A welding current is applied during operation, it is possible to use power sources of up to 220 A nominal power in the PAW system. All Fronius batch-produced power sources for nonconsumable-electrode argon-arc welding by variable polarity asymmetrical current (power sources of MW series) can be used as power sources for PAW.

Application of FPA 2003-Plasma system for welding process control allows significant expansion of the capabilities of PAW of aluminium

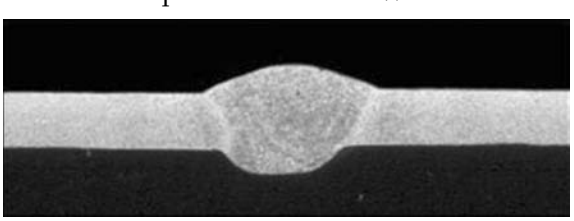

Figure 8. Macrosection of welded joint of D16 alloy 2 mm thick produced by PAW in downhand position

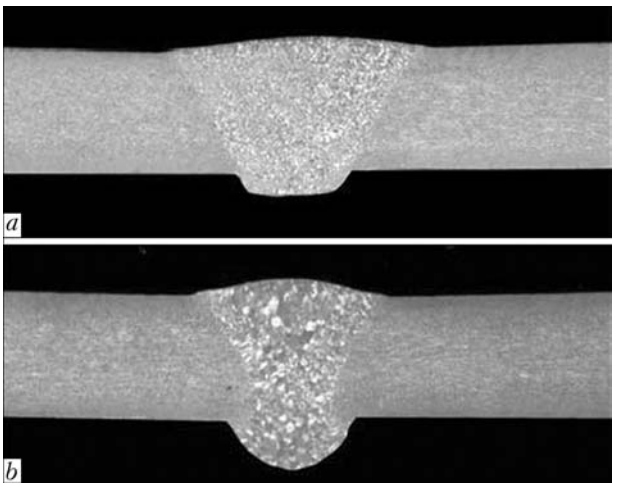

Figure 9. Macrosection of welded joint of 6 mm alloy 1420 (Al–Li–Mg) produced by downhand PAW on a backing with forming groove (*a*) and in keyhole mode of plasma jet through-thickness penetration (*b*)

alloys by variable polarity asymmetrical current. So, the possibility of pulsed feed of plasma gas allows effectively preventing porosity in aluminium alloy welding, and welding current modulation and filler wire feeding at variable rate provides sound formation of welds in orbital welding of position butt joints. Investigations conducted at PWI confirmed that more precise regulation of parameters of PAW by variable polarity asymmetrical current, using FPA 2003-Plasma welding process control system, allows application of this welding process to produce permanent joints of thin (1–2 mm) aluminium semifinished products (Figure 8), as well as to perform welding in the mode of through-thickness penetration of the plasma jet (Figure 9) [27].

Availability of machine and manual plasmatrons in the equipment range, as well as switching of plasma module operation allows equally efficient application of Fronius equipment for both automatic and manual plasma welding.

At present FPM plasma module has already been removed from production, and the new PlasmaModule-10 with digital control, unfortunately, does not provide PAW by variable polarity asymmetrical current.

Over the recent years several approaches have emerged to development of equipment for PAW of aluminium alloys by variable polarity asymmetrical current, namely development of specialized PAW systems and plasma modules (consoles) for connection to batch-produced power sources for tungsten electrode welding. In our opinion, application of additional plasma modules for creation of PAW system based on power sources for nonconsumable electrode welding will allow reduction of costs for setting up a welding station for constricted arc welding, improvement of versatility of

equipment complex application, variation of the value of required power of welding sources, more complete realization of the technological capabilities of modern power sources for nonconsumable electrode welding.

Laser-plasma welding of aluminium alloys. Laser beam, being electrically neutral, can combine readily with consumable and nonconsumable electrodes at running in a common pool. Laser beam combines equally well in hybrid welding processes with nonconsumable-electrode constricted arc, running both at DCRP and variable polarity asymmetrical current. Hybrid laser-plasma welding of aluminium alloys allows narrowing the weld, increasing the penetration depth and welding speed, compared to regular PAW [28, 29].

Plasma-arc welding with powder application as filler. Aluminium alloy wire was traditionally used as filler material in PAW of aluminium alloys, both by direct and variable polarity current. Scientists of Chemnitz and Ilmenau Universities (Germany), suggested application of aluminium powder as filler material in PAW of aluminium alloys [30]. Aluminium powder application in PAW has several advantages, namely, interference from filler wire guides at movement of robotic «arms» is eliminated, it is possible to select filler material composition in a broad range, and quickly change the welding direction without turning the plasmatron with wire feed system fastened on it. The main disadvantage of application of aluminium powder as filler material is the large area, covered by oxide film, compared to filler wire. Extensive powder surface coated by oxide film, limited application of this welding process for joining less than 2 mm thick parts. The oxide film does not effectively break up in the arc at small values of welding current. At this moment the possibility of increasing arc power through application of helium-containing mixtures is being studied [31].

Two-sided plasma-arc welding and nonconsumable electrode welding. US scientists proposed joint application of plasmatron and nonconsumable electrode torch for aluminium alloy welding (Figure 10). In such a scheme the nonconsumable electrode torch is connected to the item instead of the cable mass [32]. Constricted nonconsumable electrode arc and freely expanding nonconsumable electrode arc, powered by one source, are simultaneously applied to the item from different sides. Such simultaneous arcing increases the voltage of both the arcs and penetration depth, and also improves the stability of through-thickness channel in welding in the mode of through-thickness penetration of the plasma arc [33].

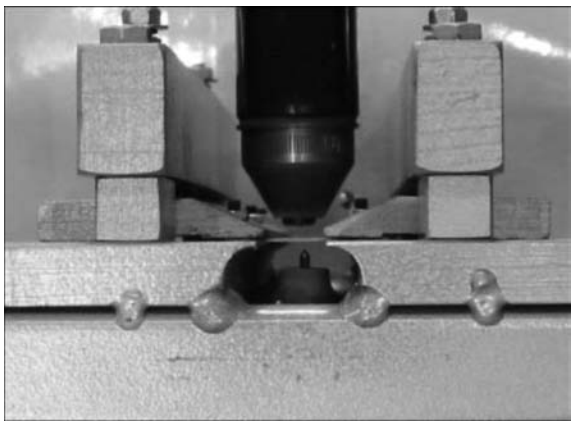

Figure 10. Two-sided PAW and nonconsumable electrode welding [32]

Combined application of plasma-arc welding and consumable electrode welding. Modern development of fabrication of aluminium structures, in particular, for extended constructions of ground and sea transportation, requires increasing the welding speed. One of the methods to solve such a task can be combined application of several welding processes, for instance, PAW and consumable electrode welding. So, in 2002–2005, PWI developed a technology of combined application of PAW by variable polarity asymmetrical current without filler material and consumable-electrode argon-arc welding (Figure 11). The distance between the two heat sources was 65 mm, and common weld pool was absent. Nonconsumable electrode constricted plasma arc performed item heating and partial removal of hydrogen from the metal being melted. Weld convexity was formed due to electrode wire melting. Combined application of PAW by variable polarity asymmetrical current and consumable-electrode argon-arc welding at

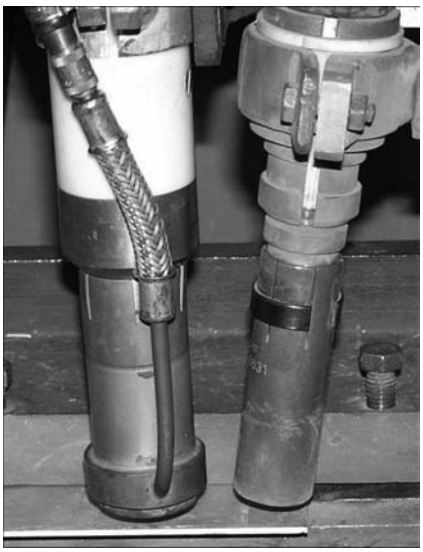

Figure 11. Position of plasmatron and consumable electrode torch at combined application of PAW and consumable electrode arc welding

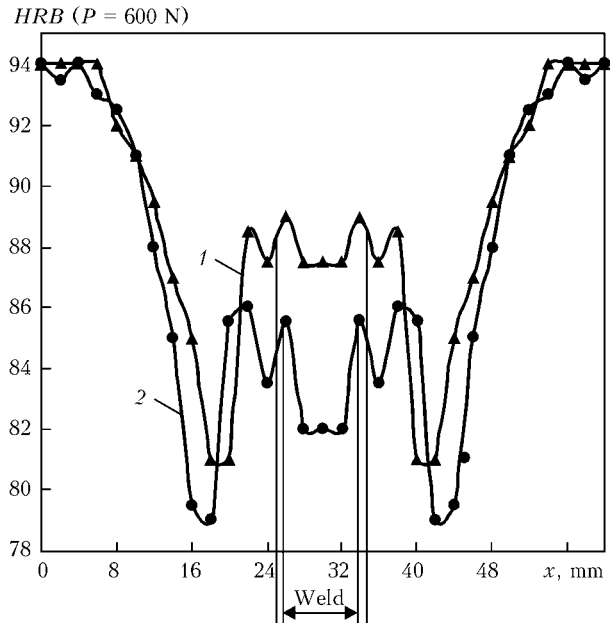

Figure 12. Hardness of deposits on 12 mm AMg6N alloy produced at combined application of PAW and consumable electrode welding (*1*) and at regular consumable electrode welding with filler wire of SvAMg6 grade (*2*)

achievement of the same penetration depth as that in regular consumable-electrode argon-arc welding, allows reducing the width of the weld and base metal softening zone in welding, as well as the degree of this softening (Figure 12).

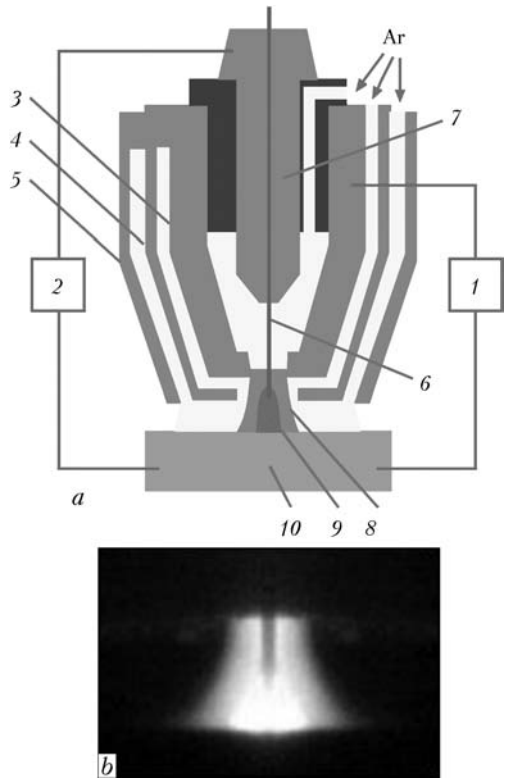

Figure 13. Schematic of the process (*a*) and appearance of consumable electrode welding arc: *1* — constricted plasma arc power source; *2* — MIG-arc power source; *3* — nonconsumable electrode; *4* — stabilizing nozzle; *5* — shielding nozzle; *6* — consumable electrode; *7* — current conduit; *8* — constricted plasma arc; *9* — MIG arc; *10* — item

Hybrid consumable-electrode plasma-arc welding. One of the promising directions of development of the processes of aluminium alloy PAW is application of simultaneous arcing from several heat sources into a common pool, such as nonconsumable electrode constricted arc and consumable electrode arc, to form the weld pool (Figure 13). It was called Plasma-MIG abroad. This process was mentioned in 1970s, and the first patent for this welding process is owned by Philips Corporation [34]. Consumable electrode arc runs inside a nonconsumable electrode constricted arc. At present there exist two main schematics of this process realization: with annular anode (Figure 14) and with lateral position of the anode (Figure 15). Such a hybrid application of both the arcs allows reducing electrode metal spatter, increasing penetration depth and welding speed, and applying the process for welding thick items with groove preparation.

Investigations of hybrid consumable-electrode PAW are pursued in many universities in the world, in particular, at Chemnitz Technical University (Germany). A device was developed there, providing switching on and simultaneous operation of power sources for nonconsumable-electrode PAW at DCRP and power sources for consumable electrode welding at DCRP [35]. Investigations in this direction are also conducted at SLV Muenchen (Germany). Similar research is performed at Perm State University (Russia) [36, 37]. In Ukraine consumable-electrode PAW was studied at Priazovsky Technical University [38]. Features of the process of consumable-electrode PAW were also studied in China, Japan and Brazil [39, 40].

TBI (Germany) set up manufacture by individual orders of PLM 500 and PLM 600 torches with annular anode for consumable-electrode PAW, which can stand up to 250 and 300 A current load of DCRP for the torch plasma part and consumable electrode assembly, respectively (see Figure 14).

Plasma Laser Technologies Ltd. (Israel) proposed a process of hybrid consumable-electrode PAW, called Super-MIG, which involves simultaneous running of nonconsumable electrode constricted arc and consumable electrode arc into a common pool. Consumable electrode arc runs to the side of nonconsumable electrode arc (see Figure 15) [41].

Despite the high interest to hybrid consumable-electrode PAW with axial feed of electrode wire, batch-production of equipment for realiza-

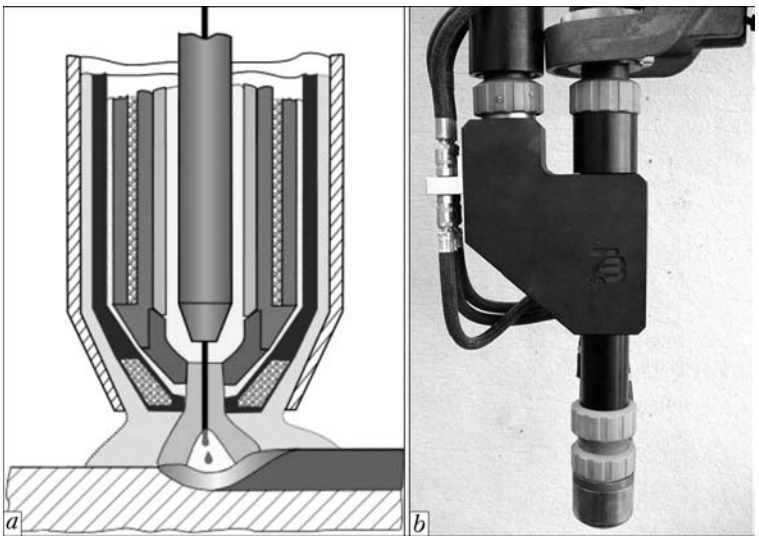

Figure 14. Schematic of the process of hybrid consumable-electrode PAW with annular hollow anode and axial feed of electrode wire (*a*) and PLM 500 welding head of TBI for this method of welding (*b*)

tion of such a process has not been organized. Such equipment has a limited range of functions that significantly narrows the technological capabilities and application of this process.

In 2014–2015, PWI within a cooperation project with Chinese-Ukrainian E.O. Paton Welding Institute developed a versatile complex of equipment PLAZER PW-HYBRID TC for plasma-arc, combined and hybrid welding. Equipment manufacturer is Science-Production Center «Plazer» (Figure 16). This equipment complex allows realizing a broad range of plasma and arc processes: performing PAW with filler wire at DCSP and DCRP and variable polarity asymmetrical current, hybrid consumable-electrode PAW with annular anode of the plasmatron and with axial feed of electrode wire, combined welding by constricted arc and consumable electrode in «soft plasma» mode (soft plasma arc welding), and automatic consumable and non-consumable electrode welding.

For realization of such a range of technological capabilities, this equipment is made to have modular design and includes the following main units:

- welding process control system, providing control of power sources, filler wire feed mechanisms, independent cooling modules, versatile multi-position manipulator for performance of various welding processes;
- inverter power source for welding plasmatron;
- inverter power source for consumable electrode;
- module for coordinating the operation of plasma welding and consumable electrode welding power sources in «Plasma + MIG» mode (hybrid and combined consumable-electrode PAW modes);
- plasmatron module for machine hybrid PAW «Plasma-MIG» with axial wire feed with cable hosepack;
- monoblock for combined «Plasma + MIG» welding with cable hosepack;

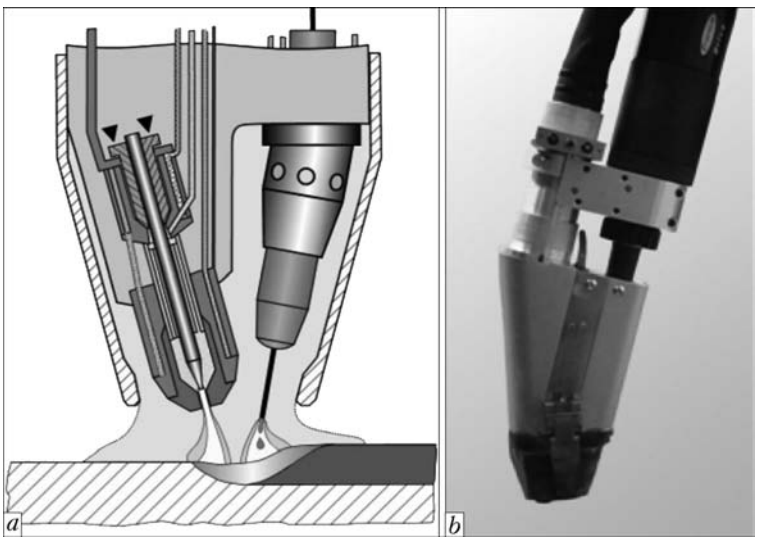

Figure 15. Schematic (*a*) and welding torch for Super-MIG process (*b*) [41]

Figure 16. Appearance of versatile equipment complex PLAZER PW-HYBRID TC for plasma-arc, combined and hybrid welding in different positions

• filler wire feed mechanism for hybrid PAW «Plasma-MIG»;

• electrode wire feed mechanism for hybrid consumable-electrode PAW «Plasma + MIG»;

• independent cooling module for plasmatron and consumable electrode torch;

• multiposition welding manipulator for hybrid plasma welding in the downhand position, on vertical plane (including performance of vertical and horizontal welds on vertical plane), as well as for welding cylindrical parts.

In addition, the functions of this equipment provide the possibility of operation in a complex with welding robot instead of welding manipulator. For this purpose an interface is envisaged in the machine control system and in power sources for connection to a robot with communication protocols applied for the main types of advanced welding robots.

Figure 17. Plasmatrons developed by PWI for nonconsumable-electrode (*a*) and hybrid consumable-electrode (*b*) PAW

This equipment complex PLAZER PW-HYBRID TC (see Figure 16) allows making welds in the downhand position, vertical and horizontal welds on vertical and inclined planes. Availability of rotating welding positioner in the system design allows performance of circumferential welds by the above techniques. The complex is fitted with plasmatrons for nonconsumable and consumable electrode welding, developed by PWI (Figure 17).

In conclusion the following can be noted. PAW of aluminium alloys was developing as a continuation of nonconsumable-electrode argon-arc welding with sinusoidal AC. The first apparatuses were based on power sources for nonconsumable electrode welding with alternating current. However, instability of running of sinusoidal AC arc, when passing through zero line, and considerable heating of plasmatron electrode assembly limited the possibility of wide application of PAW at sinusoidal AC of commercial frequency, both in FSU territory and abroad.

The next stage of development of PAW of aluminium alloys is application of DCRP for powering the constricted arc. This process has several advantages: equipment design simplicity, good cleaning of the surface of aluminium alloys and weld pool from oxide film inclusions. Large width of welds, higher susceptibility to hydrogen porosity formation, considerable overheating of plasmatron electrode assembly, leading to increase of plasmatron overall dimensions, should be regarded as disadvantages of this process, as well as greater wandering of DCRP constricted arc at small current amplitudes. At this moment this welding process is used occasionally, both for production and for research purposes.

Development of the next generation of power sources with rectangular current waveform for PAW allowed regulation in a broad range of straight and reverse polarity current amplitude, duration of straight and reverse polarity current flowing, as well as frequency of variable polarity current. Welding current form close to a rectangular one, simplified the processes of nonconsumable electrode arc excitation during reverse polarity half-wave at its transition through zero. Appearance of power sources with the possibility of creation of amplitude and time asymmetry of welding current provided a new impetus for development of PAW of aluminium alloys. In particular, VPPA welding process was the main one in manufacture in 1980–1990s of cryogenic fuel

tanks from high-strength aluminium–lithium alloys for Space Shuttle system.

Simplification of the design of equipment for PAW by variable polarity asymmetrical current, as well as its cost reduction, is a favorable factor for introduction of this method not only into aerospace industry, but also into other mechanical engineering industries. Transition from specialized systems for PAW to modular design of the complex of equipment for PAW based on batch-produced sources for nonconsumable electrode welding also has a positive effect. Modular design in development of the equipment complex allows more precise adjustment for production engineering tasks.

Further promising direction of development of PAW of aluminium alloys is combined and hybrid application of two and more heat sources at welded joint formation. This will allow increasing the welding speed, reducing electrode metal spatter, and lowering the level of welded structure distortion. One of the promising fields is hybrid consumable-electrode PAW with plasmatron hollow annular anode and axial feed of electrode wire.

1. Gage, R.M. *Arc torch and process*. Pat. 2806124 US. Publ. 10.09.1957.
2. Lathi, K., Jenstroem, P. (1999) Plasma welding aluminium. *Svetsaren*, **3**, 26–28.
3. Dzelnitzki, D. (2000) Aluplasmaschweissen: Gleich- oder Wechselstrom? *Technica (Suisse)*, 49(**10**), 44–53.
4. Dudko, D.A., Lakiza, S.P., Vinogradsky, F.M. et al. (1966) Alternating current constricted arc welding. *Avtomatich. Svarka*, **7**, 47–49.
5. Dudko, D.A., Kornienko, A.N. (1967) Thermal effectiveness of alternating current plasma arc welding process. *Ibid*., **11**, 27–30.
6. Rubinchik, Yu.L. (1974) *Mechanized welding of hull structures from aluminium alloys*. Leningrad: Sudostroenie.
7. Cooper, G., Palermo, J., Browning, J.A. (1965) Recent developments in plasma welding. *Welding J*., 44(**4**), 268–276.
8. Bykhovsky, D.G., Belyaev, V.M. (1971) Specifics of weld formation in plasma (constricted) arc welding of reverse polarity. *Svarochn. Proizvodstvo*, **9**, 25–26.
9. Bykhovsky, D.G., Belyaev, V.M. (1971) Power characteristics of plasma arc at reverse polarity. *Avtomatich. Svarka*, **5**, 27–30.
10. Nekrasov, S.A., Salkin, G.P., Bychkov, A.S. et al. (1976) Application of plasma arc welding in production of cryogenic equipment from aluminium alloys. *Svarochn. Proizvodstvo*, **4**, 16–17.
11. Gorbach, V.D., Bochkarev, V.P., Nazaruk, V.K. (2009) Technology of plasma welding of aluminium alloys. *Mir Svarki*, **3**, 22–25.
12. Kiselev, G.S. (2010) *Development of plasma welding technology of AMg5 aluminium alloy with pulsed feed of plasma-forming gases*: Syn. of Thesis for Cand. of Techn. Sci. Degree. Tula.
13. Tatarinov, E.A., Kiselev, G.S. (2009) To calculation of volt-ampere characteristic of plasma welding with pulsed feed of argon or helium. *Svarka i Diagnostika*, **5**, 11–14.
14. Bychkovsky, S.L., Novikov, O.M., Radko, E.P. et al. *Method of plasma arc welding*. Pat. 2351445 Russia. Appl. 2007121870/02, 14.06.2007.
15. Ruge, J., Lutze, P., Norenberg, K. (1989) Eignung von Aluminiumdruckguss zum Plasma- und Elektronenstrahlschweissen — Entgasungmechanismen und Nahtgute. *Schweissen und Schneiden*, 43(**7**), 327–332.
16. Schweinkhart, G. *Plasma welding torch*. Pat. 6215089B1 US. Pat. 10.04.2001.
17. Paton, B.E., Dudko, D.A., Gvozdetsky, V.S. et al. *Method of plasma welding*. USSR Author's cert. 221477. Int. Cl. B 23K9/16. Appl. 1164345/25–27, 17.06.67.
18. Cert. 73735584 of VPPA trade mark registration. *http*://www.tmfile.com/mark/?q=737355845. Latest appeal 16.07.2015.
19. Micheli, J., Pilcher, C. (2000) Advanced variable polarity plasma arc welding. *The Fabricator*, **November**.
20. Nunes, A.C., Bayless, O.E., Jones, C.S. (1983) *The variable polarity plasma arc welding process: Its application to the Space Shuttle External Tank*: 1st report, June. Marshall Space Flight Center.
21. Clower, F.R. (1980) Welding of the external tank of the Space Shuttle. *Welding J*., 54(**8**), 17–26.
22. Tomsis, M., Barhorst, S. (1984) Keyhole plasma arc welding of aluminium with variable polarity power. *Ibid*., 63(**3**), 25–32.
23. (1998) Lockheed Martin Michoud Space Systems. *Weld. Des. and Fabr*., 71(**11**), 32.
24. Brik, E.Yu. (1989) Alternating current plasma arc welding of aluminium alloys. In: *Abstr. of 1st Int. Conf. of Junior Sci. in Welding and Related Technologies* (Kiev, 16–20 May 1989), 91–92.
25. Zaparovany, A.G., Ignatchenko, G.N., Yarinich, L.M. et al. (1989) Power supply of pilot arc for variable polarity current plasma welding of aluminium. *Avtomatich. Svarka*, **9**, 73–74.
26. Labur, T.M., Grinyuk, A.A., Poklyatsky, A.G. (2006) Mechanical properties of plasma welded joints on aluminium-lithium alloys. *The Paton Welding J*., **6**, 32–34.
27. Labur, T.M., Grinyuk, A.A., Taranova, T.G. et al. (2007) Features of micromechanism of fracture in joints of aluminium-lithium alloys produced by plasma welding. *Ibid*., **9**, 11–16.
28. Krivtsun, I.V., Shelyagin, V.D., Khaskin, V.Yu. et al. (2007) Hybrid laser-plasma welding of aluminium alloys. *Ibid*., **5**, 36–40.
29. Ternovoj, E.G., Shulym, V.F., Khaskin, V.Yu. et al. (2007) Properties and structure of hybrid laser-plasma welded joints in aluminium alloys. *Ibid*., **11**, 10–15.
30. Wesling, V., Schraem, A., Bock, A. et al. (2004) Plasmapulververbindungsschweissen von Aluminumblechen. *Praktiker*, **10**, 288–294.
31. (2005) Untersuchung der metallurgischen Grundlagen zum Plasma-Pulver-Verbindungsschweissen duenner Aluminiumbleche. *Schlussbericht fuer den Zeitraum*: 1.6.2003 bis 31.5.2005. AiF Vorhaben 13.770 B/4. Technische Universitaet Ilmenau.
32. Zhang, Y.M., Zhang, S.B. (1998) Double side arc welding increases weld joint penetration. *Welding J*., **6**, 57–61.
33. Moulton, J.A., Weckman, D.C. (2010) Double side arc welding of 5182-O aluminum sheet for tailored welded blank applications. *Ibid*., **1**, 11–23.
34. *Method of plasma-MIG welding*. Pat. 3809824 U.S. Pat. 24.06.75. U.S. Philips Corporation.
35. Matthes, K.-J., Kusch, M. (2000) Plasma-MIG-Schweissen. *Praktiker*, **5**, 182–188.
36. Shchitsyn, Yu.D., Tytkin, Yu.M. (1986) Consumable electrode plasma welding of aluminium alloys. *Svarochn. Proizvodstvo*, **5**, 1–2.
37. Shchitsyn, Yu.D., Shchitsyn, V.Yu., Herold, H. et al. (2003) Plasma welding of aluminium alloys. *Ibid*., **5**, 36–42.
38. Makarenko, N.A., Nevidomsky, V.A. (2003) Thermal cycles in plasma-MIG surfacing. *The Paton Welding J*., **1**, 43–45.
39. Yan, B., Hong-Ming, G., Ling, Q. (2010) Droplet transition for plasma-MIG welding on aluminium alloys. *Transact. of Nonferrous Met. Soc. China*, **20**, 2234–2239.
40. Tiago Vieira da Cuhna, Jair Carlos Dutra (2007) Processo plasma-MIG contribuicao do arco plasma na capacidade de fusao do arame. *Soldagem Insp. Sao Paulo*, 12(**2**), 89–96.
41. (2007) Hybrid welding: An alternative to SAW. *Welding J*., **10**, 42–45.

Received 21.07.2015

APPLICATION OF N–O–C–H GAS SYSTEMS FOR SYNTHESIS OF STRENGTHENING COMPONENTS IN PLASMA COATINGS

V.N. PASHCHENKO
NTUU «Kiev Polytechnic Institute»
37 Pobeda Ave., 03056, Kiev, Ukraine. E-mail: vn.paschenko@ukr.net

Possibility of strengthening component synthesis during plasma spraying with application of plasma-chemical reactor is considered. Thermodynamic analysis of systems based on bottled gases N_2, CO_2, C_3H_8–C_4H_{10}, CH_4, as well as air (N_2 and O_2 mixture) and a number of powder materials was performed. Iron-based materials and powders with sufficiently high titanium content were selected as model ones. Fundamental possibility of producing carbides, nitrides and oxides in the condensed state is demonstrated, ranges of thermodynamic parameters, in which they exist, dependence of synthesized compound content in the system on process temperature, pressure and quantity of initial solid product were established. It is found that organization of spraying process with concurrent synthesis of strengthening components is impossible without availability of objective data on energy capabilities of plasma equipment, consisting of plasmatron–plasma-chemical reactor complex. A series of experiments were performed on plasma coating spray-deposition and testing them for abrasive wear. 8 Ref., 6 Figures.

Keywords: *complex gas systems, plasmatrons, plasma-chemical reactor, plasma spraying, strengthening component synthesis*

Rising requirements to service properties of parts and structures necessitate application of more complex compositions of materials, from which the functional surface layers are formed. Traditionally, initial material chemical composition is made more complicated by introduction of alloying elements or composite material application [1, 2]. Combination of plasma spraying with purpose-oriented chemical transformations can be an alternative [3].

Application of complex plasma-forming mixtures provides a potential possibility for running of reactions of interaction of plasma active gas components with the initial material that may result in synthesis of strengthening components in the produced coating [4, 5]. For instance, in [6] ultrafine particles of titanium nitride were found in splats produced with plasma-chemical reactor application under the conditions of supersonic spraying in nitrogen atmosphere. A number of powders were selected, after analyzing the possible variants of formation of strengthening components, which can be synthesized in plasma-forming media of N–C–H–O, N–C–H or N–O system, and taking into account the condition of availability of initial materials, on the base of which synthesis will be performed. These materials are batch produced and are available in the market of Ukraine [7]. They can be conditionally subdivided into four main groups:

- iron-based materials (PZh R3, self-fluxing iron-based), in which iron carbides and, partially, silicon and chromium carbides (in the case of presence of these elements in the initial material) can form; alternatively, the initial material can be strengthened by synthesized iron oxides;
- nickel-based materials (PG-10N-03, PKh40N60, PG-SR3, PG-SR4, PG-19N-01), which have sufficiently high content of carbide-forming components — chromium, silicon, boron in their composition;
- materials, containing considerable amount of titanium (PT65Yu35, PN55T45), and in which nitride and carbide synthesis is possible;
- aluminium-based materials (PAD, ASD-T, PT65Yu35, PN70Yu30), in which strengthening components of aluminium oxide can form under certain conditions.

Thermodynamic calculations were conducted with application of TERRA software package. Systems, based on the above spraying materials and N_2, CO_2, C_3H_8–C_4H_{10}, CH bottled gases, as well as air (N_2 and O_2 mixtures), were studied. Fundamental possibility of producing carbides, nitrides and oxides in the condensed state was established, as well as the range of thermodynamic parameters, in which they exist, and dependence of these compounds content in the system on process temperature, pressure and quantity of initial solid product.

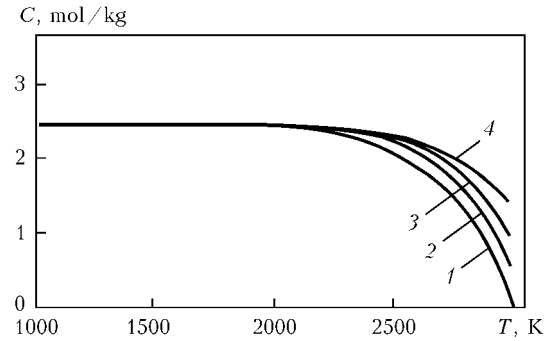

Figure 1. Dependence of target product (40.39 % Fe, 35.38 % N_2, 24.23 % C_3H_8) yield on process temperature: *1* — pressure of 0.1; *2* — 0.3; *3* — 0.3; *4* — 0.4 MPa

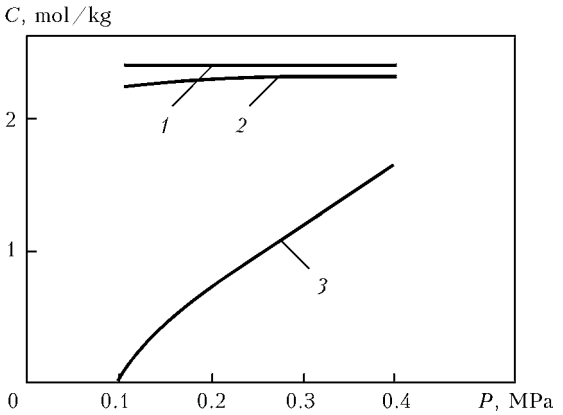

Figure 2. Dependence of target product (40.39 % Fe, 35.38 % N_2, 24.23 % C_3H_8) yield on pressure in reaction space: *1* — T = 1000–2000; *2* — 2500; *3* — 3000 K

Special attention was given to two materials, which had been selected as model ones: iron and nickel–titanium. We will assign Fe_3C iron carbide as the target product, which will be synthesized at spraying of iron-based powder. Fe_3C synthesis is possible in the presence of a sufficient amount of carbon in the system and prevention of its binding by plasma medium oxygen. Among the possible variants of reaction medium composition, which were studied, the composition formed by plasma-forming nitrogen and propane turned out to be the most effective. Propane was fed into pre-formed gas-powder flow within the plasma-chemical reactor.

Figures 1 and 2 show the dependencies of the yield of iron carbide condensed phase on process temperature and pressure in the reaction volume. Presented dependencies reveal that the temperature range of target product (Fe_3C condensed phase) yield depends on the content of hydrocarbon gas in the reaction medium. Within this temperature range, the level of target product yield practically does not change.

Temperature range is maximum wide in the case of hydrocarbon gas content of 19–25 wt.% and becomes narrower in the case of going beyond this interval with appearance of explicit maximum of product yield at 1800–1900 K. Exceeding 2500 K temperature level markedly reduces the product yield. It is found that pressure in the zone of plasma-chemical reaction running practically does not influence the target product yield within the process working temperature range, and has a significant influence on temperature range boundaries. Figure 3 shows the dependencies of target product yield on the quantity of loaded initial material under the condition of unchanged quantity of the gaseous phase, and of target product yield on the quantity of hydrocarbon gas, fed into the reaction zone.

Increase of hydrocarbon component content from 8.6 to 12.4 wt.% increases the carbide yield practically 2 times, but further increase of hydrocarbon gas quantity in the system practically does not lead to increase of synthesis process efficiency.

Increase of the quantity of loaded initial material, proceeding from calculation results, reduces the quantity of synthesized product (provided the values of other mode parameters remain unchanged).

Presence of a small (up to 45 wt.%) quantity of titanium in PN55T45 alloy composition creates the prerequisites for possible synthesis of tita-

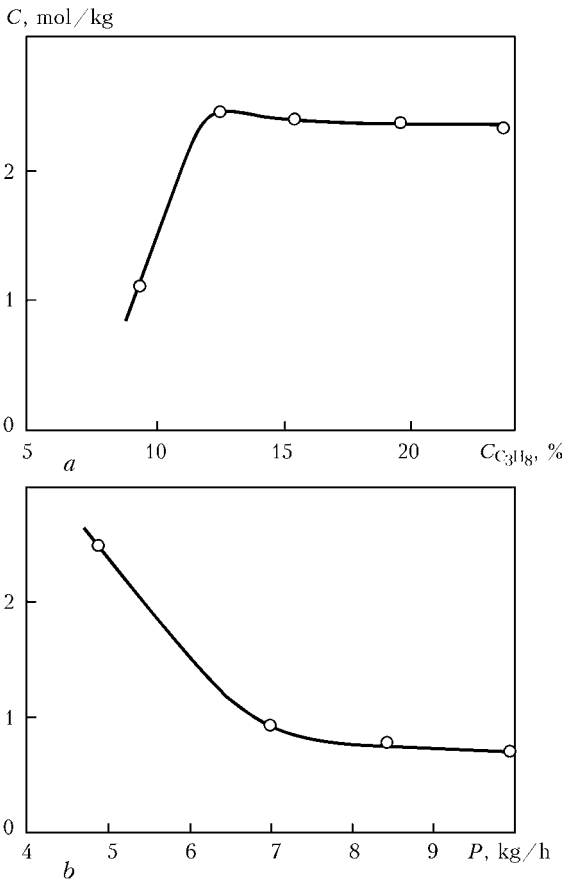

Figure 3. Dependence of synthesized carbide quantity on propane content in reaction medium (*a*) and quantity of loaded dispersion material (*b*)

nium nitride (TiN). High activity of titanium makes higher requirements to reaction medium composition. Preliminary estimates show the rationality of application of plasma-forming nitrogen, in order to create the conditions for titanium nitride synthesis, with subsequent addition of reaction nitrogen into the pre-formed gas-powder flow within the plasma-chemical reactor.

According to calculations, temperature range of target product (TiN condensed phase) yield depends on the ratio of interacting solid and gaseous phases, and in the studied range of this ratio change it becomes narrower at lowering of gaseous phase content. Increase of nitrogen content from 75.77 to 86.22 wt.% widens the temperature range by 100 K. In this case, absolute quantity of synthesized nitride will rise.

Pressure increase in the reaction space widens the temperature range of existence of titanium nitride condensed phase. Thus, it is rational to conduct the process of heating of dispersed nickel–titanium material within the plasma-chemical reactor at nitrogen content of 75–85 wt.%, in the temperature range of 2000–2400 K and about 0.1 MPa pressure in the reaction medium. Under these conditions, required fixing of synthesized product is performed by feeding hardening nitrogen into the reactor end part.

Process of coating deposition with simultaneous synthesis of strengthening components is implemented in a special spraying device, which consists of plasma sprayer and plasma-chemical reactor, tightly and rigidly combined in one unit.

Initial material together with carrier gas is fed into plasmatron arc channel. A jet of high-temperature gas flows out through outlet electrode orifice into reaction space (within the plasma-chemical reactor), in which the dispersed material is heated and accelerated.

During heating the material of initial particle surface layer evaporates with temperature rise with formation of a vapour cloud around the liquid or ductile core. Additional gas is fed into reaction space behind plasmatron nozzle edge. As a result of interaction with it, synthesis of appropriate chemical compound begins in the vapour phase surrounding the particles. Part of synthesized strengthening component can condense on the surface of carrier-particles, and the other part is in the gaseous phase around the core.

At reaction zone outlet hardening gas is fed into the unit, which, while lowering system temperature, creates the conditions for condensation of formed refractory compound on the surface of carrier-particles. Here, the particle proper remains in the liquid or ductile state, that promotes the process of mixing of the particle liquid surface layer with the condensed compound and coagulation of synthesized ultrafine particles with those of initial material.

Strengthening component composition depends on chemical composition of initial material, plasma, carrier, reaction and hardening gases.

Process of synthesis of coating strengthening components during heating and acceleration of initial material envisages application of plasma generators, capable of creating flows of low-temperature plasma from complex, reactive gaseous plasma-forming mixtures in a broad range of variation of energy parameters, and, in particular, of specific enthalpy. Plasma flow components should take an active part in synthesis, or, at least, not hinder its running.

Successful practical implementation of the process is possible in the case of availability of sufficiently complete data on energy characteristics of the used plasmatron and their interrelation with plasma generation mode parameters. Comprehensive studies of the above characteristics of plasmatrons, generating plasma of N–O–C–H system [8], allowed application of exactly this gas system for producing strengthened plasma coatings. In the specific case, straight polarity two-electrode plasmatron with stepped anode of up to 35 kW total power was used, which is capable of stable operation in nitrogen, air and mixtures of air with hydrocarbon gases (methane, propane, butane).

Proceeding from the results of these studies, criterial dependence of specific enthalpy on mode and geometrical parameters of plasma sprayer operation was established. This dependence is the basis for preliminary calculation of mode parameters of the process, at which strengthening components synthesis is possible with maximum yield of synthesized product during coating deposition.

In the simplified variant (for the applied design) in the case of air application, the criterial dependence has the following form:

$$\varepsilon = 3.984 I^{0.648} Q_{\text{air}}^{-0.33} d_1^{0.092} d_2^{-0.035} p^{0.357}, \quad (1)$$

where I is the arc current, A; Q is the plasma gas flow rate, m^3/h; d_1 and d_2 are the diameters of the narrow and wide part of outlet electrode arc channel, mm; p is the pressure at plasmatron inlet, N/m^2.

For nitrogen:

$$\varepsilon = 3.684 I^{0.66} Q_{\text{N}}^{-0.318} d_1^{0.092} d_2^{-0.058} p^{0.357}. \quad (2)$$

For a mixture of hydrocarbon gases with air (without combustion within the plasma-chemical reactor):

$$\varepsilon = 0.273 I^{0.6} Q_{\Sigma}^{-0.214} d_1^{-0.297} \times \times d_2^{0.303} p^{0.633} (l/l_1)^{-0.034} n^{0.099}. \quad (3)$$

For a mixture of hydrocarbon gases with air (with running of the process of mixture component combustion within the plasma-chemical reactor):

$$\varepsilon = [0.273 I^{0.6} Q_{\Sigma}^{-0.214} d_1^{-0.297} \times \times d_2^{0.303} p^{0.633} (l/l_1)^{-0.034} n^{0.099}] + + [0.0895 a Q_{a.g} I^{-0.132} Q_{\Sigma}^{-0.69} d_1^{-0.119} \times \times d_2^{-0.059} p^{0.241} (l/l_1)^{0.079} n^{0.064}]. \quad (4)$$

Plasma-chemical reactor is a system of individual sections sequentially and tightly connected to each other. Two kinds of sections were used: sections for feeding reaction gases and feed-through sections, the purpose of which is creation of a certain reaction volume. Each feed-through section has individual water cooling. Sections for gas feeding are cooled by those gases, which are fed through them. Geometrical dimensions and configuration of all the sections (except for the first one) are unified, that allows changing the reactor overall length by increasing the number of feed-through sections. Accordingly, location of sections for gas feeding within the reactor can be also changed, depending on process requirements.

Longitudinal geometrical size of reactor inner space (time of material particles staying in the reaction zone) is determined by number of sections, used in the structure.

Reaction zone diameter was selected constant, proceeding from preliminary information about the angle of opening of the heterogeneous flow during spraying with the plasmatron of the used design (proceeding from the condition of elimination of dispersed material deposition on the reactor inner wall during the process). Overall schematic of the technological process of spraying practically does not differ from the traditional process of plasma spraying, although its individual stages have certain specific behavioural features.

Typical preparation of initial material usually envisages powder drying and its sieving to remove possible contamination and separation of fractions of a certain range, suitable for forming the coating. The proposed process envisages application of essentially narrower range of possible dimensions of individual particles. Range narrowing improves the stability and predictability of the process of strengthening component synthesis, as it runs in the vapour cloud around the particles. Reduction of initial powder particle size can lead to complete evaporation of the particle, and its increase — to its insufficient heating and slowing down of the process of surface layer evaporation.

Requirements to temperature mode of the base become more stringent. Thermal insulation of the plasma jet from the environment by reactor walls promotes preservation of high level of heat flows to the base at spraying distances. This leads to base overheating, acceleration of the processes of oxide film growing on item surface and, consequently, to lowering of the strength of coating adhesion with the base. In the case of application of gas mixture hydrocarbon components, the fragments of which burn down at reactor outlet during sucking of oxygen from the air, additional measures are required for more intensive cooling of the item as natural cooling becomes insufficient. Here, higher requirements are made to stability of parameters of plasma sprayer and initial material feed system. Random change of carrier gas flow rate and dispersed material quantity disturbs the spatial arrangement of gas-powder flow within the plasma-chemical reactor, leading to powder particle deposition on reactor walls, and destabilizes the process of plasma-chemical synthesis.

The synthesis process is also sensitive to change of working medium energy level and it can be disturbed as a result of instability of sprayer input parameters and electrode fracture because of erosion. The required nominal mode parameters of heterogeneous flow generation (arc current, plasma gas flow rate and its chemical composition, gas pressure, arc channel geometrical dimensions, reaction and hardening gas flow rates) are calculated beforehand.

The main thermodynamic parameters, determining the probability of running of plasma-chemical reaction of strengthening component synthesis (in the condensed form), are pressure and weight-average temperature in the reaction space. Temperature, in its turn, is the derivative of the amount of energy, applied to a unit of volume (mass) of reaction medium (specific enthalpy).

Schematic of preliminary determination of mode parameters for conducting the process can be as follows:

- proceeding from analysis of chemical composition of spraying material and assigned strengthening component, element composition

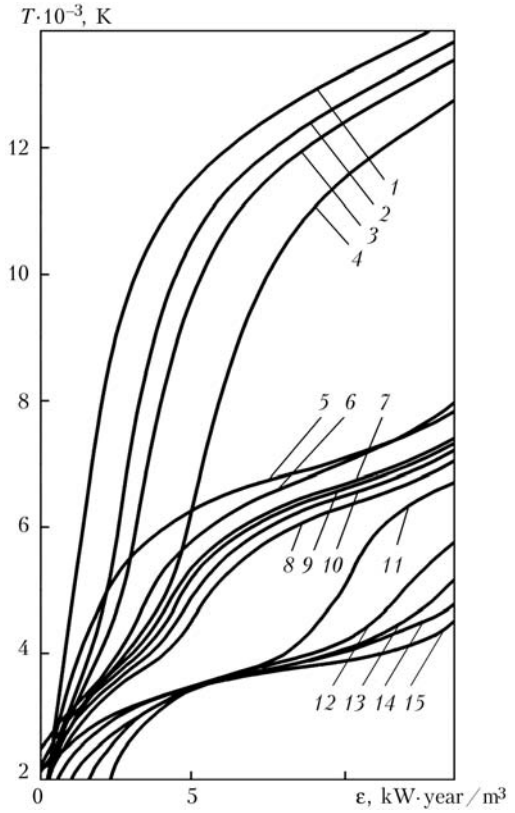

Figure 4. Dependence of plasma jet weight-averaged temperature on specific energy input into plasma gas: *1* — Ar; *2* — Ar + 15 % H_2; *3* — Ar + 25 % H_2; *4* — Ar + 50 % H_2; *5* — N_2; *6* — air; *7* — air + CH_2, α = 1; *8* — air + CH_4, α = 0.4; *9* — air + CH_4, α = 0.8; *10* — air + CH_4, α = 0.6; *11* — CO_2; *12* — products of carbon dioxide conversion of natural gas; *13* — NH_3; *14* — products of steam conversion of natural gas; *15* — H_2O

of gas system, in which the process is to be implemented, is determined;

• element composition of gas system is provided with application of the respective plasma gas, which contains the chemical elements from the required list, and reaction gas, which with its chemical composition complements the system as to chemical element list and their content;

• thermodynamic calculations of created systems (allowing for solid phase presence) are conducted in a broad range of thermodynamic parameters variation — process pressure and temperature;

• complete range of the above parameter values, in which formation of target product is possible, and values, at which product yield will be maximum, are established;

• required value of considered gas system specific enthalpy is determined (by dependencies similar to those given in Figure 4), which provides the required process temperature level (in case of ensuring appropriate pressure in reaction space);

• equations of (1)–(4) type are used to determine the required values of mode and geometrical characteristics of the process.

The process of coating spray-deposition begins from starting the plasma sprayer with complete plasma gas mixture or with its main component, at arc current, usually, below the nominal value. After the plasma sprayer has reached the working mode in terms of current, composition and flow rate of plasma gas, feeding of dispersed material into the reaction space begins.

Appearance of heated particle flow at the outlet of plasmatron–reactor system is the signal to start feeding reaction and hardening gases into the reactor. Here, the dimensions and shape of gas flow at reactor outlet change visually (Figure 5).

Functional properties of coatings from iron powder, which at this moment is the cheapest initial material for plasma spraying, can be essentially improved, by adding to coating composition iron carbides or its oxides synthesized during spraying. Selection of reaction medium chemical composition is performed, depending on chemical composition of target product. Thermodynamic calculations confirm the theoretical possibility of carbide synthesis during spraying in a mixture of carbon-containing gases.

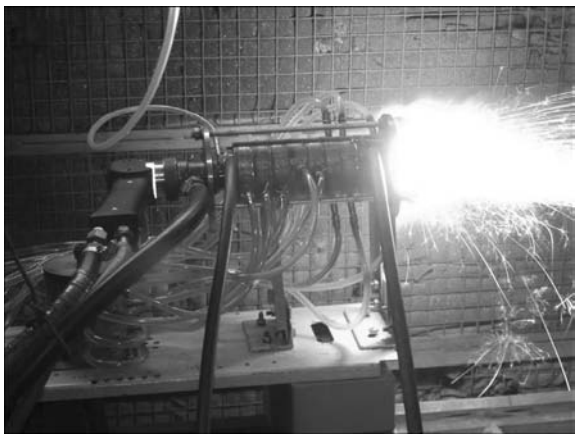

Figure 5. Process of coating spray-deposition

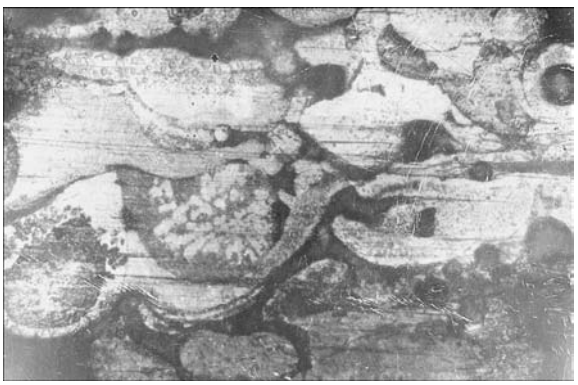

Figure 6. Microstructure (×1000) of coating, spray-deposited with PZh R3 material in a complex gas system using plasma-chemical reactor

Similar calculations show the theoretical possibility of oxide synthesis in the case of the change of spraying conditions.

In order to produce coating with synthesized iron carbide in iron matrix, the spraying process was conducted in nitrogen plasma with feeding of carbide-forming propane-butane into the reaction space.

Plasma gas flow rate was equal to 3.5 m^3/h, reaction gas flow rate was 0.7 and 1.5 m^3/h, arc current was 150 A. At these parameters voltage did not exceed 105–110 V. Coating material spraying efficiency was 5 kg/h, main size of dispersed material fraction was 63–100 μm.

Samples for spraying were mounted practically at the edge of plasma reactor last section. Spraying distance was equal to 230–250 mm, that is essentially greater than the optimum value in spraying by the traditional schematic. Increase of the distance during plasma-chemical spraying practically does not influence the value of particle velocity at the moment of colliding with the base surface and greatly increases particle temperature, as a result of limiting the air suction from the environment.

Figure 6 shows the microstructure of the produced coating. Coating has a characteristic laminated structure, which forms from molten particles. Presence of a certain quantity of particles of a globular shape, which have passed into the coating from unmolten state, is observed at the same time. All kinds of boundaries and pores are visible.

In addition to compounds, which were synthesized in the gas phase during gas medium interaction with material vapour phase and which coagulate with carrier-particles, intensive gas absorption by molten particle material occurs during spraying. Under the conditions of high cooling rates (about 10^5 K/s) gases dissolved in particles are fixed in the solid solution with formation of oversaturated solid solutions. Relaxation of metastable state leads to precipitation of ultrafine, nanosized excess phases in the cooling particles.

Quantitative microanalysis of sample microsection reveals considerable increase of carbon content: from 0.05 % in the initial material up to 5.0–5.6 % in the coating. Samples with identical coating were studied in parallel under the conditions of abrasive wear in LKI-3 instrument. The load was 150 N; fused corundum with main particle size of 300–400 μm was used as abrasive.

It is found that resistance of a sample with coating, containing a strengthening component, under identical test conditions is 7–7.5 times higher than that of a sample, sprayed without running of plasma-chemical reaction (mass loss was equal to 0.02583 g/m compared to 0.00343 g/m in a sample with strengthening component).

Conclusions

1. Use of plasma-forming media of N–O–C–H system creates prerequisites for synthesis of strengthening components (carbides, nitrides and oxides) during plasma spraying of protective coatings. Thermodynamic analysis of the respective systems allows evaluation of quantitative characteristics of target product yield and energy conditions of the process.

2. Practical realization of the technology of spray-deposition of coatings with concurrent synthesis of strengthening components is possible in case of availability of objective data on energy characteristics of applied plasma equipment and regularities of these characteristics connection to process mode parameters.

3. Results of studying coatings from PZh R3 powder reveal an abrupt (by 2 orders of magnitude) increase of carbon content in the coating, compared to initial material, and respective wear resistance increase (by more than 7 times) under conditions of abrasive wear.

1. Smirnov, I.V., Selivestrov, I.A., Chyorny, A.V. et al. (2011) Improvement of wear resistance of plasma coatings based on composite powder with SiO_2 nanoparticles. *Visnyk NTU «KhPI»*, **2**, 70–74.
2. Borisov, Yu.S., Borisova, A.L., Kolomytsev, M.V. et al. (2015) Supersonic plasma gas air spraying of cermet coatings of the (Ti, Cr)C–NiCr system. *The Paton Welding J.*, **2**, 19–25.
3. Ronald, W.S., Emerging, U.S. (1993) Thermal plasma materials processing research and development. In: *World Progress in Plasma Applications Conf. Proc.* (Palo Alto, Febr. 9–11, 1993), 1–16.
4. Pashchenko, V.M., Kuznetsov, V.D. (2002) Plasma heat sources in surface engineering processes. *Problemy Tekhniky*, **3**, 26–32.
5. Borisov, Yu.S., Petrov, S.V. (1993) Application of supersonic jets in thermal spraying technology. *Avtomatich. Svarka*, **1**, 24–34.
6. Petrov, S.V. (1997) Plasma synthesis in thermal spraying technology. *Poroshk. Metallurgiya*, **9/10**, 34–38.
7. Borisov, Yu.S., Kharlamov, Yu.A., Sidorenko, S.L. et al. (1987) *Thermal coatings from powder materials*: *Refer. Book*. Kiev: Naukova Dumka.
8. Pashchenko, V.N. (2009) Effect of the composition of plasma air-gas mixture on parameters of the plasmatron jet. *The Paton Welding J.*, **4**, 27–31.

Received 28.09.2015

EVALUATION OF THERMAL STRESSED STATE IN WELDED JOINT OF ALLOY Inconel 690

N.O. CHERVYAKOV
E.O. Paton Electric Welding Institute, NASU
11 Bozhenko Str., 03680, Kiev, Ukraine. E-mail: office@paton.kiev.ua

The results of evaluation of thermal stressed state in welded joint of nickel alloy Inconel 690 are presented. The experimental-calculation analysis of thermal processes and mathematical modeling of stress-strain state in single-pass welding was performed. The verification of the data by comparing the experimental thermal cycles with the calculated ones showed a good similarity of results of both as to the sizes of a weld as well as to the thermal cycles in the zones at the different distance from the fusion line. The kinetics of stress-strain state in different zones of welded joint was analyzed considering the probability of hot crack formation. It is shown that under the conditions of modeling linear one-pass welding of plates of 3 mm thickness with energy input of 304 J/mm the arising stresses and deformations do not exceed the critical values and, at the same time do not create the conditions for hot crack formation. The applied mathematical model can be used in evaluation of kinetics of stress-strain state for different variants of welding (change in energy input, different filler material, etc.). 7 Ref., 1 Table, 5 Figures.

Keywords: *nonconsumable-electrode arc welding, nickel alloys, thermal processes, thermal cycles, mathematical modeling, stresses, deformations*

The nickel-based alloys play an important role as corrosion-resistant materials in the nuclear and chemical industries, especially under conditions of operation at the high temperatures, considerable stresses and aggressive environments. The widely used nickel-based alloys at the present time are alloys of Ni–Cr–Fe alloying system. One of such alloys is Inconel 690 with high chromium content (30 %) [1]. The welded joints of Inconel 690 with appropriate filler materials showed a high sensitivity to hot crack formation, particularly under the conditions of welding of thick-walled structural elements. The alloys manifest the highest tendency to the formation of ductility-dip cracks [2, 3].

As was shown previously [4], the ductility-dip cracks in welding of alloys of alloying system Ni–Cr–Fe occur at the temperature range of 1050–650 °C, the value of critical deformation of crack formation ε_{cr} is about 1.2 %.

The thermal processes in fusion welding have a decisive influence on the nature and kinetics of changes in the stress-strain state, structure and properties of weld and HAZ. In this regard, the analysis of temperature fields in welding of alloys of Ni–Cr–Fe alloying system with the aim of further investigations of kinetics of stress-strain state and evaluation of tendency to hot crack formation is an urgent problem.

The aim of the work was a comparative experimental and calculation analysis of temperature fields and modeling of stress-strain state in one-pass argon-arc welding of alloy Inconel 690.

The computer prediction and calculation allow determining the temperature fields for different values of thermal power of the arc. Using the calculation procedure the efficiency coefficient of the arc is established, which varies depending on the method and conditions of welding, etc. To specify the input data of mathematical model the experimental plotting of thermal cycles and their comparison with the calculated values is required.

The recording of welding thermal cycles was carried out on the Inconel 690 specimens of 170 × × 40 × 3 mm size. TIG welding in argon without fillers was carried out at the following conditions: I_w = 72 A, U_w = 10.5 V, v_w = 7.2 m/h. The gas consumption in welding amounted to 5 l/min.

For measurements of thermal cycles of welding in the HAZ the thermocouples of type K (chromel-alumel) were used. The diameter of thermoelectrodes was 0.2 mm, the diameter of hot junction was smaller than 0.5 mm. The junction of thermocouple was produced by fusion of thermoelectrodes using manual argon arc welding. The calibration of thermocouples was carried out according to the melting temperatures of commercially pure aluminum and copper.

The record of thermal cycles was carried out in real time using ADC Expert 9018R and specialized software PowerGraph 3.0 allwoing the automatic convertion of the values of thermal EMF to the temperature.

To the surface of plates the junctions of thermocouples were fixed by capacitor-type welding, that ensured a permanent stable contact of the

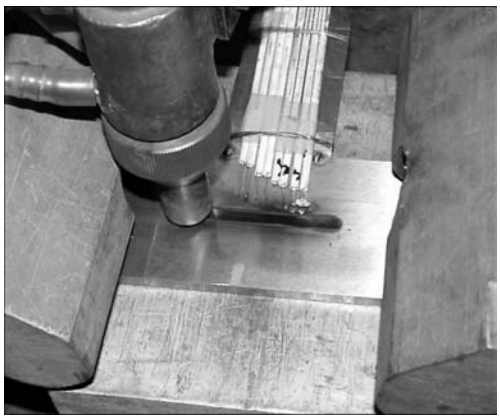

Figure 1. General view of specimen with weld and thermocouples after welding

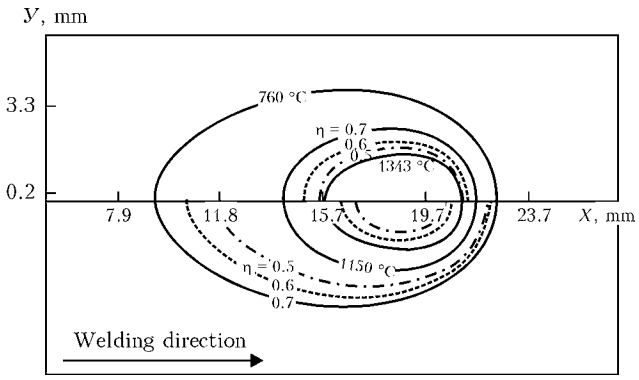

Figure 2. Influence of values of arc efficiency factor η on temperature distribution in the high-temperature region

junction with the metal in a wide temperature range. The appearance of the specimen with welded-in thermocouples after welding is shown in Figure 1.

After welding the weld and thermocouples in the HAZ were photographed in binocular microscope with 25-fold magnification and the measurement of distances from the fusion line to the thermocouple junctions was carried out. In addition, on the macrosections the weld width and penetration depth were measured.

The calculated evaluation of thermal stressed state was performed using the specialized software «Welding of nickel alloys», created on the basis of algorithms developed at the E.O. Paton Electric Welding Institute, and describing the distribution of temperatures and stress-strain state near the weld pool of complex-alloyed alloys based on nickel. For the considered plate, in the process of welding heating the temperature field $T(x, y, z, t)$ in time was determined. Then, according to the average values of temperature $T(x, y, t)$ the problem of kinetics of the stresses and deformations was solved [5, 6]. It was based on the method of successive tracking in time with pitch Δt and the finite element method in space, i.e. the considered area was represented by a totality of elementary volumes of $h_x \times h_y \times h_z$ sizes. The size of a single element in the model amounts to 0.5 × 0.5 × 0.5 mm.

For evaluation of the regularities of temperature distribution in the weld and HAZ joints using calculation method the temperature dependencies of change in heat capacity and thermal conductivity of the investigated material were used. These values for alloy Inconel 690 were chosen according to the data of literature sources, and also considering the own investigations [1, 7].

The arc efficiency factor η, used in the calculations, for TIG process amounts to 0.50–0.75. The temperature fields at the values of this factor of 0.5, 0.6 and 0.7 were calculated. Figure 2 shows that there is a significant influence of arc efficiency factor both on the heat distribution, as well on the shapes of isotherms. In modeling η = 0.70–0.75 was selected, as far as the appropriate temperature field correlates well with the experimental results.

The first stage of modeling was the determination of temperature fields, taking into account

Temperature dependence of thermophysical properties of alloy Inconel 690

Temperature, °C	Young's modulus, MPa	Yield strength, MPa	Coefficient of thermal expansion, 1/deg	Thermal conductivity, W/(cm·deg)	Heat capacity, J/(g·deg)
20	205,000	348	0.00001406	0.115	0.453
100	204,000	281	0.00001406	0.130	0.474
200	193,000	248	0.00001431	0.155	0.496
300	187,000	240	0.00001453	0.173	0.523
400	185,000	231	0.00001480	0.190	0.557
500	177,000	225	0.00001519	0.212	0.574
600	167,000	215	0.00001570	0.227	0.608
700	158,000	200	0.00001618	0.250	0.633
800	152,000	190	0.00001660	0.269	0.660
900	145,000	175	0.00001701	0.285	0.690
1000	135,000	150	0.00001741	0.303	0.715
1100	125,000	125	0.00001779	0.318	0.739
1200	100,000	100	0.00001800	0.332	0.769

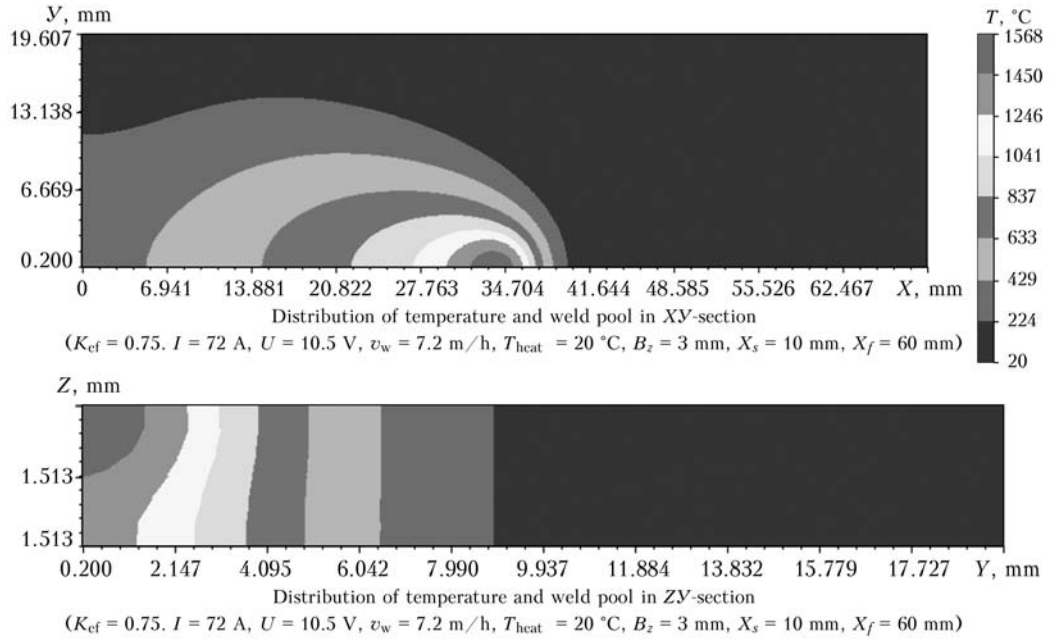

Figure 3. Distribution of temperature fields in the plane XY and across the plate thickness

the temperature-dependent properties of material (specific heat, thermal conductivity) and temperature losses as a result of convection and radiation.

The temperatures of melting and solidification were taken as 1377 and 1343 °C, respectively [1].

Figure 3 shows the results of calculation of temperature distribution along the surface of source movement at the steady state in the area of weld pool and HAZ. Due to symmetry of the solved problem a half of the plate is shown in this Figure.

The verification of the calculated temperature fields with the thermal cycles and actual sizes of the weld, measured using thermocouples, were carried out. The comparison of the data showed a good similarity of results both as to the sizes of weld (weld width and penetration depth in the experiment were 4.2 and 1.3 mm, respectively, in modeling they were 4.1 and 1.4 mm) as well as to the thermal cycles at the points at different distances from the fusion line. Thus, the validity of using the initial thermophysical characteristics for calculation of temperature distribution in welded joint in welding of alloys of Ni–Cr–Fe alloying system was confirmed.

The modeling of stress-strain state was performed taking into account the temperature dependence of physical and mechanical properties of the alloy, including modulus of elasticity, yield strength and coefficient of thermal expansion. All these characteristics were determined experimentally within the temperature range of up to 1100 °C. The yield strength and modulus of elasticity were determined in installation MTS-810, the evaluation of linear expansion coefficient was performed in the contact-free laser dilatometer. The data on thermal and mechanical properties are presented in the Table.

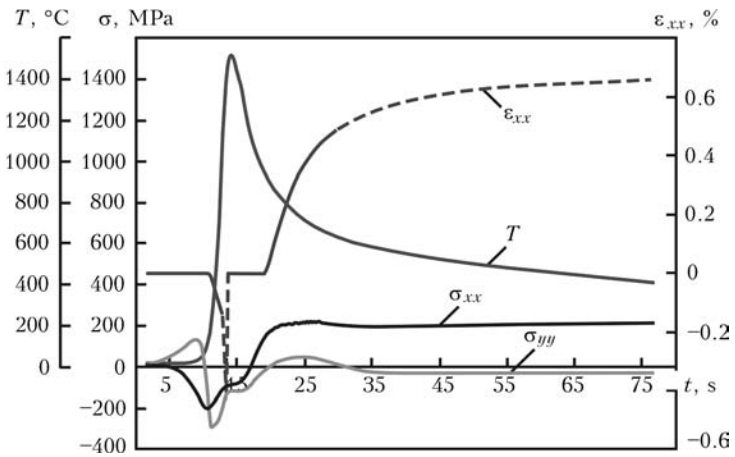

Figure 4. Kinetics of change in temperature T, longitudinal σ_{xx} and transverse σ_{yy} stresses and longitudinal plastic deformations ε_{xx} along the weld axis during welding

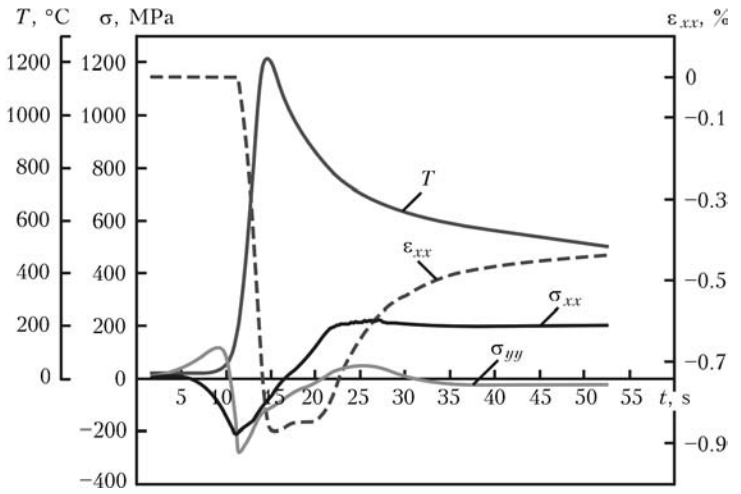

Figure 5. Kinetics of change in temperature T, longitudinal σ_{xx} and transverse σ_{yy} stresses and longitudinal plastic deformations ε_{xx} in HAZ at 0.5 mm distance from the fusion line during welding

Taking into account the calculated temperature fields the modeling of stress-strain state during welding was performed. The distributions of temporary and residual stresses and deformations for different zones of welded joint were obtained.

The investigations of weldability of alloys of Ni–Cr–Fe alloying system showed [4] that the crack formation in the weld and HAZ is possible at distance of 0.5–3.0 mm from the fusion line. In this regard, the kinetics of thermal stressed state was considered in the weld and HAZ at distance of 0.5 mm from the fusion line (Figures 4 and 5).

At the beginning of heating cycle, the metal is subjected to compressive longitudinal σ_{xx} and transverse σ_{yy} stresses. The longitudinal plastic deformations ε_{xx} are also compressive, their value reaches 0.9 %. At the subsequent cooling, the tensile stresses of both longitudinal and transverse nature occur. The longitudinal stresses reach 215 MPa and are significantly larger than the transverse ones, which are equal to 40 MPa. The longitudinal stresses reach maximum values during cooling to 650 °C. With the further cooling, the longitudinal stresses remain at a constant level, and the transverse ones are gradually decreasing. The longitudinal plastic deformations during cooling have positive increments to 0.5 %.

Basing on these results it can be concluded that for the given conditions of modeling of single-pass welding, the maximum increments of plastic deformation coincide with the temperature range of brittleness of the alloy and are propagated simultaneously with increase in the longitudinal tensile stresses, but they are not sufficient for the ductility-dip crack formation.

Conclusions

1. Using experimental and calculation procedure the evaluation of temperature fields in single-pass welding of nickel alloy Inconel 690 was carried out. The comparison of the data showed a good similarity of results of both as to the sizes of the weld and also as to the thermal cycles at the points at different distance from the fusion line, that confirms the validity of using the initial thermophysical characteristics of metal for calculation of temperature distribution in the welded joint.

2. Taking into account the experimentally determined physical and mechanical properties of the alloy, the mathematical modeling of stress-strain state was performed and the kinetics of changes in stresses and deformations was considered for different zones of welded joint. It is shown that under the conditions of modeling of linear single-pass welding of plates of 3 mm thickness at energy input of 304 J/mm the occuring stresses and deformations do not exceed the critical values, and the conditions for hot crack formation are not created.

1. (2009) Inconel® alloy 690. URL: *http://www.specialmetals.com/documents/Inconel%20alloy%20690.pdf*
2. Kiser, S.D., Zhang, R., Baker, B.A. (2009) A new welding material for improved resistance to ductility dip cracking. In: *Proc. of 8th Int. Conf. on Trends in Welding Research* (Pine-Mountain, GA, 2009), 639–644.
3. Nishimoto, K. (2006) Microcracking in multipass weld metal of alloy 690. Pt 1: Microcracking susceptibility in reheat weld metal. *Sci. and Techn. of Welding and Joining*, 11(**4**), 455–461.
4. Yushchenko, K.A., Savchenko, V.S., Chervyakov, N.O. (2011) Comparative evaluation of sensitivity of welded joints on alloy Inconel 690 to hot cracking. *The Paton Welding J.*, **11**, 2–7.
5. Makhnenko, V.I. (1976) *Computational methods for investigation of kinetics of welding stresses and strains*. Kiev: Naukova Dumka.
6. Yushchenko, K.A., Makhnenko, V.I., Savchenko, V.S. et al. (2007) Investigation of thermal-deformation state of welded joints in stable-austenitic steels and nickel alloys. *Welding in the World*, 51(**9/10**), 51–55.
7. Yushchenko, K.A., Savchenko, V.S., Zvyagintseva, A.V. et al. (2014) Physical-mechanical characteristics of In690 type weld in high-temperature range of ductility deep. In: *Proc. of 55th Int. Conf. on Actual Problems of Strength* (Kharkov, Ukraine, 2014), 189.

Received 28.09.2015

PHYSICAL AND MECHANICAL PROPERTIES OF TRANSITION ZONE OF BIMETAL PRODUCED BY AUTONOMOUS VACUUM BRAZING OF COPPER ON STEEL

M.G. ATROSHENKO, M.A. POLESHCHUK, A.V. SHEVTSOV, A.L. PUZRIN, D.D. MISHCHENKO, I.P. SEREBRYANIK and **A.I. BORODIN**
E.O. Paton Electric Welding Institute, NASU
11 Bozhenko Str., 03680, Kiev, Ukraine. E-mail: office@paton.kiev.ua

The physical and mechanical properties of the joining zone of metal produced by autonomous vacuum brazing of copper M1 on steel billets were determined. During tensile test the fracture of standard specimens occurred always in the copper part. At the same time, the strength properties of brazed copper layer in the initial state exceeded the reference values for wrought and annealed copper M1. The ultimate tear strength of brazed copper layer determined on the special specimens is equal to the temporary rupture strength of steel 20. The investigations of physical characteristics of the joining zone showed that during technical calculations the additional electrical and thermal resistances of the contact zone can be neglected. 13 Ref., 1 Table, 7 Figures.

Keywords: *autonomous vacuum brazing steel-copper bimetal, mechanical properties of joining zone, electrical and thermal resistance of contact*

During the production of separate units of machines and devices, in some cases the bimetal copper-steel billets are used manufactured beforehand. The use of such billets allows producing parts operating reliably under high electrical, thermal and mechanical loads. During their operation the physical and mechanical properties of metal in the zone of copper with steel joining are essentially important. The transition steel–copper zone should have a minimum electrical and thermal resistance and a sufficiently high mechanical strength.

It is obvious that the specific values of these variables depend on the method of manufacture of copper-steel billet.

The bimetallic strips of up to 4 mm thickness used for production of electric engineering power equipment are manufactured mainly by joint rolling of steel and copper strips or multilayer packets [1, 2]. The billets of other shapes with a large cross-section can be produced by diffusion welding in vacuum [3], explosion welding [4], friction stir welding [5], and also high-temperature brazing [6]. For manufacture of large-size billets such as water-cooled hearth electrodes of arc steel-melting furnaces of direct current, sliding bearings of large diameters, etc., different methods of fusion welding are applied [7], including electro-slag welding [8], pouring of molten copper on steel heated to 900 °C is used [9].

Recently, the method was developed to produce large-size copper-steel billets by melting copper in autonomous vacuum. The method is based on using autovacuum effect, which consists in spontaneous cleaning the surfaces of steel billets from oxide films at their heating to the temperature above 1000 °C under the conditions of a closed volume. In this case, oxygen in the composition of oxide film diffuses deep into the steel billet. At the same time, the oxidation of its surface by oxygen from the closed volume occurs. The diffusion process continues as long, unless all the oxygen of the closed volume is consumed and oxide film disappears. The time of oxide film removal from the surface of steel billet can be reduced by preliminary pumping out of air from the closed volume [10].

For manufacture of bimetal product, a closed volume is created on the billet steel part, the future interface of bimetal. The copper is placed into it in the amount necessary to produce the copper part of the billet. After sealing the volume with copper the assembly is heated to 1130–1150 °C. At this temperature the cleaning of steel surface from oxide film occurs resulting in formation of a strong metallic bonding with steel after copper melting [11].

The aim of this work is the determination of physical and mechanical characteristics of the

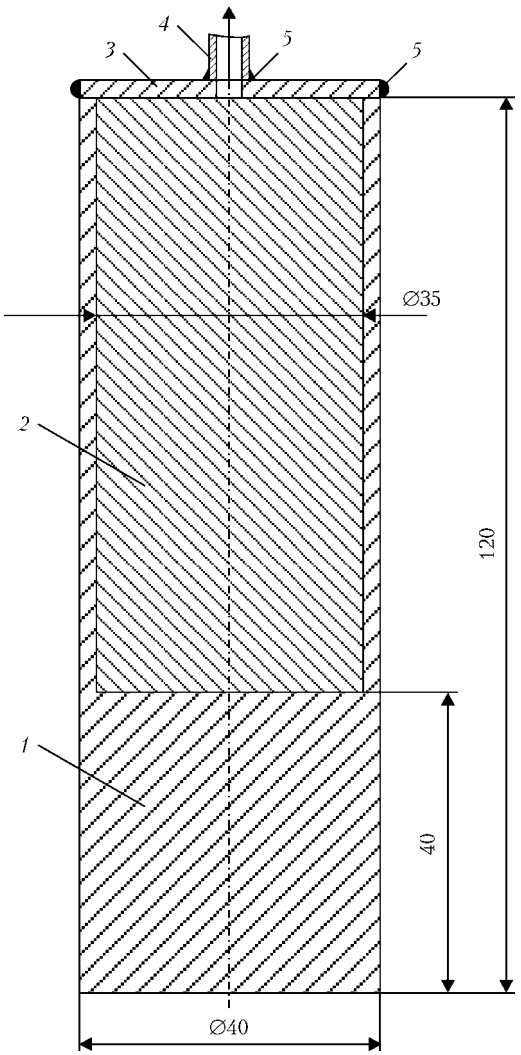

Figure 1. Sketch of pilot billet for brazing: *1* — hollow cylinder; *2* — melting component (copper); *3* — cover; *4* — branch pipe for vacuuming; *5* — sealing welds

steel–copper transition zone, produced by melting copper in autonomous vacuum, namely, of electrical and thermal resistance, mechanical strength, tensile and tear strength.

To carry out investigations the hollow cylinders with a massive bottom of steel 20 were manufactured. The cavities of cylinders were tightly filled with cuttings of copper sheet M1 of 2.5 mm thickness. The opening of the cavity was closed by steel cover, to the center of which a thin-walled steel pipe was welded-in. The cover was sealed by argon arc welding (Figure 1).

The cylinders prepared for testing were placed in the thermal furnace with a usual atmosphere. The branch pipe-vacuum conductor was brought out to the outside and connected to the forevacuum pump through the gate valve with a manovacuum gauge (Figure 2).

Before heating, the evacuation was created inside the cylinders by the forevacuum pump and the gate valve was closed. The thermal furnace was heated to 1150 °C and after 30 min of isothermal holding it was switched off and the door was opened. The cylinders were left inside the furnace until their complete cooling. During heating the evacuation inside the cylinders according to the indications of the manovacuum gauge was almost unchanged.

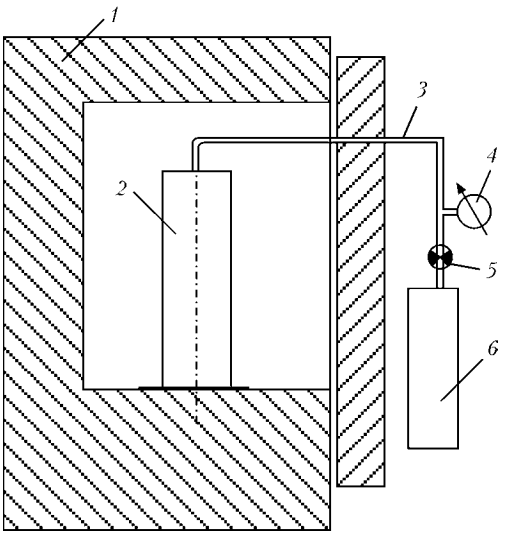

Figure 2. Scheme of carrying out autonomous vacuum brazing: *1* — thermal furnace; *2* — pilot billet; *3* — vacuum conductor; *4* — manovacuum gauge; *5* — gate valve; *6* — forevacuum pump

After cooling each cylinder was cut along the forming part into the four equal parts, of which the specimens for mechanical tests were manufactured, the measurements of electrical resistance and study of microstructure of the transition zone were carried out.

Figure 3 shows a photo of macrosection of the longitudinal template of cylindrical copper-steel billet. The visual inspection of macrosection using magnifying glass of 10-fold increase did not reveal defects, violating the integrity of metal in the brazed copper and in the zone of its joining with steel.

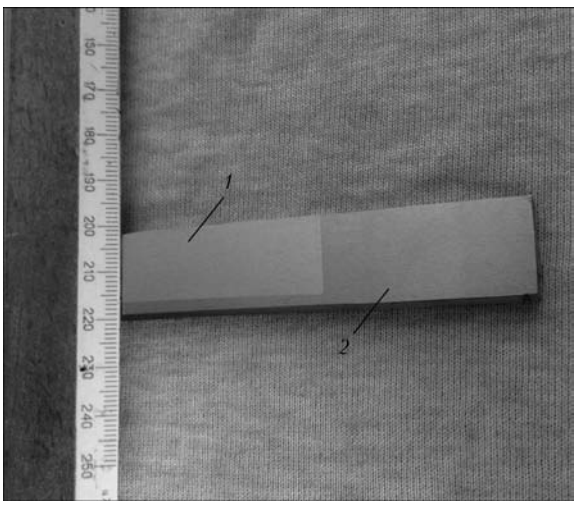

Figure 3. Macrosection of steel-copper bimetal joint: *1* — copper; *2* — steel

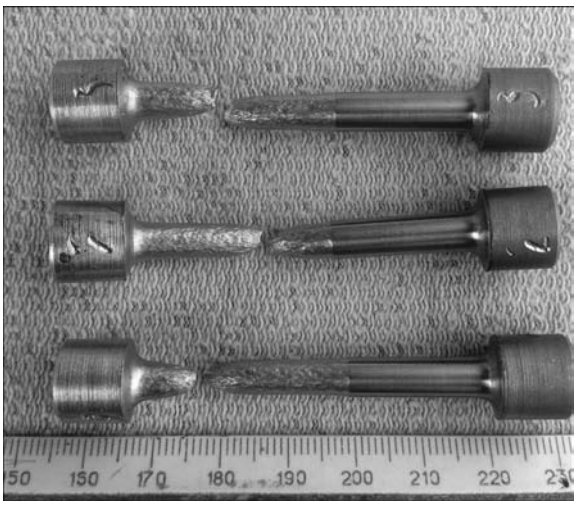

Figure 4. Specimens after tensile tests

To carry out mechanical tensile tests the specimens with 6 mm diameter of rupture part and 40 mm length were manufactured. The steel–copper contact was located in the middle of the rupture part. During tests the fracture of all the specimens occurred along the copper part (Figure 4). This means that the strength of the copper–steel contact is higher than the tensile strength of copper.

The test results are given in the Table.

The given data evidence that the values of mechanical properties of the tested specimens are higher than those of the deformed and annealed copper according to the reference values [12].

The main characteristic of quality of bimetal joint is the tear strength of the brazed layer. To obtain the reliable data on tear strength the specimens of a special type should be tested, which have a ring-type groove on a stronger joint element (Figure 5).

Such a groove reduces the area of contact of copper with steel, at the same time preserving constant diameter of the copper part of the specimen [13]. The tests showed that the fracture occurred along the line of joining. The average value of ultimate tear strength was 480 MPa, that corresponds to the value of ultimate rupture strength of annealed steel 20 [12].

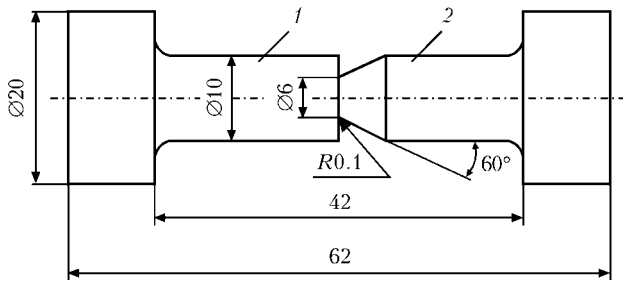

Figure 5. Sketch of specimen for testing on static tear: *1* — copper; *2* — steel part

Thus, the results of above-mentioned mechanical tests evidence that the method of autonomous vacuum brazing allows producing the copper-steel bimetal with high strength of layer joining.

The other important characteristics, which provide a reliable operation of bimetal at high electrical and thermal loads, are the values of electric and thermal resistance in the steel–copper contact. The lower are these resistances, the better is heat removal through the interface and lower the electrical losses of current passing through it. In the transition zone the change of coefficients of electrical and thermal conductivity occurs from values, inherent to steel, to those of copper. At the absence of a large number of pores, cracks and other defects in it violating the density of metal, these changes occur smoothly. Therefore, in the transition zone the value of these coefficients may be taken as an average value between the coefficients of copper and steel parts. On this assumption the total electrical and thermal resistances of transition zone are determined only by its width. The transition zone of steel-copper bimetal joints, produced using different methods of welding and melting, is determined as the area of propagating the solid solutions of copper into steel and steel into copper on both sides of the interface. These solid solutions have lower values of electrical and thermal conductivity than the pure copper [7]. Thus, by measuring the thermal or electrical conductivity of the bimetal specimen in the direction perpendicular to the joining line, the width of the transition zone can be experimentally determined.

In metallic conductors a direct connection between electrical and thermal resistance exists, determined by the Wiedemann–Franz law in its modern interpretation. Thus, knowing one of these values it is always possible to determine the other one. Methodically it is much easier to measure the electrical resistance. Therefore, we conducted its evaluation using the procedure, proposed in work [7].

Mechanical properties of steel-copper specimens as compared to properties of copper

Specimen number	Yield strength, MPa	Tensile strength, MPa	Reduction in area, %
1	110.3	282.5	70
2	113.5	281.0	73.1
3	127.4	282.8	73.1
Average	117.06	282.7	72.06
Copper, wrought and annealed [12]	74	216	75

From the cylinders the specimens of 4 × 4 × × 40 mm were manufactured so that the steel–copper interface was in the middle.

The measurements were carried out using the ammeter-voltmeter method in the differential variant by moving the potentiometric fork with the separation of electrodes of 2.3 mm at 1 mm pitch from the steel part to the copper one perpendicular to the fusion line. The measurement results are shown in Figure 6.

The diagram in this Figure shows that the change in electrical resistance at the steel–copper interface is concentrated on the length of about 4 mm. However, the size of this length can not be identified with the transition zone width of our joint. In fact, it is much smaller. This is evidenced by the nature of curve of changes of electrical resistance in the area of steel–copper interface.

In fact, judging from the diagram, the initial change in resistance occurs smoothly from steel to copper during more than 2 mm and then decreases sharply down to the value inherent to copper. Such a form of the curve indicates that the width of transition zone is smaller than the distance between electrodes of the potentiometric fork. Therefore, the resolving capacity of the method proposed in [7], does not allow evaluating the width of thin transition zones, but only determining the average value of electrical resistance in it.

To reveal the sizes of transition zone is possible by metallographic method through investigation of microsections. Figure 7 shows microstructure of bimetal joint produced by autonomous vacuum brazing of copper on steel surface.

As a result of interaction of melt of copper M1 with steel 20 at 100 magnification the fusion line of increased etching is observed. At 1000 magnification the initial stage of penetration of copper into steel is visible. The structure of steel (ferrite + pearlite) near the fusion line is not essentially different from the rest array. Around the whole volume of the brazed copper the fine non-metallic inclusions occur, the concentration of which increases near the interface at the distance of 40–50 μm.

The microhardness was measured at 50 g load in the direction perpendicular to the fusion line. On the side of steel a sharp increase in microhardness was noted. So, in the main array of steel the microhardness amounts to about 1880 MPa. At the distance of 10–15 μm from the fusion line and ahead of it the microhardness reaches to 3000 MPa. On the side of copper the abrupt changes in microhardness are not observed.

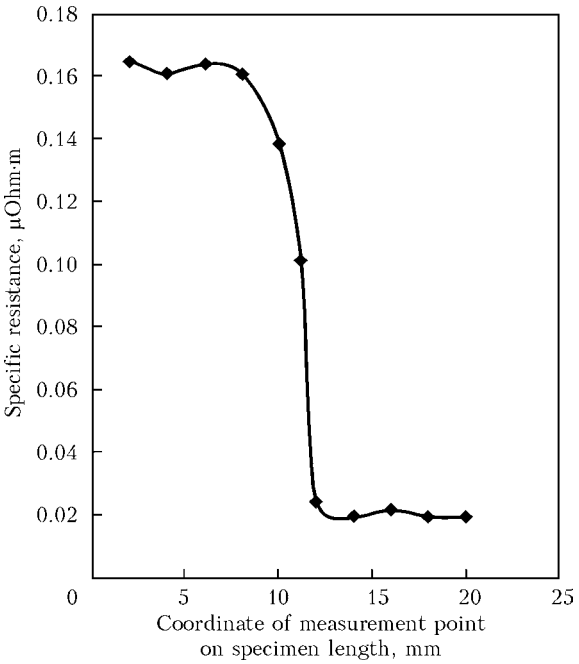

Figure 6. Diagram of changes in electrical resistance of transition zone of steel-copper bimetal produced using autonomous vacuum brazing

Across the whole cross-section of the brazed copper it amounts to 920–1080 MPa.

Thus, studying microstructure of bimetal joint on both sides of interface two anomalous regions were revealed, where the change of coefficients of electrical and thermal conductivity may occur. On the side of steel this is the area of increased

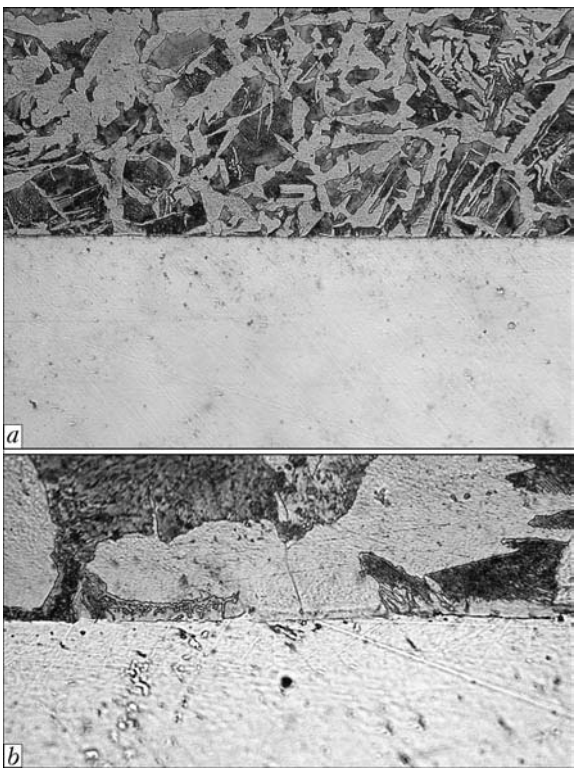

Figure 7. Microstructure of bimetal joint produced using autonomous vacuum brazing of copper on steel: *a* — ×100; *b* — ×1000

microhardness, and on the side of copper this is the area of high concentration of non-metallic inclusions.

The total length of these regions does not exceed 70 μm. Therefore, the size of this area may be identified with the width of transition zone from steel to copper.

This width is at least 3 times smaller than the width of each component of steel-copper bimetal. Consequently, the total additional electrical and thermal resistances of transition zone, determined as the product of mean values of resistances in it by its width, will be also 3 times lower than the resistance of each part of the bimetallic contact. Therefore, during engineering electrical and thermal calculations of bimetal steel-copper joint, produced using autonomous vacuum brazing, these additional resistances can be neglected.

Conclusions

1. The contact between steel and copper in bimetal joints, produced by autonomous vacuum brazing-on of copper, during electrical and thermal calculations can be considered perfect.

2. During tensile test the fracture of standard bimetallic specimens occurs along copper. At the same time, the strength properties of brazed copper layer exceed the reference values for deformed and annealed copper M1.

3. The ultimate tear strength of the brazed copper layer determined on the special specimens corresponds to the ultimate rupture strength of steel 20.

4. The technology of autonomous vacuum brazing can be used to produce bimetal consisting of carbon steels and copper of other grades.

1. Kuniharu, M. et al. *One-sided cladding of steel sheet*. Pat. 52-123824 Japan. Int. Cl. 12A 220 C 23 C 1/00. Fil. 15.10.77. Publ. 8.05.79.
2. Bukov, A.A. (1979) Corrosion-resistant bimetal sheet products. *Stal*, **6**, 446–450.
3. Nikolaev, G.A., Olshansky, I.A. (1975) *Special methods of welding*. Moscow: Mashinostroenie.
4. Kudinov, V.M., Koroteev, A.Ya. (1978) *Explosion welding in metallurgy*. Ed. by E.S. Karakozov. Moscow: Metallurgiya.
5. Nikityuk, Yu.A., Grigorenko, G.M., Zelenin, V.I. et al. (2013) Technology of restoring repair of slab mold of continuous-casting machine with friction stir surfacing. *Sovr. Elektrometallurgiya*, **3**, 51–55.
6. Paton, B.E., Rossoshinsky, A.A. (1982) Some problems of development of brazing technology. In: *Modern methods of brazing*, 3–12.
7. Lakomsky, V.I., Bogachenko, A.G., Mishchenko, D.D. et al. (2013) Welded joint of copper with steel in hearth-level electrode of direct current arc furnace. *Sovr. Elektrometallurgiya*, **4**, 7–9.
8. Paton, B.E., Medovar, L.B., Shevchenko, V.E. et al. (2003) Electroslag technologies in production of bimetal billets. *Advances in Electrometallurgy*, **4**, 7–10.
9. Golovanenko, S.A., Meandrov, L.V. (1966) *Production of bimetals*. Moscow: Metallurgiya.
10. Puzrin, L.G., Bojko, G.A., Atroshenko, M.G. (1975) *Autovacuum brazing*. Kiev: Znanie.
11. Serebryanik, I.P., Buravlev, Yu.M., Ivanitsyn, N.P. et al. *Method of production of cooled panels*. USSR author's cert. 1235075. Fil. 28.06.84.
12. Keloglu, Yu.P., Zakharievich, K.M., Kartashevskaya, M.A. (1977) *Metals and alloys*: Refer. Book. Kishinev.
13. Ovsyannikov, V.G., Shejko, V.I., Malyshev, V.A. et al. (1976) Method of determination of tearing resistance of bimetal clad layer. *Zavod Laboratoriya*, **3**, 339–340.

Received 30.07.2015

DETERMINATION OF FORCE CAUSED BY HEATING OF RING-TYPE PRODUCTS IN FLASH-BUTT WELDING

A.V. MOLTASOV, K.V. GUSHCHIN, I.N. KLOCHKOV, P.N. TKACH and **A.I. TARASENKO**
E.O. Paton Electric Welding Institute, NASU
11 Bozhenko Str., 03680, Kiev, Ukraine. E-mail: office@paton.kiev.ua

In flash-butt welding of products of a closed shape the force, which welding machine should provide for high-quality formation of welded joint in a solid phase, is determined not only by upsetting force but also by force spent for bending the part itself, and by force caused by heating of shunting part. Therefore, when choosing the equipment for welding of any product of closed shape it is necessary to determine the total force, which welding machine should provide. The experimental measurements of temperature in different characteristic points at the final stage of the process of FBW of the ring of steel 20 in machine K-724 were carried out. It was established that the temperature in the shunting part is changed both along the circumferential as well as along the radial coordinate. The existing procedure for description of temperature field was improved so that in determination of the Fourier coefficients not only the experimental data were used, but also the data obtained by computer modeling. Basing on the postulates of the proposed model the function of general form was obtained, which allows determining the temperature at any point of the shunting part using an unlimited number of terms of approximated series. The calculation of power parameters of FBW with pulsed flashing of the investigated ring was carried out. As a result, it was established that the force caused by heating of the shunting part, amounted to 9.1 % of the total force required for quality formation of the joint. The value of temperature force is connected with the value of equivalent temperature displacement. The estimated value of this displacement, corresponding to the proposed model, correlates well with the results of numerical modeling of temperature displacements in the welded billet. 11 Ref., 1 Table, 3 Figures.

Keywords: *flash-butt welding, ring-type products, shunting currents, temperature field, Fourier series, temperature force*

The advantages of flash-butt welding (FBW) determine its wide application in manufacture of structural elements such as frame rings, bands, turntables, stiffening rings, wheel rims and other products of a closed shape [1].

At the E.O. Paton Electric Welding Institute a number of machines for FBW of ring-type products was developed, which are able to develop the force from several dozens to several thousands kilonewtons [2], and some of them have also limitations on the minimum inner diameter of the product being welded [3]. Therefore, the producer encounters often a difficult task to select the optimum equipment from the existing number of machines for welding the certain ring product.

In FBW of parts of an open shape the power parameters are determined by a specific upsetting pressure of material of the part and the area of its cross-section [4]. In the process of FBW of ring-type products the bending of the part itself and the shunting of electric current through it occur [5].

In work [6] it was proved that heating of the shunting part contributes to arising of thermal stresses, which affect the volume of the force required for formation of quality welded joint during FBW. However, the procedure of description of the temperature field, demonstrated in the present work, allows using a limited number of terms of the series, with the help of which it is not always possible to obtain the desired accuracy. Furthermore, no expression was given for the force generated by thermal stresses in the shunting part.

Therefore, the aim of this work is the improvement of the procedure for description of temperature field and force caused by heating of the shunting part.

The experimental measurements of temperatures were carried out during FBW of the ring of steel 20 with cross-section of 55×25 mm^2 and inner diameter of 270 mm (Figure 1, *a*) in five controllable points (Figure 1, *b*).

According to the results of measurements it was established that the temperature in the shunting part is changed both around the circumference θ, as well as around the radial coordinate r. As the determination of force caused by heating of the shunting part is based on solving the relevant problems of theory of elasticity, it is necessary to preset the temperature as a continuous

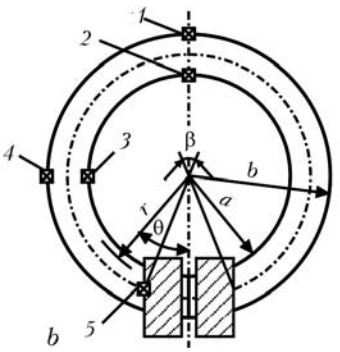

Number of point	θ, deg	T, °C
1	π	460
2	π	510
3	π/2	480
4	π/2	450
5	≈π/6	130

Figure 1. Ring workpiece in clamping devices of welding machine K-724 (*a*), and layout of points 1–5 (*1–5*) of temperature control (*b*)

function of the coordinates. In solving the problems in polar coordinates the most convenient for description of change in temperature is the even part of the Fourier series around the circumferential coordinate θ:

$$T(\theta) = A_0 + \sum_{1}^{n} A_n \cos n\theta. \tag{1}$$

To determine the unknown Fourier coefficients A_n it is necessary to create the system of equations for temperature values in the different points around the circumferential coordinate θ of the shunting part. As far as the experimental data allow presetting only three temperature values at the outer and inner diameters, namely, $T(\pi/6)$, $T(\pi/2)$ and $T(\pi)$, the other ones can be determined by computer modeling of the temperature field (Figure 2, *a*). The number of equations of the system determines the accuracy of description of the temperature field. Using the first six terms of the series (Table) allows describing the temperature field with the accuracy of up to 3 °C. You can be sure that the values of temperatures, taken from the diagram (Figure 2, *b*), coincide with the results of computer modeling.

As is seen, the value of the coefficients decreases according to the absolute value, so the introduction of the following coefficients will not make a considerable amendment to the values of temperatures.

The change in the temperatures in the radial direction is determined from the differential equation of thermal conductivity [7]:

$$\frac{1}{\chi}\frac{\partial T}{\partial t} = \frac{\partial^2 T}{\partial r^2} + \frac{1}{r}\frac{\partial T}{\partial r} + \frac{1}{r^2}\frac{\partial^2 T}{\partial \theta^2}, \tag{2}$$

Calculated Fourier coefficients in points 1–5 acc. to Figure 1, *b*

Coefficient	A_0	A_1	A_2	A_3	A_4	A_5
$T_{\text{in.dia}}$, °C	373	−221	−122.5	−51	−51	−3
$T_{\text{out.dia}}$, °C	339	−192	−106.5	−48	−51	−3

where χ is the coefficient of thermal conductivity.

As far as the temperature field is considered at the moment when the temperature reaches its maximum value, but not its change in time, then the left side of equation (2) turns to zero (solution of such equation is given in work [6]).

As a result the function of general view was obtained corresponding to the proposed model, which allows determining the temperature at any point of the shunting part:

$$T(r, \theta) = K_0 = H_0 \ln r + \sum_{1}^{n} \left(K_n r^n + \frac{H_n}{r^n} \right) \cos n\theta, \tag{3}$$

where

$$K_0 = \frac{A_0(a)\ln b - A_0(b)\ln a}{\ln b - \ln a};$$

$$K_n = \frac{A_n(b)b^n - A_n(a)a^n}{b^{2n} - a^{2n}};$$

$$H_0 = \frac{A_0(b) - A_0(a)}{\ln b - \ln a}; \tag{4}$$

$$H_n = \frac{a^n b^n}{b^{2n} - a^{2n}} [A_n(a)b^n - A_n(b)a^n].$$

(For procedure of determination of stresses caused by the presence of temperature field described by the Fourier series see works [8, 9].)

So, stress components have the following form:

$$\sigma_r = B_0 \frac{1}{r^2} + 2C_0 + D_0(1 + 2\ln r) + \left(2B_1 r - \frac{2C_1}{r^3} + \frac{D_1}{r} \right) \cos\theta;$$

$$\sigma_\theta = -B_0 \frac{1}{r^2} + 2C_0 + D_0(3 + 2\ln r) + \left(6B_1 r + \frac{2C_1}{r^3} + \frac{D_1}{r} \right) \cos\theta; \tag{5}$$

$$\tau_{r\theta} = \left(2B_1 r - \frac{2C_1}{r^3} + \frac{D_1}{r} \right) \sin\theta,$$

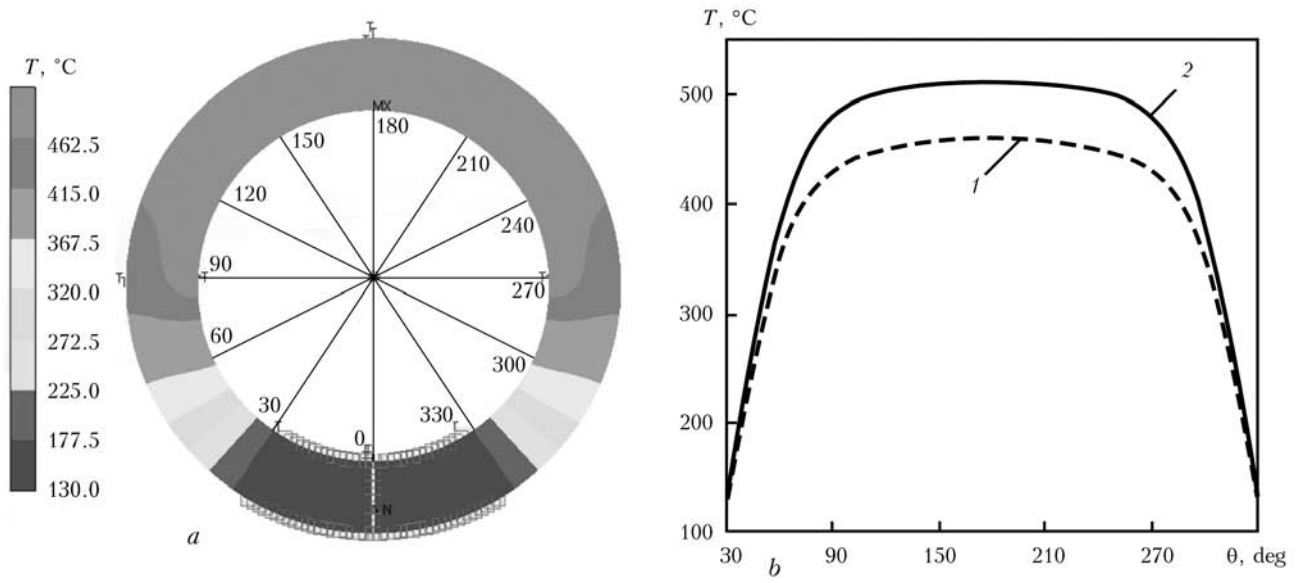

Figure 2. Temperature fields in the ring (*a*), and diagrams of temperature distribution along the outer (*1*) and inner (*2*) diameter (*b*)

where

$$B_0 = -\frac{\alpha E H_0}{2(b^2 - a^2)} a^2 b^2 \ln \frac{b}{2}; \quad B_1 = \frac{\alpha E H_1}{4(a^2 + b^2)};$$

$$C_0 = \frac{\alpha E H_0}{4} \frac{b^2 \ln b - a^2 \ln a}{b^2 - a^2} + \frac{\alpha E H_0}{8};$$

$$C_1 = -\frac{\alpha E H_1}{4(a^2 + b^2)} a^2 b^2;$$

$$D_0 = \frac{\alpha E H_0}{4}; \quad D_1 = \frac{\alpha E H_1}{2},$$

where α is the coefficient of linear expansion; E is the modulus of elasticity of material.

The relation of the displacement components with the stress components was found in [10].

Therefore, stresses (5) in the closed ring are equivalent to circumferential displacement of the ring moving edge with a gap for the value of

$$\delta_t = -(2\pi - \beta)\alpha \left(H_0 \frac{a + b}{2} + H_1 \right). \qquad (6)$$

As far as in our case, according to (4), H_0 and H_1 are negative, then the displacement δ_t is directed towards the increase of coordinate θ, i.e. is equal to increase of the gap.

In our case the temperature displacement amounted to 2.88 mm. To confirm this result a numerical modeling of displacement fields in the ring workpiece was carried out during heating, being similar to that realized in the ring shunting part in FBW (Figure 3).

According to the results of numerical modeling it was established that the temperature movement of the left edge amounted to 3.04 mm, that is 5.3 % higher than the value obtained by analytical calculation according to formula (6), corresponding to the temperature field (3).

As far as this displacement is directed opposite from displacement of the moving clamping device of the welding machine, a part of the force is spent to overcome it. The relation between the displacement and the corresponding force was established in work [10]. Thus, to prevent the displacement (6) it is necessary to apply the force

$$P_t = -\alpha E t \frac{2\pi - \beta}{4\pi} \times \qquad (7)$$

$$\times \left(H_0 \frac{(b^2 - a^2)^2 - 4a^2 b^2}{2(a + b)(b^2 - a^2)} + H_1 \frac{a^2 - b^2 + (a^2 + b^2) \ln \frac{b}{2}}{a^2 + b^2} \right).$$

For the investigated ring the calculation of power parameters of FBW with pulsed flashing

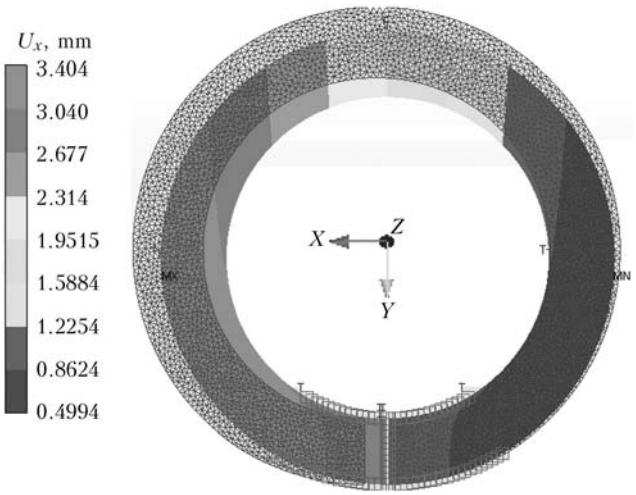

Figure 3. Field of displacements in the ring (mesh indicates the deformed state)

was performed [11]. The force, spent for bending of the part, is determined by the formula obtained in [10]:

$$P_{\text{bend}} = -\frac{E\delta_{\Sigma}t}{4\pi(a^2 + b^2)}\left[a^2 - b^2 + (a^2 + b^2)\ln\frac{b}{a}\right], \quad (8)$$

where δ_{Σ} is the sum of the initial gap and allowances for flashing and upsetting.

As a result, it was established that the thermal force amounts to more than 9 % of the total force, which the welding machine should provide to form the quality welded joint in solid phase.

The calculation of power parameters of FBW with pulsed flashing of the investigated ring was carried out at the following initial data: inner diameter 270 mm; cross-section F = 55 × × 25 mm^2; specific upsetting pressure 40 MPa; modulus of elasticity 210 GPa; coefficient of linear expansion $1.4 \cdot 10^{-5}$ 1/deg; initial gap 2 mm; allowance for flashing 9 mm; allowance for upsetting 7 mm.

Obtained were the dummy displacement from heating δ_t = 2.88 mm; thermal force P_t = 14.8 kN; upsetting force P_{ups} = 55 kN; bending force P_{bend} = 92.6 kN; total force P_{Σ} = = 162.4 kN; P_t/P_{Σ} = 9.1 %.

Conclusions

1. The procedure was improved, which allows describing the temperature field in the shunting part in FBW of ring-type workpiece in the form of even part of the Fourier series around the circumferential coordinate on the basis of discrete data obtained by experimental measurements and computer modeling.

2. In accordance with the postulates of the proposed model the function of general form was obtained, which allows determining the temperature at any point of the ring shunting part using unlimited number of series terms.

3. For the first time an analytical expression was obtained for determination of the force acting on the butt caused by heating of the shunting part. For the ring of steel 20 with inner diameter of 270 mm and cross-section of 55 × 25 mm^2 the power parameters of FBW using pulsed flashing were calculated. As a result, it was established that the force caused by heating of the shunting part amounts to 9.1 % of the total force, which welding machine should provide.

1. Pavlichenko, V.S. (1964) *Resistance welding of closed-shape products*. Moscow: Mashinostroenie.
2. Kuchuk-Yatsenko, S.I. (1992) *Flash butt welding*. Kiev: Naukova Dumka.
3. Kuchuk-Yatsenko, S.I, Chvertko, P.N., Semyonov, L.A. et al. (2013) Flash butt welding of products of high-strength alloys based on aluminium. *The Paton Welding J.*, **7**, 2–6.
4. Gelman, A.S. (1952) *Technology of electric resistance welding*. Moscow: Mashgiz.
5. Kabanov, N.S. (1973) *Welding on resistance machines*. Moscow: Vysshaya Shkola.
6. Moltasov, A.V., Samotryasov, S.M., Knysh, V.V. et al. (2014) Influence of non-uniformity of heating on upsetting force value and forging time in flash-butt welding of flat ring. *The Paton Welding J.*, **10**, 11–14.
7. Karslou, G., Eger, D. (1964) *Thermal conductivity of solids*. Moscow: Nauka.
8. Timoshenko, S.P., Goodier, J. (1975) *Theory of elasticity*. Moscow: Nauka.
9. Boli, B., Ueiner, J. (1964) *Theory of temperature stresses*. Moscow: Mir.
10. Chvertko, P.N., Moltasov, A.V., Samotryasov, S.M. (2014) Calculation of upsetting force in flash butt welding of closed-shape products. *The Paton Welding J.*, **1**, 46–50.
11. Kuchuk-Yatsenko, S.I., Didkovsky, V.A., Bogorsky, M.V. et al. *Method of flash butt welding*. Pat. 46820 Ukraine. Publ. 17.06.2002.

Received 11.02.2015

INFLUENCE OF METAL SHRINKAGE IN LONGITUDINAL WELDS OF SLEEVES ON CONTACT PRESSURE IN MAIN GAS PIPELINE REPAIR

O.I. OLEJNIK
E.O. Paton Electric Welding Institute, NASU
11 Bozhenko Str., 03680, Kiev, Ukraine. E-mail: office@paton.kiev.ua

Effectiveness of main pipeline repair in service is largely determined by contact pressure, created at sleeve mounting on pipe defective section. At correct selection of contact pressure value, long-term performance of the repaired section is ensured through partial unloading of the pipe wall. Such a result is achieved due to lowering of pressure in the main line before repair, and tight pressing of the sleeve around the pipe with a special device. Arc welding of sleeve reinforcing elements also is of considerable importance, resulting in formation of contact pressure, caused by shrinkage of multilayer longitudinal butt welds. In the work computational method was used to study the influence of sleeve wall thickness and pipeline diameter on the magnitude of contact pressure caused by deposited metal shrinkage. It is shown that contact pressure caused by metal shrinkage during welding performance has the strongest influence on unloading of a defective pipe wall in pipelines of 1020 mm and smaller outer diameter. Further increase of contact pressure magnitude caused by metal shrinkage can be achieved by increasing sleeve wall thickness. Such a technique is not effective for pipes of 1220 mm and greater diameter. 5 Ref., 5 Figures.

Keywords: *main gas pipeline, sleeve, repair, arc welding, deposited metal shrinkage, contact pressure*

Keeping Ukrainian gas transportation system in the appropriate technical condition by repair welding without taking the damaged sections out of service is an important scientific-practical task. Technologies involving application of reinforcing welded sleeves currently prevail in practical repair of corrosion damage of pipes of main gas pipeline linear part [1]. Such structures consist of two symmetrical half-shells, which are pressed around the pipe outer surface during mounting to create tight contact (interference). As a rule, such operations are performed under the condition of inner pressure lowering in the main line.

It is known that contact pressure ΔP_l arising at sleeve mounting on the pipe has an important role in ensuring reliable operation of repaired section [2]. This is associated not only with force pressing of half-shells during assembly by various devices, but also additional redistribution of loads between pipe and sleeve walls at inner pressure increase from repair value P_{rep} up to working pressure P (Figure 1). As the assembly process involves multilayer welding of half-shells to each other by two parallel longitudinal butt welds, contact pressure ΔP_{sh} arises additionally, as a result of deposited metal shrinkage.

The objective of this work consists in determination through calculation of ΔP_{sh} value for evaluation of the degree of its influence on total level of contact pressure ΔP_l.

Calculation was based on the idea of determination of reactive stresses σ_r in a closed shell, which arise after making the longitudinal welds and act in the circumferential direction (Figure 2). Assuming that stresses σ_r are uniformly distributed across sleeve wall section, and con-

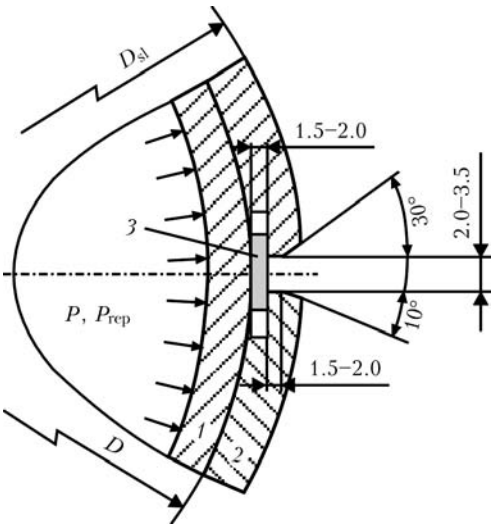

Figure 1. Schematic of edge preparation in sleeve half-shells for butt welding: *1*, *2* — pipe and sleeve wall; *3* — backing plate; D, D_{sl} — pipe and sleeve outer diameters, respectively; P, P_{rep} — pressure inside the pipeline in working mode and during repair, respectively

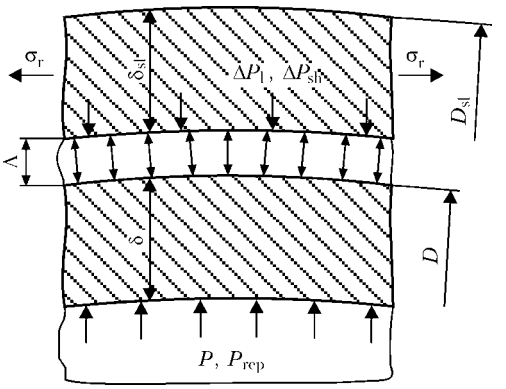

Figure 2. Stress-strain state of pipe and sleeve walls under the impact of inner pressure: δ, δ_{sl} — pipe and sleeve wall thickness, respectively; ΔP_l — contact pressure of sleeve on the pipe; ΔP_{sh} — contact pressure of sleeve on the pipe caused by weld shrinkage

dition of dense contact ($\Lambda >> 0$) is fulfilled, average contact pressure ΔP_{sh} can be found from the following formula:

$$\Delta P_{sh} = \sigma_r \frac{2\delta_{sl}}{D + 2\delta_{sl}}, \quad (1)$$

where D is the pipeline outer diameter; δ_{sl} is the nominal thickness of sleeve wall.

Known from theoretical fundamentals of welded structure design [4] is the calculated dependence for calculation of reactive stresses for the cases of transverse location of welds relative to the action of reactive stresses:

$$\sigma_r = -\mu' E \frac{q_{h.i}}{F}, \quad (2)$$

where F is the welded element section in the direction normal relative to weld axis; $q_{h.i}$ is the average welding heat input; E is the material modulus of elasticity; μ' is the coefficient characterizing weld transverse shrinkage and determined by graphic dependence $\mu' = f(m)$ (Figure 3).

For the sleeve the section will be defined as

$$F = \pi(D + 2\delta_{sl})\delta_{sl}. \quad (3)$$

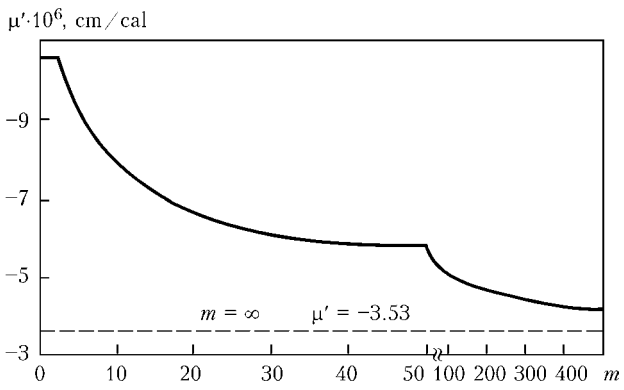

Figure 3. Coefficient μ' versus relative rigidity m

Parameter m, which reflects relative rigidity, is calculated from the following formula for such a structure:

$$m = 0.125 \cdot 10^6 \frac{4F}{v_w q_{h.i}^2}, \quad (4)$$

where v_w is the welding speed.

In butt welding in several passes the conditional heat input is calculated by the following formula:

$$q_{con} = 340 \left(F_{gr} + \frac{2}{\cos \theta/2} r\delta_{sl} \right), \quad (5)$$

where F_{gr} is the area formed by butt weld groove; θ is the total groove angle; $r = 43.5 \cdot 10^{-3} \sqrt{q_{h.i}}$.

Considering that sleeve half-shells were welded to each other by two butt welds, formula (2) can be written as

$$\sigma_r = -\mu' E \frac{2q_{con}}{F}. \quad (6)$$

Let us consider an example of calculation of the magnitude of contact pressure ΔP_{sh} for the case of sleeve repair of corrosion damage with overall dimensions of 250 × 150 mm in the longitudinal S and circumferential C directions and maximum depth a = 4 mm. Pipe of X60 strength class of D = 1020 mm, δ = 10.5 mm was used with sleeve wall thickness δ_{sl} = 10.5 mm ($\delta = \delta_{sl}$). For calculation we will assume the following welding mode, characteristic for 4 mm electrode: I = 140 A, U = 24 V, η = 0.7, v_w = 0.2 cm/s.

Then, $q_{h.i} = 0.24IU\eta(v_w)^{-1} = 2822$ [cal/cm]; r = 2.31 cm; F_{gr} = 0.44 cm^2.

We will determine welded element section in the normal direction from formula (3)

$$F = \pi(D + 2\delta_{sl})\delta_{sl} = \pi(102 + 2 \cdot 1.05) \cdot 1.05 = 244 \text{ cm}^2.$$

We will calculate conditional heat input by formula (5), considering that groove angle θ = 40° and $q_{con} = 340(0.53 + 2 \cdot 2.31 \cdot 1.05(\cos 20°)^{-1} =$ = 1905 cal/cm.

Sleeve relative stiffness is equal to

$$m = 0.125 \cdot 10^6 \frac{4F}{v_w q_{h.i}^2} = 108.$$

Then, the coefficient, which determines weld transverse shrinkage, will correspond to value $\mu' = -4/97 \cdot 10^{-6}$ cm/cal.

Reactive stress magnitude in keeping with (6) is equal to

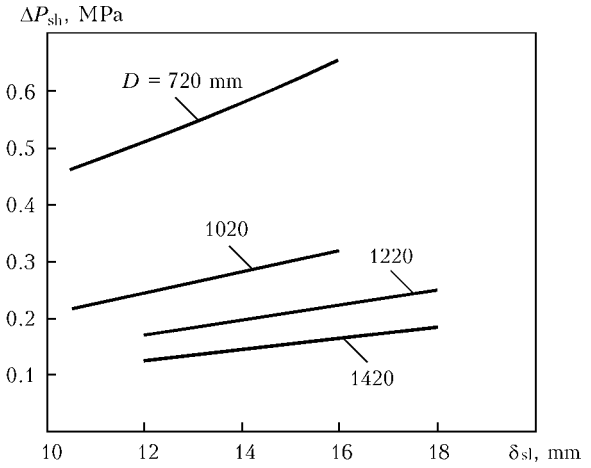

Figure 4. Influence of sleeve wall thickness δ_{sl} on magnitude of contact pressure caused by longitudinal weld shrinkage ΔP_{sh} depending on pipeline diameter D

$$\sigma_r = -\mu E \frac{2q_{con}}{F} = 110 \text{ kg/cm}^2.$$

Magnitude of average contact pressure between the sleeve and pipe ΔP_{sh} is determined as

$$\Delta P_{sh} = \sigma_r \frac{2\delta_{sl}}{D + 2\delta_{sl}} = 2.22 \text{ kg/cm}^2 \text{ or } \Delta P_{sh} = 0.22 \text{ MPa}.$$

Figure 4 presents in the graphic form the results, obtained with application of the above calculation method, showing the dependence of ΔP_{sh} on sleeve wall thickness δ_{sl} and pipeline diameter D. To evaluate the degree of ΔP_{sh} influence on level of contact pressure ΔP_l it is necessary to have the diagrams of admissible linear dimensions of pipe wall thinning, the sample of which is shown in Figure 5, and criterion of grounded selection of ΔP_l value. The latter has the following form [5]:

$$\Delta P_l \geq P - [P] - \chi_1(P - P_{rep}), \quad (7)$$

where $[P]$ is the admissible pressure for pipe wall thinning, determined by diagrams of admissible linear dimensions;

$$\chi_1 = \left(1 + \frac{(0.5D_{sl})^2\delta}{(0.5D)^2\delta_{sl}}\right)^{-1}.$$

In view of the requirements of normative documents on repair in operating gas pipelines that $P_{rep} = 0.7P$ (P = 5.4 MPa), for the considered example $[P] = 0.75P$, $\chi_1 = 0.49$. Then, in keeping with (7), $\Delta P_l = 0.55$ MPa. Comparing the calculated value with $\Delta P_{sh} = 0.22$ MPa, one can say that in this case contact pressure caused by longitudinal weld shrinkage makes up a significant part (about 40 %) of minimum required contact pressure. Their total value contributes to the margin for ensuring the performance of gas pipeline section repaired using the welded sleeve.

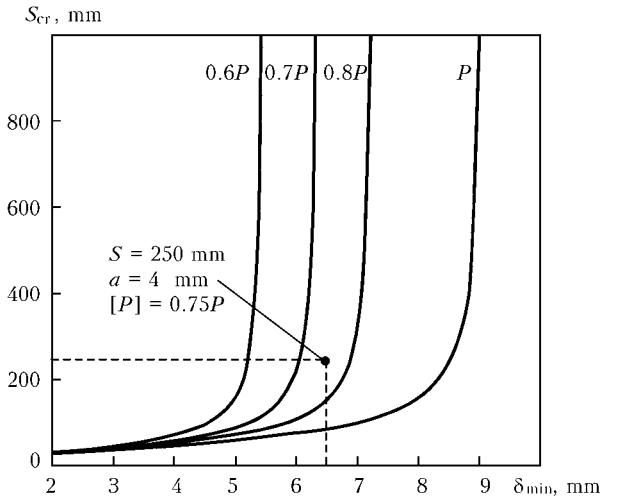

Figure 5. Diagram of admissible linear dimensions of pipe wall thinning depending on pipe wall minimum thickness δ_{min} for 1020 × 10.5 mm gas pipeline from steel of strength category X60 with maximum working pressure P = 5.4 MPa

At the same time, it should noted that with increase of pipe diameter D, value of admissible pressure $[P]$ will decrease for a defect with the same overall dimensions, that will require increasing the minimum needed contact pressure ΔP_l, accordingly. This leads to the conclusion about a decreasing role of ΔP_{sh}.

Thus, it can be stated that shrinkage in welding of sleeve longitudinal welds on gas pipelines with outer diameter of 1020 mm and less will have the strongest influence on unloading of pipe defective wall. In repair of the main gas pipelines with 1220 mm and greater outer diameters, attention should be focused on providing the required value of contact pressure ΔP_l, while influence of value ΔP_{sh} should be regarded as insignificant. A certain increase of ΔP_{sh} value can be achieved by increasing sleeve wall thickness δ_{sl}. Such a technique, however, has quite limited practical application, as a result of deterioration of mounting conditions, because of half-shell rigidity and complexity of ensuring the required value of contact pressure ΔP_l.

1. *GBN V.3.1-00013741-12:2011*: Main gas pipelines. Repair by arc welding in service conditions. Kiev: Ministry of Energy and Coal Industry of Ukraine. Introd. 06.09.2011.
2. Kiefner, J.F. (1977) Repair of line pipe defects by full-encirclement sleeves. *Welding J.*, **6**, 26–34.
3. Aginej, R.V., Puzhajlo, A.F., Aleksandrov, Yu.V. et al. (2012) Methods of safety assurance of long-term service gas pipelines prone to stress-corrosion. *Korroziya Territorii Neftegaz*, 23(**3**), 50–61.
4. Okerblom, N.O. (1964) *Structural-technological design of welded structures*. Moscow-Leningrad: Mashinostroenie.
5. Makhnenko, V.I., Olejnik, O.I., Shekera, V.M. (2013) Determination of contact pressure of reinforcing sleeve in repair of pipelines with surface defects. *The Paton Welding J.*, **6**, 11–14.

Received 09.10.2015

NEW WELDING WIRE MANUFACTURER IN UKRAINE

A.N. Alimov,
Technical Director of Company VITAPOLIS

Manufacture of special-purpose metal structures from high-alloyed corrosion-resistant, high-temperature, heat-resistant and high-strength steels is developing at a faster pace all over the world. This is due to advance of technology in petrochemical industry, power engineering, construction industry, intensification of transport operation, and designers' desire to reduce the weight and overall dimensions of metal structures. Consumable-electrode arc welding, gas-shielded welding and submerged-arc welding still remain the main technologies in fabrication and repair of such metal structures.

The structure of Ukrainian manufacturers of welding wires for all arc welding processes, also those for stick electrode manufacture, includes only manufacturers of wires from low-carbon and some low-alloyed steel grades. Production of special-purpose wires: high-alloyed corrosion-resistant, heat-resistant, nickel-based, high-strength, etc., was absent in Ukraine until recently. All the above-mentioned types of wires were imported from China, India, Russia, Italy and other countries.

In 2010, a group of enthusiasts from Boyarka (Kiev suburb) took a decision to set up modern manufacture of special-purpose welding wires in their facility. The group included graduates of Welding Chair of Kiev Polytechnic Institute, having experience of working at PWI and in welding consumable production, businessmen and financial people. After detailed study of Ukrainian market of high-alloyed corrosion-resistant, high-temperature and other special wires (including welding wires), preparation of detailed business plan, selection of production area, preparation of engineering lines and communications, the team began implementation of the project. During project preparation the most recent advances of the technology of wire product processing were analyzed, namely features of wire rod preparation for drawing, influence of various types of drawing tools and process materials on the quality of the produced wire, kinds of finished wire surface treatment to meet the expectations of consumers, used to working with wire, complying with the requirements of European and US standards. At this stage of project preparation, special attention was given to power efficiency of production process, as well as minimizing or complete elimination of adverse environmental impact of future production. Technological scheme and set of equipment for process lines were selected only on the basis of achieving maximum possible consumer characteristics of finished wire.

As a result of analysis of equipment supplier proposals, one main manufacturer — well-known company Lamnea Bruek, and several sub-suppliers of a number auxiliary devices from Germany, Italy, Austria, USA and India, were selected from a number of potential manufacturers, proceeding from detailed technological scheme of production. It should be noted that various auxiliary devices are key elements of the technological chain in manufacture of high-alloyed and special-purpose wires. Without these specialized additional devices the drawing line can only support production of general-purpose wires.

All the potential manufacturers and suppliers of process equipment were first inspected (visiting and auditing the production), in order to obtain information on the engineering level and service properties of the proposed equipment, its reliability, ease and safety of service. Finally, it was possible to combine in one production line all the best currently known engineering solutions in manufacture of special-purpose wires.

Start of production was organized by VITAPOLIS company, which began manufacturing marketable wire in July, 2015. The wires were assigned registered KHORDA trade mark.

When putting the line into operation, we performed commissioning work, using Sv-08GS and Sv-08G2S wire rods. Testing of produced general-purpose wires showed that these wires produced by our process scheme, in terms of their welding-technological properties are in no way inferior to such known wire grades as AristoRod 12.50 (ESAB) and EMK-6 Top (Boehler).

Our production line is capable of preparing for drawing and cleaning in a sound and highly reproducible manner the surface of wire rods, having difficult-to-remove or slight unforeseen contamination, possible deviations of diameter, ovality, etc. Here, already at the inlet of the first drawing block, the rod surface has characteristic uniform metal luster, as after grinding by an abrasive tool. Ovality of wire leaving the first drawing block with rotating die, is not more than 0.01 mm, and its surface is super smooth. Further wire drawing is performed with application of water-soluble stearates of sodium, calcium and drawing tools of Bremer and Paramount companies. Finish preparation of drawing tools is performed in our die shop in Bremer semi-automatic machine.

Remains of drawing lubricant are removed from the surface of finished wire by hot water at high pressure, which is followed by further polishing of the wire and covering its surface with a thin layer of antifriction current-conducting coating, containing corrosion inhibitor. Finished wire is wound on standard consumer reels of 200, 300 or 415 mm diameter, packed into plastic bags and cardboard boxes. At the request of the customer, the wire can be additionally packed into vacuum bags.

It should be noted that manufacture of a wide range of special-purpose wires, including those designed for welding low-alloyed and high-strength steels, high-alloyed corrosion-resistant and heat-resistant steels, nickel-based alloys and armour steels, requires close monitoring and control of all the technological process stages.

For these purposes, testing and measuring laboratory is functioning at VITAPOLIS enterprise from the first days of its operation. The laboratory includes a range of equipment and set of devices for mechanical testing, chemical analysis, metallographic examination of raw materials and finished products. Welding-technological testing section is fitted with stations for gas-shielded semi-automatic welding and mechanized submerged-arc welding.

Before the start of production, we paid special attention to training production personnel, realizing that even in the best equipment high-quality products with appropriate consumer properties can be produced only in the case of its operation by trained, qualified workers. Our engineers provided detailed descriptions of all the elements of technological process, working in close contact with equipment manufacturers, technologists from Germany, Sweden and Austria. After competitive selection process, all the workers had production training directly in our Enterprise, in accordance with developed technological and operating manuals. Personal responsibility of each worker for the performed technological operation was introduced, with recording and documenting of the performed operations. Quality management system, corresponding to ISO 9001, is in force at the Enterprise.

In October 2015, VITAPOLIS presented their products at the International Exhibition «Arms and Safety-2015» (Kiev), which aroused considerable interest of representatives of defence industry enterprises of Ukraine and a number of foreign countries.

By now, the first orders have been fulfilled for supplying welding wires to«Frunze Elektrod», «Gefest» and other companies. At present the Enterprise production facilities allow producing about 100 tons of welding wire of 15 different grades per month. Company investment program envisages putting into production about 30 more wire grades in 2016.

A.N. Alimov, VITAPOLIS

PATON PUBLISHING HOUSE

www.patonpublishinghouse.com

SUBSCRIPTION

«The Paton Welding Journal» is Published Monthly Since 2000 in English, ISSN 0957-798X.

«Avtomaticheskaya Svarka» Journal (Automatic Welding) is Published Monthly Since 1948 in Russian, ISSN 005-111X.

«The Paton Welding Journal» is Cover-to-Cover Translation of Avtomaticheskaya Svarka» Journal into English.

If You are interested in making subscription directly via Editorial Board, fill, please, the coupon and send application by Fax or E-mail.

The cost of annual subscription via Editorial Board is $348 for «The Paton Welding Journal» and $180 for «Avtomaticheskaya Svarka» Journal.

«The Paton Welding Journal» can be also subscribed worldwide from catalogues subscription agency EBSO.

SUBSCRIPTION COUPON

Address for journal delivery _____

Term of subscription since _____ **20** **till** _____ **20**

Name, initials _____

Affiliation _____

Position _____

Tel., Fax, E-mail _____

We offer the subscription all issues of the Journal in pdf format, starting from 2009.

The archives for 2009–2012 are free of charge on *www.patonpublishinghouse.com* site.

ADVERTISEMENT

in «Avtomaticheskaya Svarka» and «The Paton Welding Journal»

External cover, fully-colored:
First page of cover (190×190 mm) — $700
Second page of cover (200×290 mm) — $550
Third page of cover (200×290 mm) — $500
Fourth page of cover (200×290 mm) — $600

Internal cover, fully-colored:
First/second/third/fourth page of cover (200×290 mm) — $400

Internal insert:
Fully-colored (200×290 mm) — $340
Fully-colored (double page A3) (400×290 mm) — $500

- Article in the form of advertising is 50 % of the cost of advertising area
- When the sum of advertising contracts exceeds $1001, a flexible system of discounts is envisaged

Size of journal after cutting is 200×290 mm

Editorial Board of Journal «Avtomaticheskaya Svarka» and «The Paton Welding Journal»
E.O. Paton Electric Welding Institute of the NAS of Ukraine
International Association «Welding»
11, Bozhenko Str., 03680, Kyiv, Ukraine
Tel.: (38044) 200 60 16, 200 82 77; Fax: (38044) 200 82 77, 200 81 45
E-mail: journal@paton.kiev.ua; www.patonpublishinghouse.com